

A Trade Space Model for Robotic Lunar Exploration

by

Zachary James Bailey

S.B., Massachusetts Institute of Technology (2008)

Submitted to the Department of Aeronautics and Astronautics
in partial fulfillment of the requirements for the degree of

Master of Science in Aerospace Engineering

at the

MASSACHUSETTS INSTITUTE OF TECHNOLOGY

June 2010

© Massachusetts Institute of Technology 2010. All rights reserved.

Author
Department of Aeronautics and Astronautics
May 21, 2010

Certified by.....
David W. Miller
Professor of Aeronautics and Astronautics
Thesis Supervisor

Accepted by.....
Eytan H. Modiano
Associate Professor of Aeronautics and Astronautics
Chair, Committee on Graduate Students

A Trade Space Model for Robotic Lunar Exploration

by

Zachary James Bailey

Submitted to the Department of Aeronautics and Astronautics
on May 21, 2010, in partial fulfillment of the
requirements for the degree of
Master of Science in Aerospace Engineering

Abstract

The last decade has seen a resurgence of interest in the moon as a target for planetary exploration. In light of the growing interest in the robotic exploration of the moon, this thesis presents a quantitative methodology for exploring the trade space of potential *in situ* robotic lunar spacecraft designs. A science value model was developed, using Multi-Attribute Utility Theory (MAUT), to estimate the effectiveness of a spacecraft design towards assessing a set of specified science objectives. An engineering model was developed to estimate the masses of spacecraft designs within the trade space. These models were integrated together to explore the objectives of minimizing mass and maximizing science return.

Two methods for exploration of the trade space were presented: a stochastic design space search method, and a multi-objective simulated annealing method. Using these techniques, the optimality of a reference mission was investigated, and ways to improve science utility performance were shown. The exploration of a trade space under uncertainty, using an ϵ -Pareto search method, was investigated, and recommendations for designers were presented.

Thesis Supervisor: David W. Miller

Title: Professor of Aeronautics and Astronautics

Acknowledgments

This thesis is dedicated to my mom, dad, and brother: Linda, Carrington, and Carl Bailey. Their love and support have been essential as I have pursued my dreams.

I would also like to thank my advisor, Prof. David Miller, for his guidance in the five years I have known him while at MIT.

This work was partially funded by the Jet Propulsion Laboratory whose contribution is greatly appreciated. I'd like to especially thank Leon Alkalai and John Elliott of JPL and the rest of the Lunette Team for their contributions over the course of this project and for the opportunity to work with them during the summer of 2009. Thanks as well to Rob Moeller, Chet Borden, Jim Chase, Tom Spilker and the JPL RMA team for the opportunity to work with them and for their inspiration. I'd like to thank my fellow interns, Alessondra Springmann and Douglas Van Bossuyt, for a great summer at JPL.

Thanks as well to my labmate and partner on this project, Alessandra Babuscia, who as been a pleasure to work with at MIT and JPL. Many others in the Space Systems Lab have been great friends and colleagues over the past two years: Brent Tweddle, Matthew Smith, Chris Pong, Joe Robinson, and John Richmond.

Finally, thanks to all of my friends at MIT over the past six years who have greatly enriched this experience, and especially to James Houghton and Zach LaBry for their great friendship and wind tunnel project ideas.

Contents

1	Introduction	19
2	Background	23
2.1	Concept Maturity Level	23
2.2	Science Traceability	25
2.3	Campaign Science Traceability	27
2.4	Trade Space Exploration & Model-Based Engineering	30
2.5	Program Systems Engineering	32
3	Optimization	35
3.1	Multi-Objective Optimization	36
3.1.1	Design Vector	36
3.1.2	Objective Function	37
3.1.3	Constraints & Bounds	38
3.2	Pareto Optimality	38
3.2.1	Pareto Filter	40
3.3	Trade Space Exploration	41
3.3.1	Size of the Trade Space	42
3.3.2	Full Factorial Analysis	42
3.3.3	Monte Carlo Analysis	43
3.3.4	Simulated Annealing	43
4	Science Value Model	47

4.1	Overview	47
4.1.1	Mission Value Flow	47
4.1.2	Multi-Attribute Utility Theory (MAUT)	49
4.2	Stakeholders and Science Goals	50
4.2.1	Lunar Science Documents	52
4.2.2	Lunar Science Objectives	53
4.3	Candidate Instruments	54
4.4	Science Objectives Weights	56
4.5	Science Value Matrix	56
4.6	Calculating the Utilities	59
4.6.1	Conditions for Using MAUT	59
4.6.2	MAUT Mathematical Framework	61
4.7	Science Concept Utility Model	63
5	Engineering Model	65
5.1	Overview	65
5.2	Design Vector	67
5.3	Instruments Subsystem	67
5.3.1	Overview	67
5.3.2	Instruments Database	68
5.4	Avionics & Data Subsystem	68
5.4.1	Overview	68
5.4.2	Data Capacity	68
5.4.3	Avionics Sizing	69
5.5	Communications Subsystem	70
5.5.1	Overview	70
5.5.2	Link Budget Analysis	71
5.5.3	Communications Subsystem Sizing	71
5.6	Power Subsystem	72
5.6.1	Overview	72

5.6.2	Power Loads	73
5.6.3	Power Subsystem Sizing: Solar Variant	75
5.6.4	Power Subsystem Sizing: Nuclear Variant	77
5.6.5	Transient Power Analysis	79
5.7	Orbits Subsystem	80
5.7.1	Overview	80
5.7.2	Low Energy Transfer Orbits	81
5.7.3	Hohmann Transfer Trajectory Analysis	82
5.7.4	Landing Trajectories	85
5.8	Thermal Subsystem	86
5.8.1	Overview	86
5.8.2	Thermal Environment Model	87
5.8.3	Energy Balance Model	88
5.8.4	Thermal Subsystem Sizing	90
5.8.5	Validation	92
5.9	Structures Subsystem	93
5.10	ACS/GNC Subsystem	94
5.11	Propulsion Subsystem	94
5.11.1	Overview	94
5.11.2	Propulsion Subsystem Design	95
5.11.3	Propulsion Validation	103
5.12	Mass Module	104
5.13	Carrier Module	105
5.14	Launch Module	105
5.15	Conclusion	108
6	<i>In Situ</i> Lunar Mission Case Study	109
6.1	Overview	109
6.2	Engineering Model Validation	109
6.2.1	Validation Reference Missions	110

6.2.2	Validation Results	115
6.3	Monte Carlo Analysis	120
6.3.1	Sampling the Design Space	120
6.3.2	Running the Model	121
6.3.3	Concept Utility Analysis	123
6.3.4	Pareto Front Interactions	124
6.4	Optimization Analysis	126
6.5	Conclusion	128
7	Uncertainty Analysis	129
7.1	Model Errors	129
7.2	Trade Space Exploration Under Uncertainty	130
7.2.1	ϵ -Pareto Set	131
7.3	Example ϵ -Pareto Set Exploration	132
8	Conclusion	135
8.1	Summary	135
8.2	Future Work	136
A	Lunar Science Value Matrix	139
B	Engineering Model Variabes	143
	Bibliography	147

List of Figures

1.1	Recent and future lunar missions	20
1.2	Diagram of the lunar interior [5]	20
2.1	Description of Concept Maturity Levels [11]	24
2.2	Concept Maturity Levels vs. NASA Project Phase	25
2.3	Flow of elements in a Science Traceability Matrix (STM)[12]	26
2.4	An example Science Traceability Matrix from Weiss, <i>et al.</i> for a generic planetary orbiter[12]	27
2.5	A Campaign Science Traceability Matrix as Applied to the 2007 Earth Science Decadal Survey[13]	28
2.6	Normalized Utility vs. Time for the 2007 Earth Science Decadal Survey Missions [13]	30
2.7	Improvements in Mission Conceptual Design [14]	31
2.8	Program Systems Engineering Process [15]	33
3.1	Example of weakly dominated, strongly dominated, and non-dominated solutions	39
4.1	Value flow in a mission from program goal identification to knowledge generation	48
5.1	N^2 Diagram of the Engineering Model	66
5.2	Diagram of a subsystem module with inputs and outputs and showing the feedback direction	66
5.3	Data Storage and Downlink vs. Time on a Representative Lunar Lander	69

5.4	Layout of the power subsystem	73
5.5	Example of power loads for instruments/subsystems 1, 2, . . . , n	74
5.6	Transient power analysis results	80
5.7	Schematic of a Weak-Stability Boundary transfer trajectory [50]	81
5.8	Schematic of a Hohmann transfer trajectory	82
5.9	Conceptual lunar landing trajectories [53]	86
5.10	Thermal Environment Data	87
5.11	Lander Heat Flow Paths	89
5.12	Thermal control mechanisms	90
5.13	Transient thermal model results	92
5.14	Lander structural mass fractions	93
5.15	Schematic of Surveyor’s Two-Stage Landing Method [59]	96
5.16	Schematic of the Apollo Lunar Module’s Landing Phase [60]	97
5.17	Comparison of Monopropellant and Bipropellant Propulsion Systems [62]	98
5.18	Liquid Propulsion System Weight Comparison [63]	99
5.19	Cutaway Diagram of a Spherical Tank	101
5.20	Launch mass vs. landed dry mass for sample lunar lander architectures	104
5.21	Launch vehicle performance vs. C^3 [64]	107
6.1	Proposed lunar lander missions	111
6.2	Missions for engineering model validation	112
6.3	Engineering model subsystem validation against JPL’s Lunette mission concept	116
6.4	Engineering model validation against NASA’s Surveyor missions, NASA’s ILN mission concept, and JPL’s Lunette mission concept	119
6.5	Monte Carlo Simulation results of science utility vs. dry mass for 2000 runs	122
6.6	Monte Carlo Simulation results of eight elements concept science utility vs. dry mass for 2000 runs	124

6.7	Concept 2 Utility vs. Dry Mass for eight concept Pareto sets	125
6.8	Pareto sets for Monte Carlo Analysis and Multi-Objective Simulated Annealing Analysis	127
7.1	Example of uncertainty in architectures	130
7.2	Plot illustrating the concept of ϵ -dominance [70]	131
7.3	ϵ -Pareto sets for $\epsilon_{i,j} \in 0, 0.2, 0.5$	132
7.4	ϵ -Pareto set with 20% mass uncertainty and 50% science utility uncer- tainty	133

List of Tables

2.1	Concept Maturity Levels	24
4.1	Documents Outlining Lunar Science Objectives	52
4.2	Candidate Lunar Instruments	55
4.3	SCEM Objectives Priority Rankings and Weights	57
4.4	Instrument Contributions to SCEM Objectives	58
5.1	Design Variables	67
5.2	Avionics Sizing	70
5.3	Link budget [45, 46]	72
5.4	Solar panel selection [45]	76
5.5	Battery selection [45]	77
5.6	Properties of past, present, and future RPSs [47]	78
5.7	Advanced Sterling Radioisotope Generator (ASRG) properties [48]	79
5.8	Summary of Earth-to-Moon Transfers from Pernicka, et al. [51]	82
5.9	Properties of the Earth and Moon	83
5.10	Solid Motor Selection [61]	97
5.11	Propellant Characteristics	99
5.12	Monopropellant Engine Selection	100
5.13	Bipropellant Engine Selection	100
5.14	Attitude Control Thruster Characteristics	103
5.15	Launch Vehicle Payload Mass [kg] vs. C^3 [km^2/s^2]	106
6.1	Validation Design Vector	115

6.2	Engineering model subsystem validation against JPL’s Lunette mission concept with differences highlighted	116
6.3	Engineering model validation against NASA’s Surveyor missions, NASA’s ILN mission concept, and JPL’s Lunette mission concept with differences highlighted	119
6.4	Design Variables	121
6.5	Instruments and objective functions for two designs in the SCEM concept 3 Pareto set	126
A.1	Lunar Science Value Matrix based on SCEM Goals	140
A.2	Lunar Science Value Matrix based on SCEM Goals (Continued)	141
B.1	Working Variables	143

Nomenclature

Acronymns

ACS	Attitude Control System
ASRG	Advanced Sterling Radioisotope Generator
BOL	Beginning of Life
CML	Concept Maturity Level
CSTM	Campaign Science Traceability Matrix
DoD	Depth of Discharge
EOL	End of Life
FY	Fiscal Year
GNC	Guidance, Navigation, and Control
GRAIL	Gravity Recovery and Interior Laboratory
ILN	International Lunar Network
JEO	Jupiter Europa Orbiter Mission
JPL	Jet Propulsion Laboratory
LCROSS	Lunar Crater Observation and Sensing Satellite
LEO	Low Earth Orbit
LMO	Low Moon Orbit
LPRP	Lunar Precursor Robotic Program
LRO	Lunar Reconnaissance Orbiter
MAUT	Multi-Attribute Utility Theory
MBED	Model Based Engineering Design

MEP	Mars Exploration Program
MEPAG	Mars Exploration Program Analysis Group
MLI	Multi-layer Insulation
MOSA	Multi-Objective Simulated Annealing
MSDO	Multidisciplinary Systems Design Optimization
NASA	National Aeronautics and Space Administration
NRC	National Research Council
NSSDC	National Space Science Data Center
PSE	Program System Engineering
RHU	Radioisotope Heater Unit
RMA	Rapid Mission Architecture
RPS	Radioisotope Power Source
SA	Simulated Annealing
SCEM	The Scientific Context for the Exploration of the Moon
SMAD	Space Mission Analysis and Design
STM	Science Traceability Matrix
SVM	Science Value Matrix
T/W	Thrust-to-Weight Ratio
TLI	Trans-Lunar Insertion
TRL	Technology Readiness Level
TSSM	Titan Saturn System Mission
WSB	Weak-Stability Boundary

Chapter 1

Introduction

The last decade has seen a resurgence of interest in the Moon as a target for planetary exploration. NASA's Vision for Space Exploration laid out in 2004, sought to return humans to the Moon under the auspices of Project Constellation.[1] In the three decades between the conclusion of the Apollo Program in 1972 and the announcement of the Project Constellation in 2004, only two US missions were sent to the Moon: Clementine in 1994, and Lunar Prospector in 1998. In the six years since 2004, two more US lunar missions have been launched: the Lunar Reconnaissance Orbiter (LRO) and the Lunar Crater Observation and Sensing Satellite (LCROSS) in 2009. Japan and India have also launched their own lunar probes, and there is ongoing interest in the commercial sector to land a privately financed rover on the Moon in order to win the Google Lunar X-Prize.[2]

Despite the cancellation of Project Constellation in the NASA FY 2011 budget [3], interest in robotic exploration of the moon has not slowed. NASA will launch a lunar gravity mapping mission (GRAIL) in 2011. MoonRise, a lunar sample return mission, is a competitor for the New Frontiers 3 competition, and NASA continues to provide funding for the Lunar Precursor Robotic Program.[4]

The reason for this sustained interest in the Moon is that many questions about it remain open. As Earth's nearest neighbor, the Moon provides a geological archive in the absence of terrestrial weathering of what the conditions in the vicinity of Earth were like over the last several billion years. Understanding the history of the



Figure 1.1: Recent and future lunar missions

Moon will help scientist gain a better understanding of the history of the Earth and the early solar system. The Moon is also a laboratory for understanding the processes that govern planetary formation and differentiation. By understanding the properties of the lunar interior (Figure 1.2 and their evolution over time, we can better understand the processes that govern Earth’s interior and create more accurate models of exoplanets in other star systems.

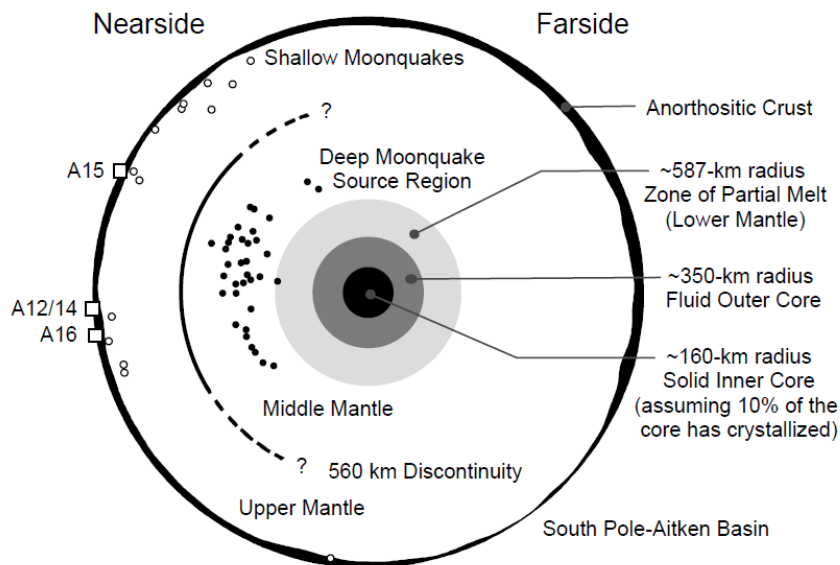


Figure 1.2: Diagram of the lunar interior [5]

Many of the lunar and planetary science goals for the coming decades involve measuring large-scale characteristics of the Moon and other bodies in our solar system. This includes studying the internal structures of the Moon and Mars, taking synoptic measurements of Martian atmosphere and weather, and measuring the lunar surface

environment. These goals are the focus of several upcoming missions, including the proposed International Lunar Network (ILN), and a possible Martian Network Science mission under the New Frontiers Program.[6, 7] JPL has also been conducting a study of a low-cost multi-lander lunar mission, “Lunette”. [8, 9, 10]

Each of these proposed missions would use a network of distributed landers, each with a payload of scientific instruments, to better study large-scale properties of the Moon and Mars. Given the many competing science goals for these missions, it is useful to have a tool to examine the trade-space of lander architectures to objectively understand how different sets of science payloads compare in their ability to satisfy the specified science and exploration goals.

The overall goal of this thesis is to build a tool to conduct trade studies for different robotic lunar lander architectures. This tool consists of three modules: a scientific utility model for determining the value of instruments towards different science and exploration objectives; an engineering model to size a lander’s subsystems; and a system model to map the trade space of architecture options.

The division of this thesis maps to the framework of this model.

- Chapter 2 covers the systems engineering background for this project: namely previous developments in building science utility models, trade space exploration, and model-based engineering.
- Chapter 3 covers multi-objective optimization and lays out the mathematical framework for the trade space exploration methods used later on.
- Chapter 4 walks through the steps of developing a spacecraft science utility model, building on decision theory and utility theory from economics.
- Chapter 5 details the engineering model used for sizing a lunar lander design.
- Chapter 6 provides a validation of the engineering model and details the results of a study on *in situ* lunar lander designs.
- Chapter 7 discusses the exploration of the trade space of lunar lander designs in the presence of uncertainty.
- Chapter 8 summarizes the results of this thesis and provides recommendations for areas of future work.

Chapter 2

Background

This chapter outlines some of the relevant research for developing a science value model and using model based engineering techniques. Section 2.1 covers the “Concept Maturity Level”, a tool of expressing the level of specificity of a design. Sections 2.2 and 2.3 discuss the development of a science traceability model. Section 2.4 discusses the concept of Model Based Engineering and how it fits into the context of trade space exploration. Finally, Section 2.5 discusses Program Systems Engineering and demonstrates how models, such as the framework developed in this thesis can fit into developing concepts and plans for the architecture of exploration programs.

2.1 Concept Maturity Level

As missions progress through the project lifecycle, they typically transition from a high-level conceptual idea spanning a large trade space of potential architectures to more complete designs with higher level of specificity, spanning a much narrower trade space.

One metric to describe the level of detail of a mission concept is the Concept Maturity Level (CML) developed by Mark Adler of JPL.[11] The CML metric is inspired by the Technology Readiness Level (TRL) widely used in the aerospace industry. An outline of the various CMLs is shown in Figure 2.1.

A description of the Concept Maturity Levels is given in Table 2.1. This metric

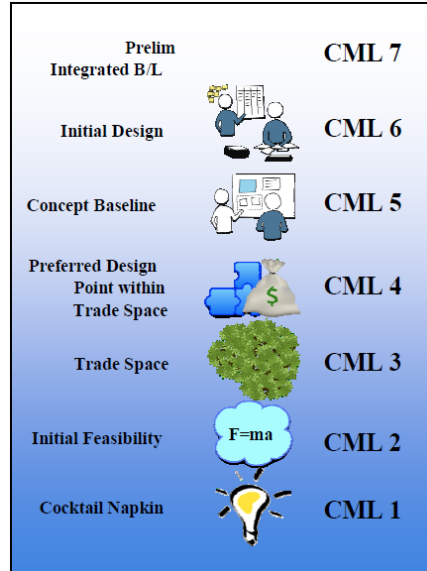


Figure 2.1: Description of Concept Maturity Levels [11]

addresses both the conceptual maturity of the science planning of a mission and as well as its engineering design. As the science goals of a mission inform its architecture, increasing levels of detail in both engineering and science formulation are highly coupled.

Table 2.1: Concept Maturity Levels

Level	Science	Engineering
1	Science Goals	High-level Description
2	Top-level Science Objectives	High-level Comparison to Similar System
3	Prioritized Objectives; Investigations	Alternate Architectures
4	Baseline & Threshold Mission Attributes; Science Traeability Matrix	System & Subsystem Block Diagrams; Configuration & CAD Drawings
5	Concept Baseline Science Requirements	Document Design
6/7	Initial Design; Level 2 & 3 Science Requirements	Preliminary Systems & Subsystem Design

The a mission’s Concept Maturity Level increases through the project lifecycle. The target CMLs for a mission are shown relative to the standard NASA mission lifecycle in Figure 2.2. At the end of the mission concept formulation (Pre-Phase

A), a mission should be at CML 5, meaning that a baseline point design should be developed with baseline science requirements and an initial documented engineering design.

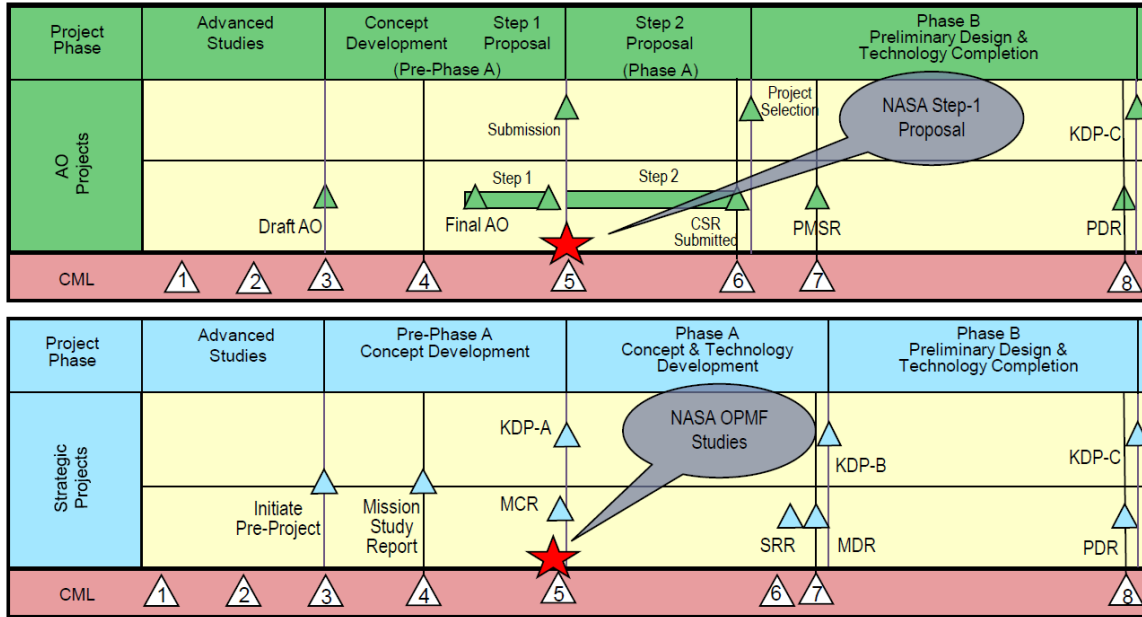


Figure 2.2: Concept Maturity Levels vs. NASA Project Phase

The goal of this project is to develop planetary exploration mission concepts to CML 3, both detailing the level to which science objectives are evaluated and identifying feasible engineering architectures for a broad set of designs.

2.2 Science Traceability

A relatively new tool being used in all NASA science mission proposals is the Science Traceability Matrix (STM). The STM is discussed in detail in a 2005 paper by J. R. Weiss, *et al.* of the Jet Propulsion Laboratory.[12]

The purpose of the STM is to relate the specific measurements and data collection of a science mission to the overarching programmatic objectives (Decadal Surveys, NASA Roadmaps, National Research Council Reports, etc.) which the mission seeks to fulfill.

The STM describes the links between the high level programmatic objectives to

specific spacecraft requirements through several layers of increasing detail: program objectives, mission objectives, measurement objectives, instrument requirements, to spacecraft and system requirements. The structure of a Science Traceability Matrix is shown in Figure 2.3.

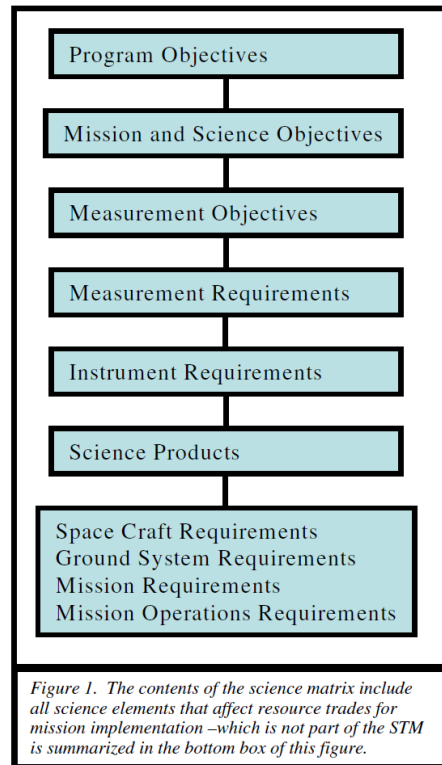


Figure 2.3: Flow of elements in a Science Traceability Matrix (STM)[12]

The STM is useful a useful too from a systems engineering perspective; it can inform how trade studies should be conducted, and it gives guidance as to the consequences of de-scoping a mission’s capability. As a tool for guiding trade studies, the STM provides indicates the flow of scientific value from the instrument level to the programmatic level. Additionally it indicates the flow of engineering requirements from the instrument level to the spacecraft subsystem level. By remapping these value and requirements flows, the effects different instrument approaches can be seen on the overall science value of a mission and the engineering requirements and design of a mission. An example STM taken from Weiss, *et al.* is shown in Figure 2.4

At the core of the methodology developed in this thesis is a science utility model

NASA Solar System Exploration Roadmap Mission Objectives	Objective #1: Learn How the Sun's Family of planets and minor bodies originated
	Objective #2: Determine how the solar system evolved to its current diverse state
	To determine the state, atmosphere and structure of "Planet" and the structures of it's satellites

Science Objectives	Measurement Objectives	Measurement Requirements	Instruments	Instrument Requirements	Data Products
Planet					
2. Internal structure	measure gravity field	Gravity moment to order 12	Radio	3 bands to recover propogation	gravity moment of order n (n~ 12)
	measure magnetic field	Magnetic moment to order 14	Vector Magnetometer	Resolution 0.1 nT, mounting orientation to 10 arcsec	magnetic moment of order n (n~14)
3. Magnetosphere structure, plasma dynamics and radiation belts	measure magnetic field, charged particle and plasma waves over a large range of latitudes, longitudes, and altitudes, and local time (need to rotate the line of apsides 180o)	Field direction to 1 degree, field resolution 0.1 nT, continuity 95%	magnetometer, plasma, low energy protons (LEP)		magnetosphere map, plasma spectrum, proton spectrum
Satellites					
1. Characterization interior, surface structure, activity and atmosphere.	multispectral IR imaging of surface	Map full surface at 3 meters/pixel	Mapping IR spectrometer	SNR 30, ifov 0.5 mrad, FOV 8.5 degrees	high resolution global coverage multispectral image data
	measure gravity field	circular orbit, global coverage for > 3 rotations, order 6	radio science		gravity field map
	measure magnetic field	circular orbit, global coverage for > 3 rotations	magnetometer	0.5 nT resolution	magnetic field map
	measure surface topography	100m track spacing	laser altimeter	30 meter spot size, 10 hz pulse, 1 nanosec gates	topography map

Figure 2.4: An example Science Traceability Matrix from Weiss, *et al.* for a generic planetary orbiter[12]

that maps the value of different instruments to science objectives, and an engineering model that levies requirements on spacecraft designs based on the instruments included in a payload. While this methodology is inspired by the STM paradigm, there are several fundamental differences.

An individual STM is developed for a specific mission and the trade studies envisioned using the STM are perturbations about that baseline mission design. This framework seeks to examine a wide trade space of instrument combinations. Rather than specifying programmatic objectives to be met by a mission and choosing instruments to meet those objectives, this framework optimizes the set of instruments based on an objective function derived from the value delivered by a set of instruments to a list of programmatic objectives.

2.3 Campaign Science Traceability

The Science Traceability Matrix proposed by Weiss, *et al.*[12], provides a good framework for analyzing the scientific value of a single mission, but is less well suited to analyzing scientific value across a portfolio of missions. Recent work by Theodore

Seher extended the STM framework to look at the utility of a campaign of related missions proposed in the 2007 Earth Science Decadal Survey (ESDS).[13] Seher developed the Campaign Science Traceability Matrix (CSTM), which outlines the specific relationships in a campaign that map the value delivered by a specific spacecraft's instruments to the high level science questions to be answered by a campaign.

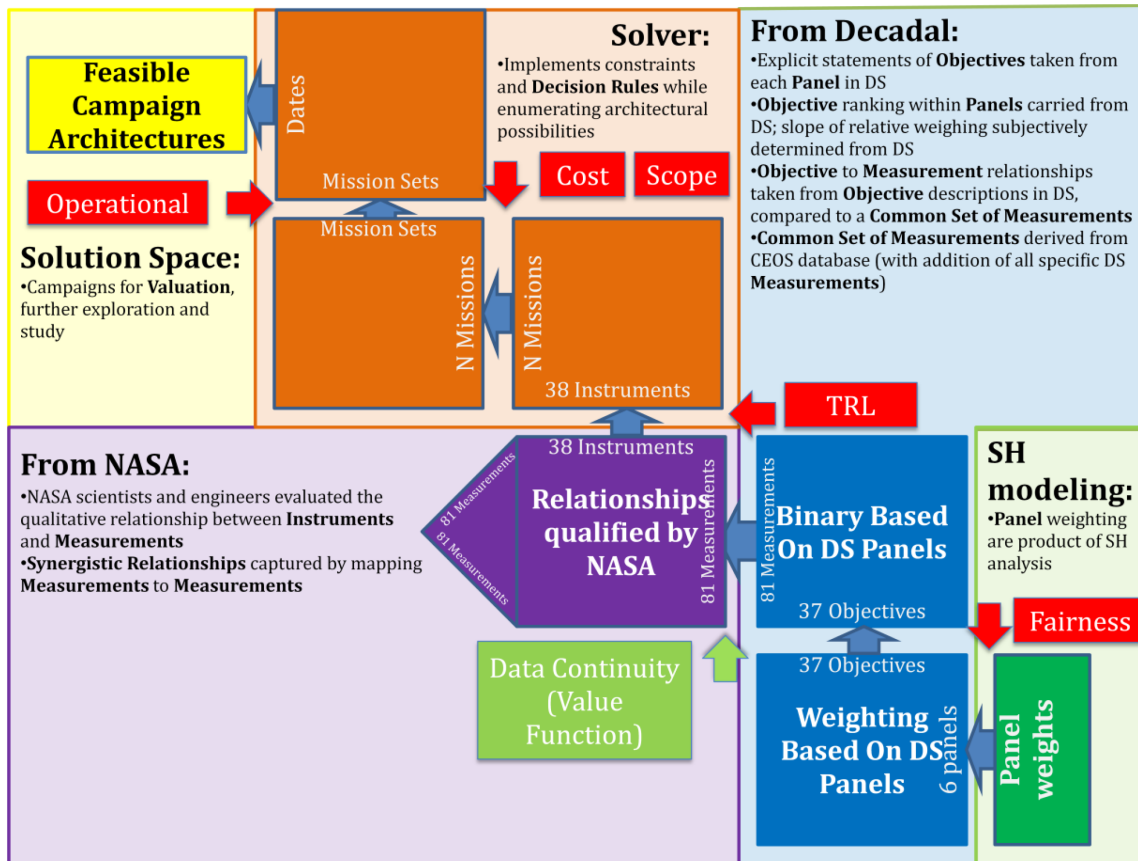


Figure 2.5: A Campaign Science Traceability Matrix as Applied to the 2007 Earth Science Decadal Survey[13]

In the CSTM framework (outlined in Figure 2.5), these relationships are broken down into multiple levels:

- The highest level is a societal level in which stakeholder analysis is done to model the societal impacts and benefits of different kinds of scientific knowledge.
- In the second level, the highest level science goals are broken down into finer resolution specific questions or objectives. This is typically done by a decadal survey panel, or some other group of subject experts.

- The third level maps concerns scientific knowledge and maps the value delivered by specific instruments to the low-level objectives outlined in the second level.
- The fourth level involves specific engineering knowledge. Here instruments are mapped to specific mission architectures and these mission architectures are evaluated for cost, mass or other relevant figures of merit.
- The fifth and final level is programmatic and involves the scheduling of missions to meet budgetary constraints, to ensure operational continuity, etc.

At each level in this framework, constraints are imposed, such as costing and operational continuity.

The primary difference between this CSTM framework and the framework developed in this thesis is that this framework focuses more on developing accurate mission design models in the fourth (Engineering) level. The CSTM focused primarily on the scheduling of decadal survey mission designs, whereas this model looks at the development mission designs as an integral step in the program design process.

A final development in the CSTM framework to mention is the ability of this model to examine the utility delivered by a portfolio of missions vs. time for each of the high level campaign objectives. In Figure 2.6, the cumulative benefit over time for each of the six Decadal Survey focus areas is shown for a baseline scenario.

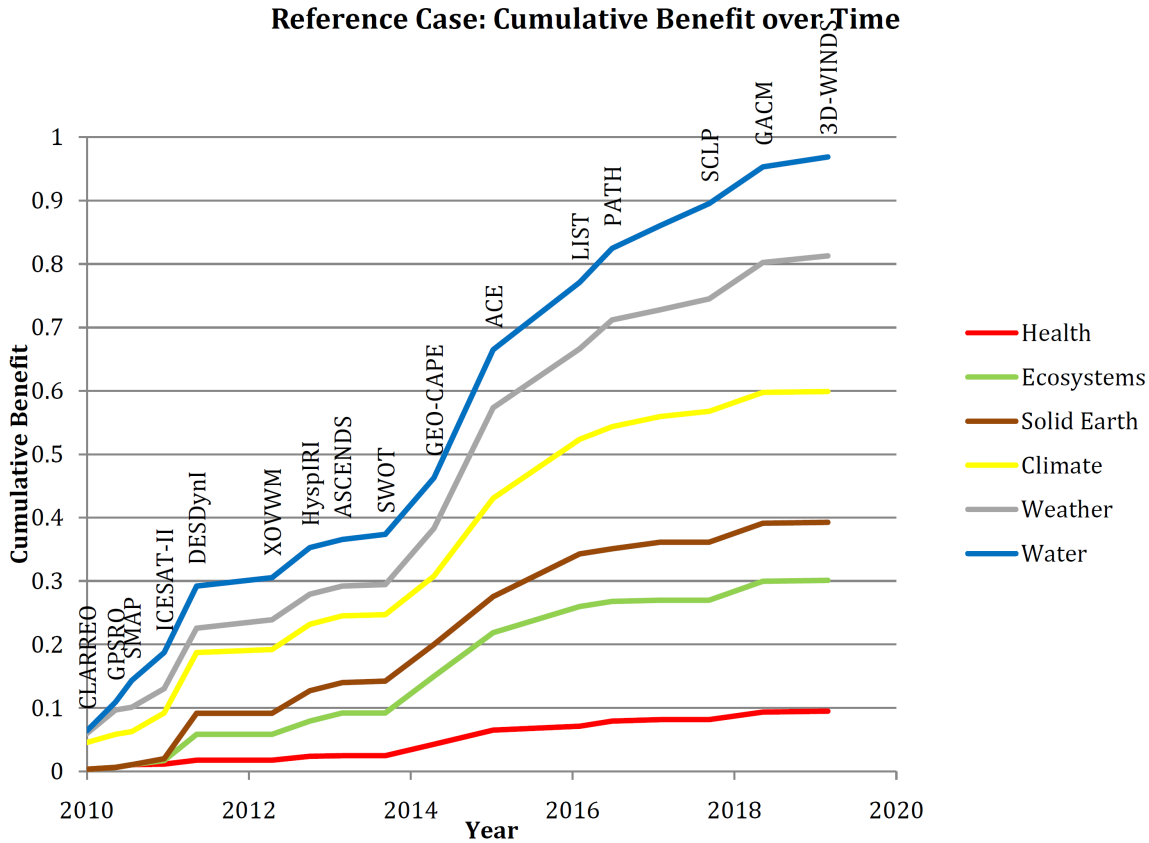
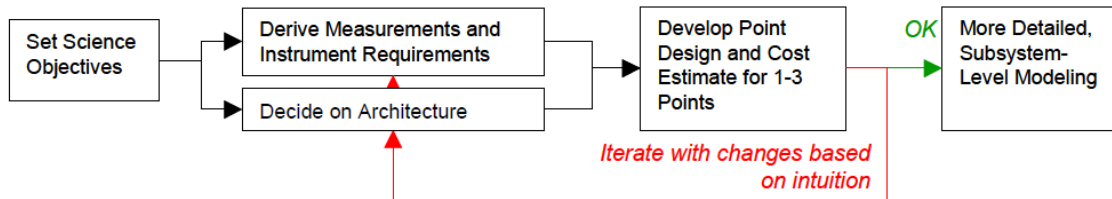


Figure 2.6: Normalized Utility vs. Time for the 2007 Earth Science Decadal Survey Missions [13]

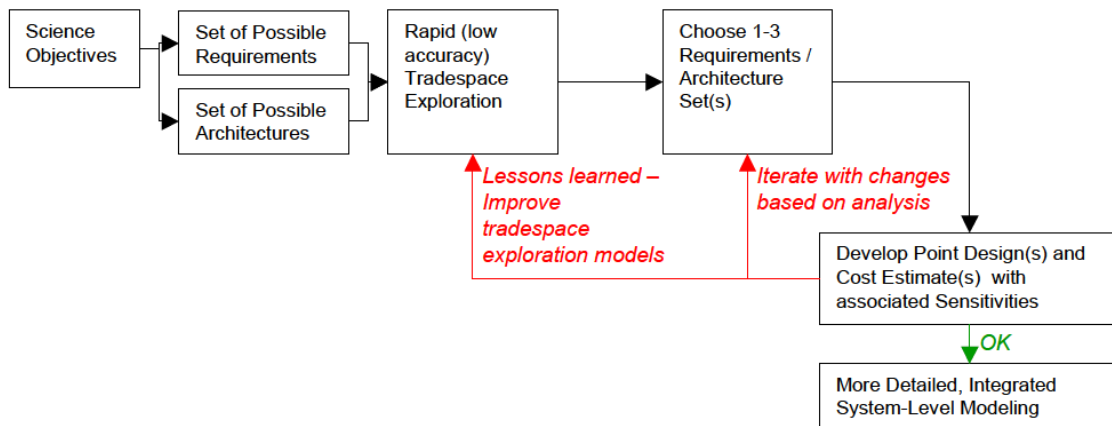
2.4 Trade Space Exploration & Model-Based Engineering

Today the design of many planetary science missions follows a linear path. This process typically consists of the following steps, outlined by Lamassoure, *et al.*[14]:

1. Top level science requirements are developed.
2. A Science Traceability Matrix (STM) is developed, mapping science goals to measurement requirements and ultimately spacecraft requirements.
3. Top level architectural trades are identified and the best choices among these trades are selected, taking into account the mission requirements and other budgetary, scheduling, and programmatic constraints.
4. Subsystem experts develop 1-3 feasible point designs.



a) Current Process, simplified for the purpose of this discussion. “Shooting in the dark” might lead to many design iterations. Developing an understanding of a large trade space is prohibitive.



b) Future Process, as envisioned in this paper. Rapid trade space exploration and sensitivities analysis serve as guide for decision making and improve the quality of the design after the first iteration.

Figure 2.7: Improvements in Mission Conceptual Design [14]

A diagram of this process is shown in Figure 2.7a. It is efficient at quickly developing a feasible design, however it has two primary shortcomings: If there are changes to the scientific objectives or programmatic constraints later in the design cycle, much additional work can be required. Also, due to the lack of a quantitative trade space exploration better suited designs may be missed in this process.

Efforts have been made recently to develop a Model Based Engineering Design (MBED) approach in which an additional step is added to this process after the development of science objectives and before the development of a point design. In this additional step (shown in Figure 2.7b) a trade space exploration is conducted prior to the selection of a point design. This trade space exploration can take many forms, but typically consists of varying many design variables, and modeling performance of these designs.

The framework developed in this thesis implements a MBED approach. A set of modular spacecraft subsystem modules are developed in an engineering model that

can determine the estimated cost and performance parameters of a spacecraft design based on the selection of an instrument suite. Due to the modular nature of these subsystem modules, varying levels of complexity can be implemented from simple parametric estimating relationships to full time domain, physics-based simulations of subsystem performance. Together these modules and the engineering model they comprise allow for the estimation of spacecraft performance in a systematic way, which enables conducting large trade space explorations.

2.5 Program Systems Engineering

In 1999 NASA undertook a restructuring of the Mars Exploration Program in the wake of the dual failures of the Mars Climate and the Mars Polar Lander. The goal of this restructuring was to create a new program guided by a unified set of science objectives, and consisting of a well-integrated portfolio of complimentary missions.[15] This undertaking required new scientific and engineering strategies for the Mars Exploration Program.

In 2001 NASA's Mars Exploration Program Analysis Group (MEPAG) released a document outlining a new program-level science strategy for Mars.[16] This document outlined four top-level goals of scientific investigation revolving around Life, Climate, Geology, and Human Exploration. These top level goals were further broken down into more detailed investigations and measurements. The cross-cutting theme of these four goals was to "Follow the water". All missions formulated as part of MEP subsequent to the development of this document trace their science investigations to these MEPAG objectives. This science framework is a living document which has been revised in 2004, 2005, 2006, 2008, and is undergoing a revision in 2010.

On the engineering side of the Mars Exploration Program formulation, a cross-cutting strategy was needed to ensure that future missions to Mars were complimentary and leveraged the scientific results of other missions. The "goal was to create a Program that was more than a loosely coupled collection of missions." [15] In pursuit of this goal, the NASA implemented a "Program System Engineering" (PSE)

approach. In developing a new MEP, the entire program trade space was opened up, with the output of this effort being a proposed mission queue, which seeks to maximize the realization of the Mars scientific goals within a constrained budgetary space, and the 26-month interval between available Mars launch windows. Other aspects of this program-level approach are technology development and program management. This PSE approach is shown in Figure 2.8.

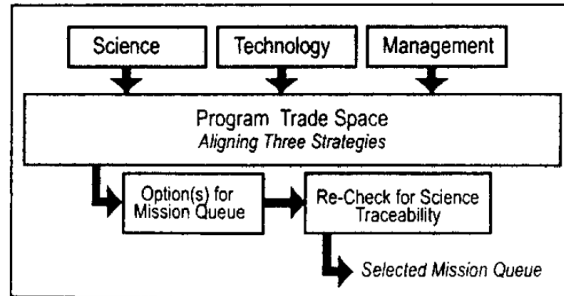


Figure 2.8: Program Systems Engineering Process [15]

In 2008 the National Research Council (NRC) conducted a review of NASA’s Solar System Exploration Program.[17] The NRC’s report stated:

NASA’s Mars Exploration Program (MEP), which was redesigned in 2000, has been highly successful to date and appears on track through the end of the current decade. . . . A key element of the success of this program is that it is not a series of isolated missions but rather a highly integrated set of strategically designed missions, each building on the discoveries and technology of the previous missions and fitting into long-term goals to expand the understanding of the planet: whether or not it ever had or does now have life, and how Mars fits into the origin and evolution of terrestrial planets.

The Program Systems Engineering approach can, therefore, be very successful if implemented properly. The two key elements required to successfully undertake such an integrated trade space exploration of a variety of mission architectures within a program are a methodology for assessing the scientific merit of these missions, and

a engineering tool to estimate the masses, costs, and other figures of merit for these missions. This thesis presents the development of a general tool which is applicable to this PSE approach and is here shown with a Lunar program case study.

Chapter 3

Optimization

Engineering is fundamentally about the art of compromise and spacecraft design is no exception to this rule. In any engineering discipline, the design effort is faced with many competing objectives. In design of planetary exploration spacecraft, examples of competing objectives include: maximizing the science return, minimizing the cost, and minimizing risk. These objective values are complex, non-linear functions of the design variables over which designers have control, and typically span multiple disciplines. Furthermore, the spacecraft design problem is not open ended; there also exist many constraints, such as program budgets, launch vehicle performance limits, schedules, and launch window availability, to name a few.

Within this complex and highly constrained trade space, engineers need a quantitative tool to help them understand the design variable trade offs and find optimal designs. Fortunately such a tool exists in the field of Multidisciplinary Systems Design Optimization (MSDO).[18] MSDO provides a rigorous and quantitative methodology for designing complex systems with mutually interacting parts.

This chapter lays out the mathematical framework for the elements of MSDO methodology used in this thesis. Section 3.1 describes the general multi-objective optimization problem, which is the underpinning of the MSDO framework; Section 3.2 describes the concept of Pareto optimality; and Section 3.3 describes several techniques for trade space exploration.

3.1 Multi-Objective Optimization

The general multi-objective optimization problem [19, 20] is the underpinning of the MSDO framework. It is stated as:

$$\begin{aligned}
 & \min_{\mathbf{x}} \mathbf{J}(\mathbf{x}, \mathbf{p}) \quad \text{where } \mathbf{x} = [x_1, x_2, \dots, x_n]^\top \\
 s.t. \quad & \mathbf{g}(\mathbf{x}) \leq 0 \quad \mathbf{p} = [p_1, p_2, \dots, p_m]^\top \\
 & \mathbf{h}(\mathbf{x}) = 0 \quad \mathbf{J} = [J_1(\mathbf{x}), J_2(\mathbf{x}), \dots, J_n(\mathbf{x})]^\top \\
 & \mathbf{x}_l \leq \mathbf{x} \leq \mathbf{x}_u \quad \mathbf{g} = [g_1(\mathbf{x}), g_2(\mathbf{x}), \dots, g_n(\mathbf{x})]^\top \\
 & \quad \quad \quad \quad \quad \quad \quad \quad \mathbf{h} = [h_1(\mathbf{x}), h_2(\mathbf{x}), \dots, h_n(\mathbf{x})]^\top
 \end{aligned} \tag{3.1}$$

In this formulation of the optimization problem, \mathbf{x} is a vector of design variables, \mathbf{p} is a vector of parameters, and $\mathbf{J}(\mathbf{x}, \mathbf{p})$ is a vector of objectives. The problem is subject to the inequality constraints, $\mathbf{g}(\mathbf{x})$, and the equality constraints, $\mathbf{h}(\mathbf{x})$. Furthermore, solutions can only exist within the specified bounds for \mathbf{x} . Here the goal is to simultaneously minimize objectives $J_1, J_2(\mathbf{x}), \dots, J_n$. Not that if the goal is to maximize a value, it can be reformulated as minimization by minimizing the negative of the objective (ie. $\max J_1 = \min -J_1$).

All of the components of our engineering design problem and present in this formulation, each of which are described in the following sections.

3.1.1 Design Vector

The design vector, \mathbf{x} , is the set of all variables which can be changed to specify the design. This list need not be exhaustive; in order to constrain the size of the design space, it can advantageous to set design variables with a small impact as parameters of the problem. For the lunar case study presented in this thesis, the design vector is given by equation 3.2:

$$\mathbf{x} = \begin{bmatrix} \text{Instrument 1} \dots \text{n} [binary] \\ \text{Lifetime} [yr] \\ \text{Landing Latitude} [^\circ] \\ \text{Power Source} [-] \\ \text{Battery Type} [-] \\ \text{Solar Panel Type} [-] \\ \text{Data Rate} [bits/s] \\ \text{Antenna Size} [m] \\ \text{Transfer Orbit} [-] \\ \text{Descent Method} [-] \\ \text{Propellant} [-] \end{bmatrix} \quad (3.2)$$

This design vector as well as the parameters, \mathbf{p} , are discussed in greater depth in Section 5.2. Together, these two vectors completely specify a design.

3.1.2 Objective Function

The objective function, $\mathbf{J}(\mathbf{x}, \mathbf{p})$, maps the design vector, \mathbf{x} , to some figures of merit which the designer cares about and will use to select a design. For a spacecraft design problem, this embodies most of the complexity and effort of the problem. For the lunar case study, the goals are to minimize the cost of the spacecraft and maximize the science return. Here landed dry mass is used as a surrogate for cost. The objective function is shown in equation 3.3:

$$\mathbf{J}(\mathbf{x}, \mathbf{p}) = \begin{bmatrix} M_{\text{Dry}} [kg] \\ -\text{Science Utility} [-] \end{bmatrix} \quad (3.3)$$

How the objective values are determined for a given design vector is the topic of Chapters 4 and 5. Two models which estimate the science utility and spacecraft mass have been implemented. These models span a number of disciplines, from planetary science to propulsion, thermal control, and power management (to name a few). Running these models together in an integrated way allows the designer to

understand how subsystem interactions may affect the overall figures of merit.

Intuitively one can see that the objectives for this problem are competing with one another: a heavier, more capable spacecraft with more instruments will have a greater science return than a lighter spacecraft with fewer instruments. By using the MSDO approach and using multi-objective optimization techniques, a designer can find out to what extent science utility must be traded against mass. To this end, the result of a multi-objective optimization study is rarely a single “best” solution, but rather a set of solutions which weight the various objectives differently. This concept, known as Pareto optimality, is expanded upon in Section 3.2

3.1.3 Constraints & Bounds

The constraints acting on a problem indirectly place limitations on which design vectors are feasible. The bounds of the problem directly place limitations on which design vectors are feasible. Typically constraint violations are determined during the same step in which the values for the objective functions are determined. For the lunar case study, there are a number of constraints determined internally (such as thermal limits, battery depth of discharge limits, etc.) which are automatically satisfied by the engineering module. The constraints which must be resolved by the designer are presented in equation 3.4:

$$\mathbf{g}(\mathbf{x}, \mathbf{p}) = \begin{bmatrix} \text{Duty Cycle}_{\text{Radio}} - 1 \\ M_{\text{Launch}} - M_{\text{LV Payload}} \end{bmatrix} \quad (3.4)$$

3.2 Pareto Optimality

In a multi-objective design problem there never any single “best” solution that outperforms all others (aside from trivial cases). When objectives are competing with one another the result of the optimization problem is a set of solutions, known as the Pareto set. The Pareto set (named for Vilfredo Pareto who published the concept in 1906) is the set of solutions for which no improvement in any objective can be made

without worsening some other objective.

If we consider a set of possible design vectors and their objective functions, J_1 and J_2 , we can place every pairing of designs into one of three categories: Design 1 weakly dominates design 2 if it is at least as good as design 2 in all objectives and is better than it in at least one area. Design 1 strongly dominates design 2 if it is better than design 2 in all objectives. If two designs do not meet either of these criteria, then they are said to be non-dominated with respect to one another. If we step through all of these potential pairings, the Pareto set consists of the designs which are non-dominated after all pairwise comparisons have been made. The mathematical descriptions of these statements are given in the following sections.

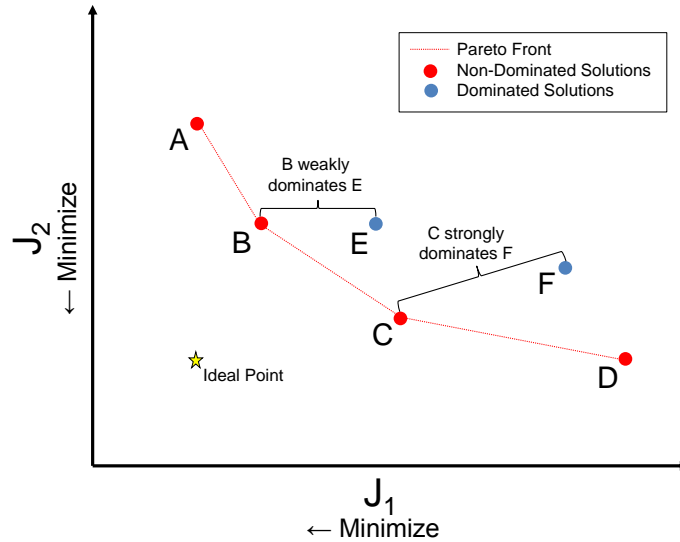


Figure 3.1: Example of weakly dominated, strongly dominated, and non-dominated solutions

This is shown graphically, in Figure 3.1. Here there are six designs, with objectives J_1 and J_2 plotted, with both objectives being minimized. Designs E and F are both dominated by other solutions in the design space. If we compare A and E, they are non dominated; however B weakly dominates E, as it is equal in J_2 , but performs better in J_1 . Because E is dominated by at least one other design it is considered to be dominated. We can also see that F is strongly dominated by design C. Designs A, B, C, & D comprise the Pareto set, as none of these designs is dominated by any

other design.

Weakly Dominated Solutions

For two objective vectors: $\mathbf{J}^1 = \mathbf{J}(\mathbf{x}^1)$ and $\mathbf{J}^2 = \mathbf{J}(\mathbf{x}^2)$ with i elements, \mathbf{J}^1 weakly dominates \mathbf{J}^2 iff:

$$\begin{aligned} \mathbf{J}_i^1 &\leq \mathbf{J}_i^2 \quad \forall i, i \in \{1, 2, \dots, n\} \\ \text{and } \mathbf{J}_j^1 &< \mathbf{J}_j^2 \quad \text{for at least one } j, j \in \{1, 2, \dots, n\} \end{aligned} \tag{3.5}$$

Strongly Dominated Solutions

A stronger case exists when all elements of \mathbf{J}^1 are more favorable than all corresponding elements of \mathbf{J}^2 . This is the strongly dominated case:

$$\mathbf{J}_i^1 < \mathbf{J}_i^2 \quad \forall i, i \in \{1, 2, \dots, n\} \tag{3.6}$$

The strongly dominated case is a subset of the weakly dominated case.

Non-Dominated Solutions

A third case exists in which neither \mathbf{J}^1 nor \mathbf{J}^2 dominate one another. This so-called “Non-dominated” case is the bases for Pareto optimality. Within the set of non-dominated solutions, no improvement to any element of the objective vector can be made without a penalty in a different element of the objective vector. A solution, \mathbf{J}^* is non-dominated if there exists no solution, \mathbf{J} , such that:

$$\begin{aligned} \mathbf{J}_i &\leq \mathbf{J}_i^* \quad \forall i, i \in \{1, 2, \dots, n\} \\ \text{and } \mathbf{J}_j &< \mathbf{J}_j^* \quad \text{for at least one } j, j \in \{1, 2, \dots, n\} \end{aligned} \tag{3.7}$$

3.2.1 Pareto Filter

In order to find the Pareto-optimal set of solutions within a larger set of solutions, a Pareto filter is needed. A general Pareto filter algorithm from Mattson, *et al.* is shown in Algorithm 1.[21] In this algorithm, a pairwise comparison is made between pairs of

points within the design space. As it is determined that a given solution is dominated by another, it is eliminated from the set of points between which comparisons are made. The remaining set of designs which are not dominated by any other designs comprise the Pareto set of non-dominated solutions.

Algorithm 1 Pareto Filter [21]

```

1:  $i \leftarrow 0, j \leftarrow 0$ 
2:  $r = [1, 1, \dots, 1]_{np \times 1}^T$ 
3:  $n_p =$  number of candidate designs
4: while  $i < n_p$  do
5:    $i \leftarrow i + 1, j \leftarrow 1$ 
6:   while  $j \leq n_p$  do
7:     if  $i \neq j$  and  $r_j = 1$  then
8:       if  $U^j$  dominated by  $U^i$  then
9:          $r_j \leftarrow 0$                                      % Remove  $U^j$ 
10:        if  $j = n_p$  then
11:          continue                                       % Drop out of inner while loop
12:        end if
13:      else if  $U^i$  dominated by  $U^j$  then
14:         $r_i \leftarrow 0$                                      % Remove  $U^i$ 
15:        continue                                       % Drop out of inner while loop
16:      else if  $j = n_p$  then
17:        continue                                       % Drop out of inner while loop
18:      end if
19:    else if  $j = n_p$  then
20:      continue                                       % Drop out of inner while loop
21:    end if
22:     $j \leftarrow j + 1$ 
23:  end while
24:  if  $j = n_p$  and  $r_i \neq 0$  then
25:     $r_i \leftarrow 2$                                      % Retain  $U^i$ 
26:  end if
27: end while

```

3.3 Trade Space Exploration

With the optimization problem formulated, and with a method in place to compute the objective functions and constraints for a given design vector, the next step is to select a method to find a Pareto optimal set of solutions. This section outlines how to

gauge the size of the trade space, and several methods used to find optimal solutions within it.

3.3.1 Size of the Trade Space

The trade space, also referred to as the design space, is the set of all possible designs. The size of the design space is an important factor in selecting the type of trade space exploration to use. If the trade space is small, it may be possible to complete a full factorial trade space search, in which every possible combination of the design variables is enumerated and evaluated. If the number of possible designs is very large, optimization methods which evaluate only a subset of the possible designs in an intelligent fashion will be needed.

The number of possible designs, Ω , for a design vector, $\mathbf{x} = [x_1, x_2, \dots, x_n]^T$, is given by:

$$\Omega = \prod_{i=1}^n L(x_i) \quad (3.8)$$

Here, $L(x_i)$, is a function describing how many “levels” element x_i of the design vector, \mathbf{x} , may take. For continuous design variables, this number is infinite. It is therefore useful to divide such continuous variables into discrete steps, for the purpose of such an estimation.

3.3.2 Full Factorial Analysis

In a full factorial analysis, every possible design vector is enumerated, and its objective functions are computed. This method is appealing, as one is guaranteed to find the true Pareto set of designs. Having a complete data set about the design space is also useful in calculating interaction effects between variables. The greatest downside to this method is that large amount of computational power and time required for all but the simplest of cases. Due to the large trade space in the lunar case study, this method was not used.

Alternative methods to a full factorial analysis only consider a portion of the design space.

3.3.3 Monte Carlo Analysis

One of the simplest methods for exploring the trade space is to use a probabilistic search, or a Monte Carlo method. In a Monte Carlo analysis, every variable in the design vector is selected according to a probability distribution function from all possible values it can take. For an even sampling of the design space, a uniform distribution of the levels of the design variables is used. The objective functions for this random sampling of the design space are computed and the process is repeated for a specified number of iterations.

The Monte Carlo method has the advantage that it is simple to implement and scalable to any number of iterations. It also gives a good approximation of the feasible and infeasible regions of the design space. The primary disadvantage of this method is that it offers no guarantee of finding the optimal Pareto set. In general, the distance of the true Pareto set from the Pareto set estimated with the Monte Carlo method is a function of the distribution of objective values in the vicinity of the estimated Pareto front.

3.3.4 Simulated Annealing

Another class of methods for trade space exploration are heuristic algorithms. These are non-gradient based methods which generally work by iteratively generating candidate solutions and evaluating them on some measure(s) of optimality. Methods in this class include Genetic Algorithms, Particle Swarm Optimization, and Simulated Annealing (which is implemented here). Ehrgott and Gandibleux [22] provide a good overview of these methods.

Simulated Annealing (SA), first proposed by Kirkpatrick, *et al.* in 1983,[23] is an optimization method that borrows from the principles of statistical mechanics to find an optimal solution to a design problem. In physical process of annealing, a metal is

heated up, then allowed to cool slowly, allowing it to recrystallize with larger grain sizes and fewer defects. Atoms may initially move through many energy states when they are at a high temperature, allowing them to find the most favorable minimum energy state.

The SA process is an iterative process conducted over a fixed number of steps. The loop is initialized with a random design variable. The elements of the iteration are: determine the “Temperature” according to a cooling schedule; select a new design which is a neighbor of the current design; determine whether the new design is an optimal design; and determine whether or not to accept the new design as the new current design based on the current “Temperature” and the relative optimality of the new design. This process is outlined in Algorithm 2.

Algorithm 2 Simulated Annealing

```

1:  $i \leftarrow 1$                                      % Initialize index
2:  $x \leftarrow x_0, j \leftarrow U(x)$              % Initialize design vector and fitness values
3:  $x_{best} \leftarrow x, u_{best} \leftarrow u$       % Set best solution to current architecture
4: while  $i < N$  do
5:    $x_{new} \leftarrow neighbor(x)$                  % Pick a nearby architecture
6:    $u_{new} \leftarrow U(x_{new})$                  % Compute fitness of the new architecture
7:   if  $u_{new} > u_{best}$  then                     % Is the fitness of this architecture the best?
8:      $x_{best} \leftarrow x_{new}, u_{best} \leftarrow u_{new}$  % Set the current architecture as best
9:      $x \leftarrow x_{new}, u \leftarrow u_{new}$ 
10:  else if  $P(u, u_{new}, temp(i/N)) > random()$  then % Move to new
    architecture?
11:     $x \leftarrow x_{new}, u \leftarrow u_{new}$ 
12:  end if
13:   $i \leftarrow i + 1$ 
14: end while
15: return  $x_{best}, u_{best}$ 

```

Multi-Objective Simulated Annealing (MOSA) algorithms have been developed by Nam and Park in 2000.[24] The primary distinction of the MOSA algorithm is that it assesses the optimality of a new design based on whether it dominates the old design. The transition probability is given by equation 3.9.

$$P = \exp \left(-\frac{1}{T_i} \frac{\sum_i^N (J_{new,i} - J_i) \frac{1}{\Delta J_i}}{N} \right) \quad (3.9)$$

Here N is the number of objectives, i is the iteration number, ΔJ_i is a scaling factor, and T_i is the “temperature” of the current iteration. In this formulation, the cooling schedule is hyperbolic:

$$T_i = \frac{T_0}{i} \quad (3.10)$$

The neighboring function simply randomly selects another value within a distance Δx_i for each variable x_i in the design vector.

This method is applied in Section 6.4.

Chapter 4

Science Value Model

4.1 Overview

One of the fundamental goals of this thesis is to develop a quantitative methodology to evaluate the science value of planetary exploration missions, so that science can be traded against engineering and programmatic figures of merit. In the context of this thesis, the science value of a mission is defined as how well a particular mission fulfills a set of pre-specified science objectives. Using such a figure of merit allows the relative scientific return of different mission concepts to be compared to one another.

4.1.1 Mission Value Flow

In order to be able to properly apply this concept, it is important to fully understand how value traces through a mission. Ultimately the value of a planetary exploration mission comes from scientific discoveries and the generation of new knowledge. Typically this knowledge is in response to questions or hypotheses posed by members of the scientific community. In between the posing of hypotheses and generating answers to these questions lie the processes of science goal identification, mission architecting, spacecraft operations, and data analysis. This overall value generation process is outlined in Figure 4.1; this process, for a given mission, can be partitioned into two sides: architecture and operations.

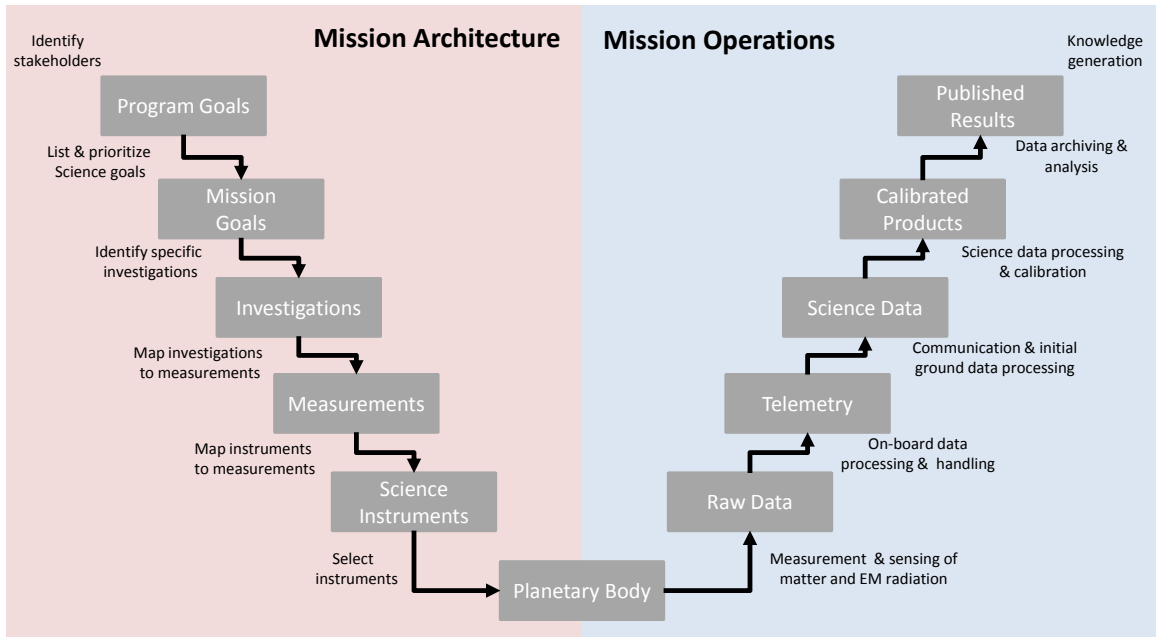


Figure 4.1: Value flow in a mission from program goal identification to knowledge generation

On the architecture side of the value flow, high level program goals are related to more specific mission investigations and ultimately to a science payload selection. This process typically consists of the following steps:

1. Stakeholder identification
2. Outlining high level science goals
3. Identifying specific science investigations and measurements
4. Identifying instrument and measurement/investigation interactions
5. Selecting an instrument suite

The operational side of the value flow is outlined in the right half of Figure 4.1. Spacecraft instruments interact with a planetary body through direct sensing of matter or EM radiation. Raw data are generated which undergo some on-board handling and processing. These science data, along with spacecraft engineering data are transmitted to the ground where they undergo further formatting and calibrating to be turned into archive able science products. These science products are analysis by investigators, ultimately leading to papers, discoveries and the creation of new knowledge (hopefully) in fulfillment of the original program goals.

4.1.2 Multi-Attribute Utility Theory (MAUT)

This chapter is concerned with the mission architecture stage of value generation. The following sections of this chapter describe a framework to estimate the science value of a mission, as applicable to some high level program goals. As a case study, examples of how to apply this framework to a lunar mission are presented.

The scientific value of a spacecraft is highly dependent on the instruments chosen for a mission. This framework seeks to develop a quantitative metric to objectively evaluate the value of a spacecraft instrument suite towards accomplishing a set of science objectives. In order to accomplish this, the concept of *utility* from economics is used. A utility function is a tool for describing preferences. Much of the original work on utility is described in great detail by von Nuemann and Morgenstern.[25]

Utility values are unitless numbers that confer the relative preference of one design to another. For a planetary exploration spacecraft, utility is dependent on generating scientific data and the ultimately ability to provide answers to questions posed by the planetary science community. Therefore, the utility of an instrument will be dependent on a number of attributes: how well it assesses a set of scientific objectives.

In this framework, we use Multi-Attribute Utility Theory (MAUT) to create a function that describes the total utility of an instrument. This is done by combining a set of single attribute utility functions in such a way as to capture how these single attributes are preferred to one another. MAUT has been used with success in the past by spacecraft designers to assess the preferences of different design trades.[26, 27, 28, 29]

A good methodology for implementing MAUT is described by Posavac and Carey.[30] The steps used in this process are as follows, with a description of how each step is applied in this framework:

1. *Identify the decision maker(s)/stakeholders:* Planetary Science Community, Spacecraft Designers
2. *Identify the issues to be addressed:* Science traceability of a spacecraft towards a set of scientific objectives

3. *Identify options to be evaluated:* Set of candidate scientific instruments
4. *Identify relevant attributes of the problem:* Contribution of an instrument towards assessing each science objective
5. *Rate attributes in order of importance:* Determine weights for each science objective
6. *Determine attribute probabilities for each option:* Populate a science value matrix with single-attribute utility values
7. *Calculate utilities:* Use MAUT formulas to combine single attribute utility values

In the following sections each of these steps is described in detail. While this method of evaluating the science traceability of different point designs is a useful approach, the tool being developed in this project will allow engineers to keep the trade space of scientific payloads open longer during the mission conceptualization phase, and quantitatively evaluate potential architecture choices in terms of their scientific impact.

4.2 Stakeholders and Science Goals

The first step in the process of determining the science value of a mission is to identify the relevant stakeholders, high-level science goals and specific science investigations to be undertaken by a mission. NASA has developed a very useful tool for this process in the Science Traceability Matrix (STM) [12] (discussed previously in Section 2.2). As outlined by Weiss, *et al.*, a well-developed STM should start with high-level science objectives taken from “Programmatic Road Maps” or stated in the Announcement of Opportunity (AO) for a mission. These high-level programmatic objectives should then be related to more specific science objectives and, in turn, measurement objectives. A candidate instrument set can then be rated against the set of measurement objectives outlined in a mission’s STM. In many cases these instrument-objective

interactions represent a many-many relationship, with each objective needing several instruments to assess it fully, and with each instrument contributing to multiple objectives.

How the specific science objectives for a mission are developed depends on the desired depth of a mission architecture study. This can range from survey past documents outlining detailed science objectives (ie. Decadal Survey reports, Nation Research Council studies, etc.), to assembling a science team to generate a more detailed set of science objectives than may already exist in the literature. For an mission architecture study the level of science detail will be proportional to the level of resources available for such a study. It is not necessary to over-specify the science objectives for a mission trade study if a low-fidelity engineering model is being used; likewise for a very detailed mission engineering analysis a detailed set of science objectives should be developed. A good metric to specify the level of detail of a mission study is the Concept Maturity Level (CML), discussed in further detail in Section 2.1. The lunar case study presented in this thesis is developed to CML 3.

For a low CML architecture study it may be suitable to identify a small number of science objectives based on expert opinion. For instance, a recent JPL Rapid Mission Architecture (RMA) study on potential Neptune System missions identifies only 10 science objectives of interest.[31] This allows a quick turnaround for science utility analysis. More detailed mission plans, such as the recent Outer Planet Flagship Mission proposals: the Titan Saturn System Mission [32] and the Jupiter Europa Orbiter Mission [33], had dedicated science definition teams that developed detailed STMs in support of these studies. For each mission study dozens of science investigations are identified, along with over 100 specific measurements. These mission studies required many man-years of effort and are completed to CML 6 or higher, which is infeasible and beyond the scope of a rapid mission architecture trade study.

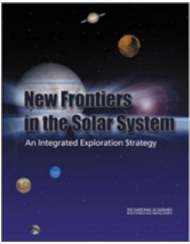


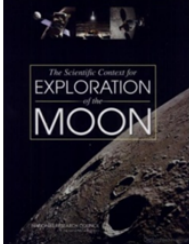

For the Lunar case study presented in this thesis, a number of documents generated by the planetary science community which outline the proposed science objectives for future lunar missions were reviewed. Programmatic science goals and science objectives were gleaned from these documents. This case study does not extend to

the depth of identifying specific measurements; only instrument-investigation interactions are identified. These documents outlining Lunar science objectives are discussed further in Sections 4.2.1 and 4.2.2.

4.2.1 Lunar Science Documents

A broad range of documents exist outlining the science objectives for Lunar exploration. These documents have been produced by a number of stakeholder groups from the science and exploration communities. Five of these documents (published since 2003) are outlined in Table 4.1.

Table 4.1: Documents Outlining Lunar Science Objectives

					
Title	New Frontiers in the Solar System [34]	Lunar Robotic Architecture Study [35]	LEAG Geological Science Report [36]	The Scientific Context for the Exploration of the Moon [37]	Lunar Science Workshop [38]
Author	National Research Council	NASA Headquarters Office of Program Analysis and Evaluation	Lunar Exploration Analysis Group	National Research Council	NASA Advisory Council Science Committee
Year	2003	2006	2006	2007	2007

The earliest document is the 2003 Planetary Science Decadal Survey, “New Frontiers in the Solar System,” published by the Space Studies Boards of the National Research Council.[34] These decadal survey reports are issued every ten years and represent the best consensus of the planetary science community about the priorities for exploration of the solar system. This particular report is divided into sections on Primitive Bodies, the Inner Solar System, Mars, Giant Planets, and Large Satellites. Each section presents a prioritized list of science goals and investigations (including

31 science investigations for the inner solar system – including the Moon).

NASA’s 2006 Lunar Robotic Architecture Study, the Lunar Exploration Analysis Group’s 2007 report, and the NASA Advisory Council’s 2007 Lunar Science Workshop focus on exploration specific and human precursor objectives.

The broadest in scope of these documents is The Scientific Context for the Exploration of the Moon (SCEM) [37] released by the National Research Council in 2007. This document (SCEM) does not explicitly address other goals, such as exploration precursor requirements and environmental characterization that are nonetheless of interest to the lunar community. For the purposes of this study, the objectives outlined in SCEM are used exclusively to evaluate mission scientific utility.

4.2.2 Lunar Science Objectives

The Scientific Context for the Exploration of the Moon[37] outlines eight broad lunar science concepts to be investigated during future lunar missions, both human and robotic. These science concepts (which are further broken down into 35 sub-objectives) are:

1. The bombardment history of the inner solar system is uniquely revealed on the Moon.
2. The structure and composition of the lunar interior provide fundamental information on the evolution of a differentiated planetary body.
3. Key planetary processes are manifested in the diversity of lunar crustal rocks.
4. The lunar poles are special environments that may bear witness to the volatile flux over the latter part of solar system history.
5. Lunar volcanism provides a window into the thermal and compositional evolution of the Moon.
6. The Moon is an accessible laboratory for studying the impact process on planetary scales.
7. The Moon is a natural laboratory for regolith processes and weathering on anhydrous airless bodies.
8. Processes involved with the atmosphere and dust environment of the Moon are

accessible for scientific study while the environment remains in a pristine state.

The full set of scientific objectives presented in SCEM are listed in full in Appendix A. At this point, these 35 science objectives could be expanded to encompass specific measurement requirements, depending on the desired fidelity of the science value model. In this study, due to resource limitations, these 35 objectives are the finest resolution science objectives considered.

4.3 Candidate Instruments

The next step in the science value framework is to develop a database of candidate instruments. From this list of candidate instruments, mission payload sets can be generated. Using this science framework, the utility of a science payload can be determined. Using the engineering model described in Chapter 5, the mass and cost of a spacecraft necessary to support the payload can be determined.

The minimum set of information that needs to be captured for each instrument for this model is:

- *Instrument Name*
- *Measurement*
- *Mass [kg]*
- *Max Power [W]*
- *Average Power [W]*
- *Daytime Duty Cycle* –Percentage of time the instrument is on when the spacecraft is illuminated
- *Daytime Frequency* –How many times instrument is on during a given daytime period
- *Nighttime Duty Cycle* –Percentage of time the instrument is on when the spacecraft is not illuminated
- *Nighttime Frequency* –How many times instrument is on during a given nighttime period
- *Data Rate [bits/s]*

- *Technology Readiness Level (TRL)*

After a significant literature review of past missions and proposed instruments, a list of fourteen relevant instruments for lunar surface exploration was developed. This list is shown in Table 4.2, with the mass, power, data rate, and day and night duty cycles for each instrument.

This dataset was drawn from instruments flown on past in-situ landers (ie. Mars Phoenix), and instruments in development found in papers in the NASA Astrophysical Data System[39] and the Lunar and Planetary Research Institute’s abstract database[40]. Much information about previously flown instruments is available from the National Space Science Data Center (NSSDC)[41].

Table 4.2: Candidate Lunar Instruments

Instrument	Measurement	Mass [kg]	Power [W]	Daytime Duty Cycle	Nighttime Duty Cycle	Data Rate [b/s]
Argon Geochronology Experiment (AGE)	Geochronology	5.7	180	0.09%	0.00%	370
Camera	Lighting	0.54	6	0.38%	0.38%	71429
Microscopy, Electrochemistry, and Conductivity Analyzer (MECA)	Regolith/Dust Grain Shape & Size, Adhesion, Chemical Reactivity, Composition, Toxicity, Dielectric Response, Optical Response, Abrasiveness	8.5	30	0.56%	0.00%	10000000
Pyrolysis Mass Spectrometer (VAPoR)	Regolith Volatile Content	10	25	1.13%	0.00%	7500
LIDAR	Topography	7.72	30	3.39%	0.00%	16000
IR Imager (MINITES)	Thermal Environment	2.1	5.4	1.97%	1.97%	720
Alpha Particle X-Ray Spectrometer (APXS)	Mineralogy/Water Maps	0.64	1.5	5.64%	0.00%	7200000
Cone penetrometer	Regolith Cohesion & Mechanical Properties	7	10	0.99%	0.00%	700000
E-field boom	Electric Field, Regolith/Dust Electrostatic Charge	3	3	100.00%	10.00%	9600
Seismometer (SEIS)	Seismic Activity/Moonquakes	2.3	3	100.00%	100.00%	7600
Radiation Assessment Detector (RAD)	Radiation Environment	1.52	4.1	100.00%	0.00%	58000
Magnetometer	Magnetic Field	0.93	0.9	100.00%	10.00%	2900
Heat Flow Probe	Heat Flux	0.5	3	100.00%	25.00%	418
Retroreflector	Orbital Elements	1	0	100.00%	100.00%	0

4.4 Science Objectives Weights

After developing the list of candidate instruments, the next step is to apply weights to the science objectives indicating their priority. In many cases, this may be done in parallel with the development of the science objectives themselves. Weights should be applied such that higher numerical weights correspond to higher priorities.

For the lunar case study, the objectives presented in SCEM were given a priority ranking by the science panel that developed the objectives. Based on a discussion with one of the panel members¹, the highest priority objective was given a weight of three times that of the lowest priority objective. The weights for all other objectives were interpolated between these values. The twenty three lowest priority objectives were not distinguished between in their ranking and were all given a weight of 1.

The formula for this weighting scheme is:

$$w_i = \frac{W_{\max} - W_{\min}}{P_{\max} - P_{\min}} (1 - P_i) + W_{\max}, \quad (4.1)$$

where w_i = Weight of i-th science objective

P_i = Ordinal rank (priority) of i-th science objective

P_{\max} = Ordinal rank of lowest priority science objective

P_{\min} = Ordinal rank of highest priority science objective

W_{\max} = Weight of highest priority objective

W_{\min} = Weight of lowest priority objective

The priority values and weights for all 35 SCEM objectives are shown in Table 4.3.

4.5 Science Value Matrix

Once the relevant science objectives have been identified and a database of candidate instruments has been built, the next step in the science value framework is to develop a “Science Value Matrix” (SVM).

¹Dr. Bruce Banerdt, Personal Communication, Oct. 14, 2008

Table 4.3: SCEM Objectives Priority Rankings and Weights

Concept	#	Objective	Rank	Weight
Bombardment History	1 a	1a. Test the cataclysm hypothesis by determining the spacing in time of the creation of lunar basins.	1	3.00
	1 b	1b. Anchor the early Earth-Moon impact flux curve by determining the age of the oldest lunar basin (South Pole-Aitken Basin).	2	2.82
	1 c	1c. Establish a precise absolute chronology.	3	2.64
	1 d	1d. Assess the recent impact flux.	12	1.00
	1 e	1e. Study the role of secondary impact craters on crater counts.	12	1.00
Interior Structure & Composition	2 a	2a. Determine the thickness of the lunar crust (upper and lower) and characterize its lateral variability on regional and global scales.	6	2.09
	2 b	2b. Characterize the chemical/physical stratification in the mantle, particularly the nature of the putative 500-km discontinuity and the composition of the lower mantle.	7	1.91
	2 c	2c. Determine the size, composition, and state (solid/liquid) of the core of the Moon.	9	1.55
	2 d	2d. Characterize the thermal state of the interior and elucidate the workings of the planetary heat engine.		3.18
Crust	3 a	3a. Determine the extent and composition of the primary feldspathic crust, KREEP layer, and other products of planetary differentiation.	5	2.27
	3 b	3b. Inventory the variety, age, distribution, and origin of lunar rock types.	10	1.36
	3 c	3c. Determine the composition of the lower crust and bulk Moon.	12	1.00
	3 d	3d. Quantify the local and regional complexity of the current lunar crust.	12	1.00
	3 e	3e. Determine the vertical extent and structure of the megaregolith.	12	1.00
Poles	4 a	4a. Determine the compositional state (elemental, isotopic, mineralogic) and compositional distribution (lateral and depth) of the volatile component in lunar polar regions.	4	2.45
	4 b	4b. Determine the source(s) for lunar polar volatiles.	12	1.00
	4 c	4c. Understand the transport, retention, alteration, and loss processes that operate on volatile materials at permanently shaded lunar regions.	12	1.00
	4 d	4d. Understand the physical properties of the extremely cold (and possibly volatile rich) polar regolith.	12	1.00
	4 e	4e. Determine what the cold polar regolith reveals about the ancient solar environment.	12	1.00
Volcanism	5 a	5a. Determine the origin and variability of lunar basalts.	12	1.00
	5 b	5b. Determine the age of the youngest and oldest mare basalts.	12	1.00
	5 c	5c. Determine the compositional range and extent of lunar pyroclastic deposits.	12	1.00
	5 d	5d. Determine the flux of lunar volcanism and its evolution through space and time.	12	1.00
Impact Processes	6 a	6a. Characterize the existence and extent of melt sheet differentiation.	12	1.00
	6 b	6b. Determine the structure of multi-ring impact basins.	12	1.00
	6 c	6c. Quantify the effects of planetary characteristics (composition, density, impact velocities) on crater formation and morphology.	12	1.00
	6 d	6d. Measure the extent of lateral and vertical mixing of local and ejecta material.	12	1.00
Regolith Processes	7 a	7a. Search for and characterize ancient regolith.	12	1.00
	7 b	7b. Determine physical properties of the regolith at diverse locations of expected human activity.	12	1.00
	7 c	7c. Understand regolith modification processes (including space weathering), particularly deposition of volatile materials.	12	1.00
	7 d	7d. Separate and study rare materials in the lunar regolith.	12	1.00
Atmosphere	8 a	8a. Determine the global density, composition, and time variability of the fragile lunar atmosphere before it is perturbed by further human activity.	8	1.73
	8 b	8b. Determine the size, charge, and spatial distribution of electrostatically transported dust grains and assess their likely effects on lunar exploration and lunar-based astronomy.	11	1.18
	8 c	8c. Use the time-variable release rate of atmospheric species such as ⁴⁰ Ar and Radon to learn more about the inner workings of the lunar interior.	12	1.00
	8 d	8d. Learn how water vapor and other volatiles are released from the lunar surface and migrate to the poles where they are adsorbed in polar cold traps.	12	1.00

As stated in Section 4.1, the utility of a mission is directly tied to its science return—specifically the relevance of that science return to the objectives of the planetary science community. In order to quantitatively assess how well different instruments feed back to the science objectives, a matrix is developed that defines how well each instrument contributes to each of the defined science objectives.

This method of determining instrument to objective correlations has been used previously in the Mars Surface Exploration Rover Modeling Tool developed at MIT by Julien Lamamy.[28] Engineers at JPL have also used this method to evaluate the

Table 4.4: Instrument Contributions to SCEM Objectives

Concept	#	Objective	Rank	Weight	Utility	Instrument															
						Geochronology	Lighting	Regolith Properties	Regolith Volatile Content	Topography	Thermal Environment	Mineralogy/Water Maps	Regolith Cohesion/Mechanical Properties	Electric Field, Regolith/Dust Electrostatic Charge	Seismic Activity/Moonquakes	Radiation Environment	Magnetic Field	Heat Flux	Orbital Elements		
						Max Power [W]	180	6	30	25	30	5.4	1.5	10	3	3	4.1	0.9	3	0	
						Power [W]	10	3	30	25	30	5.4	1.5	10	3	3	4.1	0.9	3	0	
						Mass [kg]	5.7	0.54	8.5	10	7.72	2.1	0.64	7	3	2.3	1.52	0.93	0.5	1	
						Utility	0.281	0.041	0.032	0.066	0.010	0.010	0.356	0.010	0.112	0.100	0.020	0.100	0.132	0.039	
The bombardment history of the inner solar system is uniquely revealed on the Moon.	1a	1a. Test the cataclysm hypothesis by determining the spacing in time of the creation of lunar basins.	1	3.00	2.00	1	0.5	0	0	0	0	0	0.5	0	0	0	0	0	0	0	
	1b	1b. Anchor the early Earth-Moon impact flux curve by determining the age of the oldest lunar basin (South Pole-Aitken Basin).	2	2.82	1.50	1	0	0	0	0	0	0	0.5	0	0	0	0	0	0	0	
	1c	1c. Establish a precise absolute chronology.	3	2.64	1.50	1	0	0	0	0	0	0	0.5	0	0	0	0	0	0	0	
	1d	1d. Assess the recent impact flux.	12	1.00	0.00	0	0	0	0	0	0	0	0	0	0	0	0	0	0	0	0
	1e	1e. Study the role of secondary impact craters on crater counts.	12	1.00	0.50	0	0	0	0	0	0	0	0.5	0	0	0	0	0	0	0	0

science capabilities of a number of Venus Flagship Mission architectures.[29]

In this model for instrument utility, each instrument-objective contribution is given a weight from 0 to 1. For this lunar case study, three strengths of contribution are defined: no contribution, significant contribution, and strong contribution. These three strengths are given weights of 0, 0.5, and 1 respectively. In Table 4.4, these contribution weights are shown for the set of fourteen instruments identified in Section 4.3 for the first two SCEM concepts. The entire matrix of 35 SCEM objectives has been populated for all fourteen instruments. (The fully populated matrix can be found in Table A.1 located in Appendix A.)

This method of defining instrument-objective contributions captures the many-to-many aspect of planetary science missions. Any given instrument is likely to contribute to several scientific objectives and any given objective will likely require several instruments to gain a high level of understanding.

Ideally this science value matrix would be populated by interviewing multiple scientists and combining their answers to obtain a mean contribution level and standard

deviation for each instrument-objective pair. Due to resource limitations the SVM for the lunar case study was populated by the author.

4.6 Calculating the Utilities

The final step in the science value framework is to calculate the instrument utilities, using all the information gathered up to this point. To calculate the instrument utilities, Multi-Attribute Utility Theory (MAUT) is used.

4.6.1 Conditions for Using MAUT

Before proceeding further it is important to understand the limitations of MAUT. There are three conditions that must be satisfied in order to use MAUT to determine an instrument utility function.[42, 43] These conditions are:

1. *Preferential Independence*
2. *Utility Independence*
3. *Additive Independence*

All of these conditions are predicated on the fact that the multi-attribute utility function is composed of single attribute utility functions. Each attribute may take different levels, each level of which can be mapped to some single-attribute utility value. An example of an attribute in the lunar case study is SCEM objective 2c, “Determine the size, composition, and state (solid/liquid) of the core of the Moon.” For a particular instrument, the “levels” of this attribute would be “no contribution”, “significant contribution”, or “strong contribution”.

Preferential Independence

To test for preferential independence, we consider two attributes x and y with levels A and B . If these attributes exhibit preferential independence, then the following must hold:

$$(x_A, y_A) > (x_B, y_A) \text{ and } (x_A, y_B) > (x_B, y_B) \quad (4.2)$$

That is to say, if level A of attribute x is preferred to level B of attribute x , then it is preferred regardless of what level attribute y takes.

It is easy to make an argument that our problem satisfies this condition. All else being equal, it will always be more advantageous to have more information about one particular science objective.

Utility Independence

A stronger statement of preferential independence is utility independence. For attribute x to be utility independent of attribute y , then the utility of attribute x must remain constant if the levels of attribute y are varied. This can be tested with a lottery question. In utility lottery questions one option is compared to a lottery of receiving two different options with probability p and $1 - p$ respectively.

For utility independence to hold, one must be indifferent between:

$$(x_A, y_A) \text{ or the lottery } \begin{array}{l} \xrightarrow{p} (x_B, y_A) \\ \xrightarrow{1-p} (x_C, y_A) \end{array} \quad (4.3)$$

and:

$$(x_A, y_B) \text{ or the lottery } \begin{array}{l} \xrightarrow{p} (x_B, y_B) \\ \xrightarrow{1-p} (x_C, y_B) \end{array} \quad (4.4)$$

It is more difficult to ensure that the utility condition is satisfied for the planetary exploration spacecraft problem. In order for this condition to be satisfied, there must be no synergistic effect between attributes. That is to say, the preference of getting data about science objective x must be independent of whether objective y has been well studied or not.

An example of this might be a mineralogical study of a particular rock. If there is no context imagery of where a rock is physically located, then a mineralogical inves-

tigation of the rock may be of lesser value than if its physical location and geological context is known.

One solution to this problem is to group similar science objectives together so that there is as little overlap between objectives as possible. This results in a trade off between the resolution of the science study and the accuracy of the utility analysis. For a more detailed enumeration of science objectives, utility independence will be violated to a greater extent; either more a more complex nonlinear multi-attribute utility function will be needed or the accuracy of the model will suffer.

We assume that the SCEM objectives defined for the lunar case study are utility independent.

Additive Independence

The last condition that must be met to use the MAUT framework is additive independence. For additive independence to be satisfied, one must be indifferent between:

$$\begin{array}{ccc}
 \text{The lottery} & \begin{array}{l} \nearrow 0.5 (x_A, y_A) \\ \searrow 0.5 (x_A, y_A) \end{array} & \text{or the lottery} & \begin{array}{l} \nearrow 0.5 (x_A, y_B) \\ \searrow 0.5 (x_B, y_A) \end{array} \\
 & & & (4.5)
 \end{array}$$

Additive independence implies that there exist known attribute weights and that the attribute weights sum to 1:

$$1 = \sum_{i=1}^n k_i \tag{4.6}$$

We assume that additive independence holds for the lunar case study.

4.6.2 MAUT Mathematical Framework

To calculate the instrument utilities, we use the MAUT mathematical framework presented by Keeney and Raiffa.[44] The general equation for a multi-attribute utility

function $U(X)$ is the solution to the equation:

$$KU(X) + 1 = \prod_{i=1}^n [Kk_i u_i(x_i) + 1] \quad (4.7)$$

where $U =$ Multi-Attribute Utility Function

$X =$ Vector of Attribute Levels

$k_i =$ Weight of the i -th Science Objective

$u_i =$ Single-Attribute Utility Function for the i -th Science Objective

$x_i =$ Level of the i -th Attribute

K is the solution to the following equation:

$$K + 1 = \prod_{i=1}^n [Kk_i + 1] \quad (4.8)$$

$$\sum_{i=1}^n k_i < 1, \quad K > 0$$

$$\sum_{i=1}^n k_i > 1, \quad -1 < K < 0$$

$$\sum_{i=1}^n k_i = 1, \quad K = 0$$

If the additive independence condition is satisfied, then $K = 0$. For this additive independent case, the multi-attribute utility function reduces to:

$$U(X) = \sum_{i=1}^n k_i u_i(x_i) \quad (4.9)$$

In this context, the values of U_i are simply the values in column j of the science value matrix corresponding to the j -th instrument. Correspondingly, k_i is the value of the weight of the i -th science objective. Note that this is a normalized weight; to find this from the weight described in Section 4.4, use the following formula:

$$k_i = \frac{w_i}{\sum_{i=1}^n w_i} \quad (4.10)$$

To find the utility of an science instrument payload, we extend this linear multi-attribute utility function. In order to calculate the utility value U for an entire payload, the instrument-objective correlation matrix (also the Science Value Matrix–SVM) u is summed over all the objectives i , and all the included instruments j , and the objective weights k . Thus payload utility value is expressed as:

$$U_{Payload} = \sum_{j=1}^m \sum_{i=1}^n k_i u_{i,j} \quad (4.11)$$

where $U_{Payload}$ = Multi-Attribute Utility Function for a Payload

n = Number of Science Objectives

m = Number of Instruments in Payload

k_i = Weight of the i -th Science Objective

$u_{i,j}$ = i -th, j -th Entry in the SVM

It is important to note that the SVM is trimmed such that only entries in the payload to be analyzed are included in the multi-attribute utility function given in Equation 4.11.

4.7 Science Concept Utility Model

One limitation of this analysis is that it may be useful to preserve some of the finer resolution information about how well an instrument suite assesses several science objectives. For instance, no-one would design a mission to answer all lunar science objectives at once, however a single mission may attempt to answer one or two high-level science objectives very completely. For this purpose we define a utility vector as a set of utility metrics which indicate the preferability of a mission in the context of one particular science concept. Here we delineate between science objectives (the lowest levels in the science traceability matrix), and the science concepts (mid-level science objectives that cover a broad discipline).

In order to determine how well different mission architectures evaluate the individual science concepts outlined in SCEM, the same general method as presented in

Section 4.6.2 is used. In this case, the summation is conducted over the science objectives contained in a given science concept, instead of over the entire set of science objectives. The formula for this utility vector is:

$$U_l = \sum_{j=1}^m \sum_{i=1}^n k_i u_{i,j} \begin{bmatrix} \text{Concept}_i = l & 1 \\ \text{otherwise} & 0 \end{bmatrix} \quad (4.12)$$

where U_l = Utility Vector for Concepts $l = 1 \dots \text{Concept}_{\max}$

Concept_i = Science Concept of the i-th Objective

Chapter 5

Engineering Model

5.1 Overview

This chapter presents an engineering tool for estimating the mass and costs of planetary exploration missions, specifically landers and orbiters. This model is designed to interface with a science model (Chapter 4), which given a suite of instruments will determine a science utility value or a science utility vector.

This engineering model will interface with a larger trade space exploration tool to map out a trade space of science performance vs. costs estimated by this engineering model.

The engineering model presented here is designed to be modular. It is composed of a set of subsystem modules (outlined in detail in the following sections), which interact with one another. Figure 5.1 is an N^2 diagram for this model, which maps the interdependencies among the various subsystems included in the model.

Each block along the diagonal of Figure 5.1 represents a separate subsystem. The numbers in the non-diagonal cells represent the inputs and outputs of these subsystem models, or the working variables of the model. (These working variables are tabulated in Table B.1.) Numbers along row indicate outputs of the model within that row, and numbers along a column indicate the inputs of that model. Numbers to the bottom-right of the diagonal represent variables that provide some feedback to earlier models from later calculations. This is illustrated in Figure 5.2 The overall model must be

run through several iterations reach convergence due to these feedback mechanisms.

In the following sections, the inner workings of each subsystem module are explained. Validation against relevant data is shown for each subsystem model, where feasible. The entire engineering model is validated against several relevant spacecraft examples in Section 6.2.

Design Vector	Param. Vector	Payload	Avionics	Comm.	Power	Orbit	Thermal	Struct.	ACS & GNC	Prop.	Mass	Launch Vehicle	Science
		1			2,4,5,6	9,10	1,3		11	9,10,11			1
				2,5,6,7	1,7,10,11	7,8,9,12	4	3		12			
			1,2		2,3		2,3				4		
				4,5	2		2				3		
					2						1,3		
							4				3,5		
										1,2		3	
					2						1		
												1	
											1		
												1	
								1			2,3		
							1	1	1	1		3	

Figure 5.1: N^2 Diagram of the Engineering Model

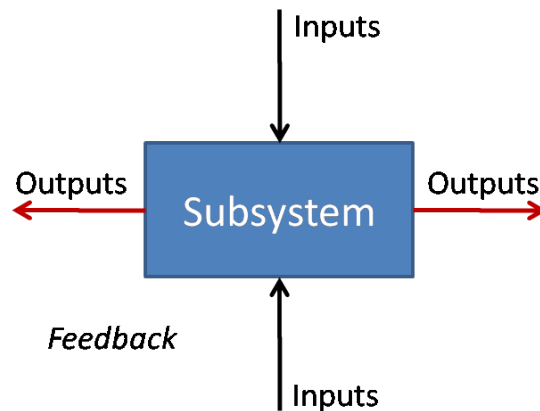


Figure 5.2: Diagram of a subsystem module with inputs and outputs and showing the feedback direction

5.2 Design Vector

The first module in the engineering model develops a design vector of input variables, which specify a design completely. The design variables considered in this model, along with the values each variable may take are shown in Table 5.1. When this model is executed, the selection of design vectors depends on the trade space exploration method used. This is discussed further in the following chapter.

Table 5.1: Design Variables

Variable	Units	Levels				
Instrument 1	[-]	0	1			
⋮						
Instrument n	[-]	0	1			
Lifetime	[yr]	1	2	5		
Landing Latitude	[°]	0	45	85		
Power Source	[-]	Solar	Nuclear			
Battery Type	[-]	Ni-Cd	Ni-H I	Ni-H II	Ni-H III	Lilon
Solar Panel Type	[-]	Si	Amorp. Si	Ga-As	In-P	Multi junction Ga-As
Data Rate	[bits/s]	5e4	5e5	5e6	5e7	5e8
Antenna Size	[m]	0.05	0.3	1		
Transfer Orbit	[-]	WSB	Hohmann			
Descent Method	[-]	Solid-Staged	Liquid-Direct			
Propellant	[-]	Monopropellant	Bipropellant			

5.3 Instruments Subsystem

5.3.1 Overview

The purpose of the Instruments Model is to provide technical data about the instruments chose in a specific spacecraft design to other subsystems. The Instruments model takes as it inputs, a database of possible instruments and their characteristics and a vector indicating which instruments are present in the current design. The model outputs a structure containing the relevant data for the selected instruments. The science utility of these instruments is computed in the Science Utility Model described in Chapter 4.

5.3.2 Instruments Database

For each instrument, the following variables are stored: *mass*, *maximum power*, *average power*, *data rate*, *daytime frequency of operation*, *daytime duty cycle*, *nighttime frequency of operation*, and *nighttime duty cycle*. A database of possible instruments has been compiled, shown in Table 4.2. Where possible this data has been collected directly from past missions, or has been estimated from several related instruments. In some cases, especially for values of *daytime frequency of operation*, *daytime duty cycle*, *nighttime frequency of operation*, and *nighttime duty cycle*, this data has been estimated.

5.4 Avionics & Data Subsystem

5.4.1 Overview

The Avionics & Data model is responsible for determining the total data storage requirements on board the spacecraft and finding the mass and power for the avionics subsystem. This shall be assumed to cover all control of the spacecraft as well as science data handling. The inputs to this model are:

- *Radio rate*: From design vector
- *Time between downlinks*: Parameter
- *Instruments' data rates*: From instruments model

The outputs are the duty cycle of the communications subsystem, the required on board data storage volume, and the mass and power of the avionics system.

5.4.2 Data Capacity

The Data model computes the on board storage requirement by integrating the instrument data rates and communications downlink rates in time. An example of such a transient analysis is shown in Figure 5.3.

The total data generated in one lunar day is:

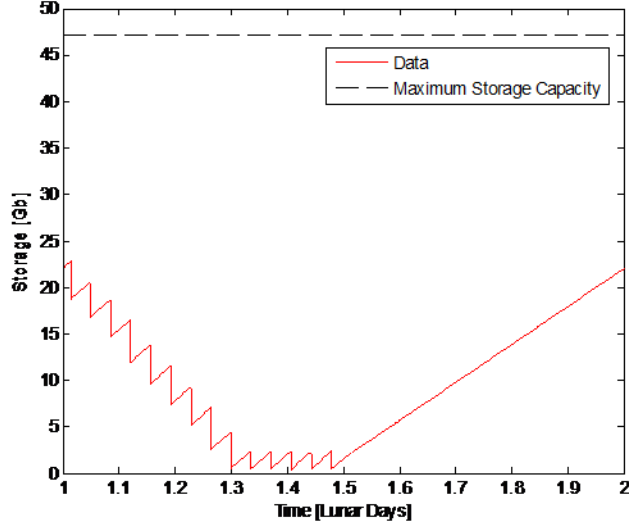


Figure 5.3: Data Storage and Downlink vs. Time on a Representative Lunar Lander

$$Data_{Total} = \left(\frac{1}{2} \sum_{i=1}^n \text{DutyCycle}_{\text{Day},i} \text{DataRate}_i + \frac{1}{2} \sum_{i=1}^n \text{DutyCycle}_{\text{Night},i} \text{DataRate}_i \right) t_{\text{LunarDay}} \quad (5.1)$$

The total data storage is set to be twice the data generated in one lunar day, as a contingency for any communications glitches. The duration of each downlink and the duty cycle of the radio are:

$$T_{radio} = \frac{Data_{Total}}{RN_{Downlink}} \quad (5.2)$$

$$\text{DutyCycle}_{\text{Radio}} = \frac{Data_{Total}}{Rt_{\text{LunarDay}}} \quad (5.3)$$

Here R is the radio rate and $N_{Downlink}$ is the number of downlink events per lunar day.

5.4.3 Avionics Sizing

The sizing of the avionics subsystem is dependent on the data throughput of the system. Estimates for power and volume are taken from SMAD.[45] See Table 5.2

below:

Table 5.2: Avionics Sizing

Data Rate	< 4 kbps	4 – 200 kbps	> 200 kbps
Mass [kg]	2.75 – 5.5	4.5 – 6.5	9.5 – 10.5
Power [W]	7 – 12	13 – 18	15 – 25

5.5 Communications Subsystem

5.5.1 Overview

The communications model is responsible for computing the spacecraft’s link budget, and determining the size and power of the communications subsystem components.

The inputs of the communications model are:

- *Radio rate*: From design vector
- *Spacecraft antenna*: From design vector
- *Ground station antenna*: Parameter
- *Time between downlinks*: Parameter
- *Communications band*: Parameter
- *Free space distance*: Parameter

The total mass, power, and duty cycle of the communications subsystem are reported to the mass and power modules. The following sections describe the communications model in further detail.

The communications model takes as its inputs the type of radio to be used, the radio rate, and the number and duration of downlink events. The outputs of the model are: the power vs. time profile, the antenna size, and communications system mass. Internal to this model is a link budget calculation which performs antenna sizing. Antenna masses are estimated using parametric relationships from past mission data. The assumed relationship for antenna mass vs. gain is shown in Figure 5.

In Figure 6, an example communications system architecture is illustrated. The primary components are: an S-band transponder, a diplexer, a switch, and a low-

and high-gain antenna.

5.5.2 Link Budget Analysis

At the core of the communications model is a link budget analysis. The link equation, given below, relates the signal-to-noise to the transmitted power, antenna gains (G_t , G_r), losses (L_l , L_s , L_a), environmental parameters (k , T_s), and the radio rate (R):

$$\frac{E_b}{N_0} = \frac{P_t L_l G_t L_s L_a G_r}{k T_s R} \quad (5.4)$$

This maps out the trades between antenna size, comm. system power, science return (in the form of downlinked data), and ground system design (choice of receiving antenna). Typically Equation 5.4 is used in its logarithmic form, with gains and losses expressed in units of decibels [dB]:

$$P = EbNo - L_l - G_t - L_s - L_a - G_r + 10 \log_{10} k + 10 \log_{10} T_s + 10 \log_{10} R \quad (5.5)$$

The terms of the link budget are taken from reference [45] and shown in Table 5.3:

To convert from the power in [dBW] as expressed in Equation 5.5 to the power in [W]:

$$P[W] = 10^{(P[dBW])/10} \quad (5.6)$$

5.5.3 Communications Subsystem Sizing

The communications subsystem is assumed to have a single high gain antenna, transceiver, switch, and diplexer. The mass of the high gain antenna is given as:

$$m_{antenna} = 15.2 \left(\frac{D_t}{1.56} \right)^2 \quad (5.7)$$

All additional equipment is assumed to have a mass of 3 [kg]. The communications

Table 5.3: Link budget [45, 46]

Symbol	Parameter	Units	Equation
c	Speed of Light	m/s	2.99792458×10^8
k			$0.13806504 \times 10^{-22}$
f	Frequency	Hz	
θ_t	Transmitter beamwidth	deg	
D_t	Transmitter antenna diameter	m	
G_{pt}	Transmitter antenna gain	dB	$10 \log_{10} \frac{\pi^2 D_t^2}{(c/f)^2}$
L_{pt}	Transmitter antenna pointing loss	dB	$-12(et/\theta_t)^2$
G_t	Transmitter antenna net gain	dB	$G_{pt} + L_{pt}$
L_s	Free space loss	dB	$10 \log_{10} \left(\frac{c}{4\pi S f} \right)^2$
θ_r	Receiver beamwidth	deg	$\frac{21}{f D_r}$
G_{pr}	Receiver antenna gain	dB	$10 \log_{10} \frac{\pi^2 D_r^2}{(c/f)^2}$
L_{pr}	Receiver antenna pointing loss	dB	$-12(et/\theta_t)^2$
G_r	Receiver antenna net gain	dB	$G_{pr} + L_{pr}$

power found in Equation 5.6 is given as an output of this model. The required duty cycle of the communications subsystem is found in the Avionics/Data model.

5.6 Power Subsystem

5.6.1 Overview

The power model is responsible for determining the size of power subsystem components, namely solar arrays and batteries. The inputs of the power model are:

- *Instrument power loads*: From instruments module
- *Other subsystem power loads*: From various subsystems
- *Power architecture (solar/nuclear)*: From design vector
- *Solar cell type*: From design vector
- *Battery type*: From design vector
- *Mission duration*: Parameter

The total mass of the power subsystem and the total internal heat loads are reported to the mass and thermal subsystem modules respectively. The power model is capable of sizing the power subsystem based on average power analysis and more

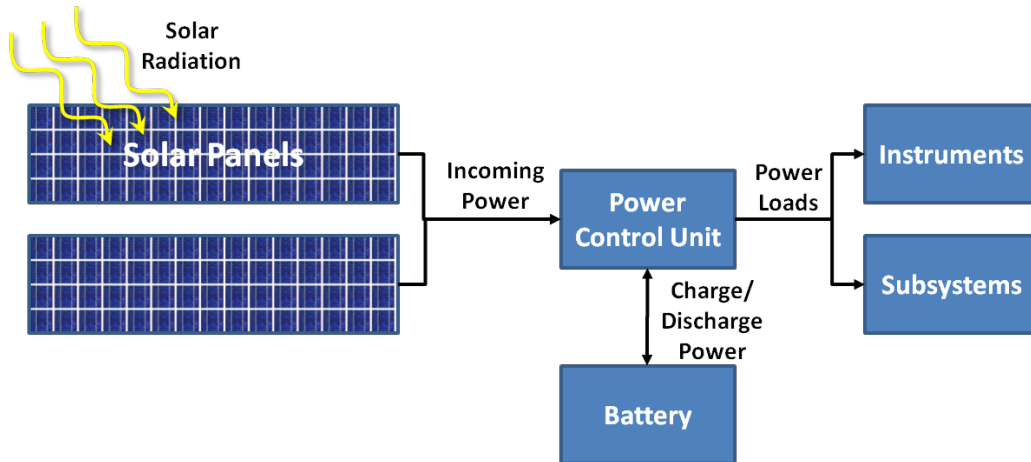


Figure 5.4: Layout of the power subsystem

computationally costly transient power analysis. A diagram of the assumed configuration of the power subsystem is shown in Figure 5.4. The following sections describe the power model in further detail.

5.6.2 Power Loads

the first step in developing a power model is to determine the power loads that it will need to supply through the course of the mission. For the purpose of this model, it is assumed that the spacecraft power loads are periodic, repeating each lunar day. Power loads are assumed to come from each of the instruments and from several subsystems (namely: Avionics, Communications, and Thermal). Each power load is described by several parameters:

- *Power*: Amplitude of the load in [W]
- *Daytime Duty Cycle*: Percentage of time the instrument is on when the spacecraft is illuminated
- *Daytime Frequency*: How many times instrument is on during a given daytime period
- *Nighttime Duty Cycle*: Percentage of time the instrument is on when the spacecraft is not illuminated
- *Nighttime Frequency*: How many times instrument is on during a given night-

time period

These values are sufficient to determine the power vs. time profile for each load, assuming that all loads can either be fully on or fully off. The period of each load's occurrence per lunar day is give as:

$$Period_{Day} = \frac{0.5[\text{day}]}{Freq_{Day}} \quad (5.8)$$

$$Period_{Night} = \frac{0.5[\text{day}]}{Freq_{Night}} \quad (5.9)$$

In Figure 5.5, several power loads vs. time are shown for representative subsystems.

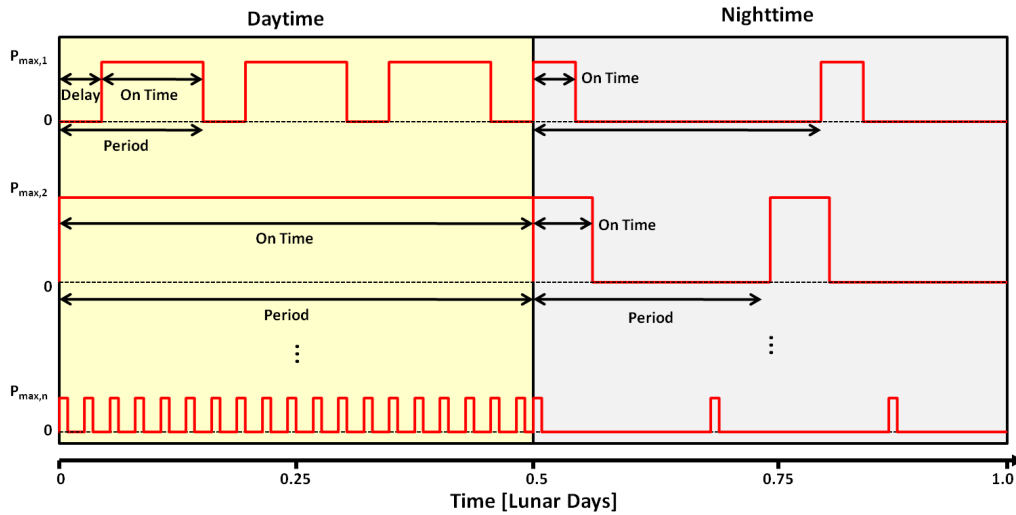


Figure 5.5: Example of power loads for instruments/subsystems 1, 2, ..., n

The average daytime, nighttime and total power can be found by multiplying each power load by its duty cycle:

$$P_{\text{Avg,Day}} = \sum_{i=1}^n \text{DutyCycle}_{\text{Day},i} P_i \quad (5.10)$$

$$P_{\text{Avg,Night}} = \sum_{i=1}^n \text{DutyCycle}_{\text{Night},i} P_i \quad (5.11)$$

$$P_{\text{Avg,Total}} = \frac{1}{2} \sum_{i=1}^n \text{DutyCycle}_{\text{Day},i} P_i + \frac{1}{2} \sum_{i=1}^n \text{DutyCycle}_{\text{Night},i} P_i \quad (5.12)$$

5.6.3 Power Subsystem Sizing: Solar Variant

The power subsystem components are sized based on the instrument and subsystem power loads, discussed in the previous section. When the power model is used in its non-transient (average power) mode, the required solar panel output and battery capacity are functions of the average daytime and nighttime power.

Solar Panel Sizing

The incoming solar radiation to the solar panels is a function of the distance from the sun, the latitude, and the time of day. At the moon, the solar radiation constant is $1367[W/m^2]$. It is assumed that the solar panels can be oriented such that the panels are perpendicular to the sun's rays at local noon. Furthermore, it is assumed that that output of the solar arrays decays at some known rate, d , over time. At the end of life (EOL), the power output of an array as a fraction of the beginning of life (BOL) power is:

$$\xi = (1 - d)^{\text{Lifetime}} \quad (5.13)$$

Solar radiation varies over the course of the day, following a sine curve:

$$P_{\text{incoming}} = \begin{cases} 1367[W/m^2] A_{\text{Solar Array}} \frac{1}{\xi} \eta \sin\left(t \frac{2\pi}{t_{\text{Lunar Day}}}\right) & \text{if } t \leq 0.5 t_{\text{Lunar Day}} \\ 0 & \text{if } 0.5 t_{\text{Lunar Day}} < t \leq 0.5 t_{\text{lunar Day}} \end{cases} \quad (5.14)$$

Integrating, the total energy output by the solar array is:

$$\begin{aligned}
E_{incoming} &= 1367[W/m^2]A_{SolarArray} \frac{1}{\xi} \eta \int_0^{0.5t_{LunarDay}} \sin\left(t \frac{2\pi}{t_{LunarDay}}\right) dt \quad (5.15) \\
&= 1367[W/m^2]A_{SolarArray} \frac{1}{\xi} \eta \frac{t_{LunarDay}}{\pi}
\end{aligned}$$

The required energy over an entire day cycle is:

$$\begin{aligned}
E_{required} &= P_{Avg,Total} t_{LunarDay} \quad (5.16) \\
&= \left(\frac{1}{2} \sum_{i=1}^n \text{DutyCycle}_{Day,i} P_i + \frac{1}{2} \sum_{i=1}^n \text{DutyCycle}_{Night,i} P_i \right) t_{LunarDay}
\end{aligned}$$

In the steady state, the incoming power must balance the required power, so the required peak solar panel power is:

$$P_{SolarArray} = P_{Avg,Total} \pi \quad (5.17)$$

The solar panel dimensions and mass are dependent on the type of solar panel selected:

Table 5.4: Solar panel selection [45]

Type	η	Degradation	Specific Power [W/kg]
Si	0.148	0.0375	25
Amorphous Si	0.050	0.0375	25
Ga-As	0.185	0.0275	25
In-P	0.18	0.0275	25
Multijunction Ga-As	0.22	0.0275	25

The beginning of life solar panel area is:

$$A_{SolarArray} = \frac{P_{Avg,Total} \pi}{1367[W/m^2] \frac{1}{\xi} \eta} \quad (5.18)$$

The mass can be found from the specific power.

Battery Sizing

The battery is sized to be able to provide the entire nighttime power load and an additionally 10% of the daytime power load. The additional 10% capacity accounts for the fact that some power may be needed at dawn when the incoming power is still very low. The battery is sized such that at its maximum discharge level it will not exceed the proscribed maximum depth of discharge (DoD).

$$E_{battery} = \left(\frac{1}{20} P_{Avg,Day} + \frac{1}{2} P_{Avg,Night} \right) \frac{t_{LunarDay}}{DoD} \quad (5.19)$$

The battery mass is dependent on the battery type selected and its specific energy density:

Table 5.5: Battery selection [45]

Type	DoD	Specific Energy Density [kJ/kg]
Ni-Cd	0.8	99
Ni-H A	0.8	140
Ni-H B	0.8	173
Ni-H C	0.8	180
LiIon	0.8	400

Other Power Equipment Sizing

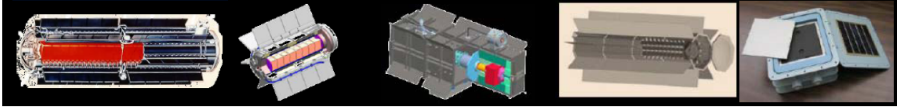
In addition to the battery and solar panels, it is assumed that there is a power control unit with a mass in [kg] equal to 4% of the average total power in [W].[45]

5.6.4 Power Subsystem Sizing: Nuclear Variant

Due to the long duration of the Moon's night, getting a solar-based power subsystem design to converge can be challenging. This is especially the case if the mission requires that science measurements be made at nighttime, leading to high power loads when there is no generating capability available. One solution to this issue is to use a Radioisotope Power Source (RPS).

A RPSs is a power generation device that does not require sunlight; instead it contains a small amount of radioactive material (typically ^{238}Pu), which gives off

thermal energy in the course of its radioactive decay. The RPSs converts this thermal energy into electrical power for the spacecraft. Radioisotope Power Sources have a long history, first being used in 1961 and having flown on over 26 missions.[47] Traditionally RPSs have used a solid state device to convert the thermal energy from ^{238}Pu into electrical energy. NASA Glenn is currently developing a Sterling Cycle RPS – the Advanced Sterling Radioisotope Generator (ASRG) – which will have a higher specific energy owing to the greater efficiency of the Sterling Cycle than solid state energy conversion methods. The properties of several variants of RPS devices are shown in Table 5.6.



	GPHS-RTG Past	MMRTG Present	ASRG In development	ARTG Future	TPV Future
Electric output, BOM, W_e	285	125	~140-150	~280 to 420	~38-50
Heat input, BOM, W_e	4500	2000	500	3000	250
RPS system efficiency, BOM, %	6.3	6.3	~28-30	~9-14	~15-20
Total system weight, kg	56	44.2	~19-21	~40	~7
Specific power, W_e/kg	5.1	2.8	~7-8	~7-10	~6-7
# GPHS modules	18	8	2	12	1
GPHS module weight, kg	25.7	12.9	3.2	19.3	1.6
^{238}Pu weight, kg	7.6	3.5	0.88	5.3	0.44

Table 5.6: Properties of past, present, and future RPSs [47]

For the purposes of this model, it is assumed that an ASRG is used. In this configuration of the power subsystem, the ASRG provides the base power load. Batteries are included to supply any peak power loads that are greater than the average power. When a RPS is used the, spacecraft does not need to tailor power consumption at night; accordingly, the instruments are assumed to run at their daytime duty cycles for the entire mission.

The following ASRG properties are used in this model:

RPS Sizing

The RPS must provide the average system power at the mission’s end of life. As with solar panels, the power output of a RPS will decrease over time owing to radioactive decay. Given this decay rate, the required beginning of life RPS power is:

Table 5.7: Avanced Sterling Radioisotope Generator (ASRG) properties [48]

Property	Unit	Value
Electrical Power	W	143
Thermal Power	W	500
Mass	kg	23
Degradation	%/yr	0.8%

$$P_{\text{Required}} = \frac{P_{\text{Avg,Day}}}{(1 - d)^{\text{Lifetime}}} \quad (5.20)$$

The number of ASRGs required is the ceiling of the required power divided by the power per ASRG:

$$N_{\text{ASRG}} = \left\lceil \frac{P_{\text{Required}}}{P_{\text{ASRG}}} \right\rceil \quad (5.21)$$

Battery Sizing

The battery is sized to provide peak power above the output of the RPS. The total energy storage required be the battery is this peak energy usage multiplied by the depth-of-discharge coefficient:

$$E_{\text{Battery}} = \frac{t_{\text{LunarDay}}}{DoD} \int_0^{t_{\text{LunarDay}}} \max \left(\sum_i P(t)_i - P_{\text{Avg,Day}}, 0 \right) dt \quad (5.22)$$

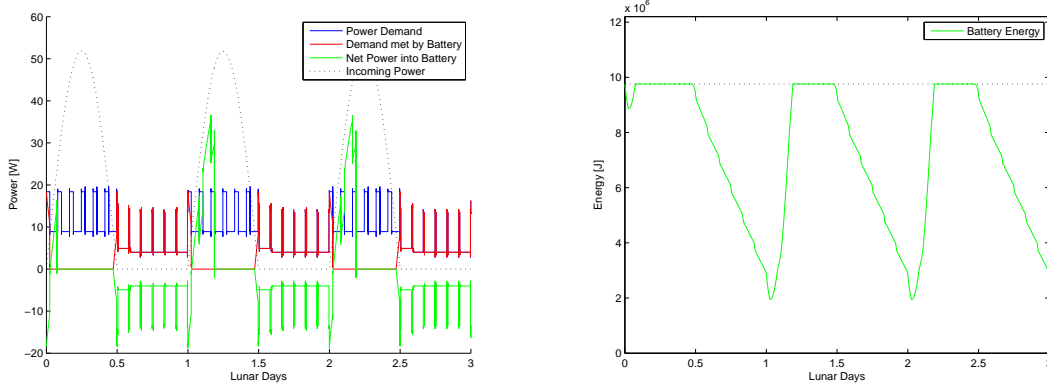
The battery mass is found in the same manner as for the solar variant. The other power subsystem masses are also the same as for the solar variant case.

5.6.5 Transient Power Analysis

To ensure that the power subsystem design can close, it is necessary to have a transient power analysis capability. This is implemented using numerical integration with Matlab's `ode45` solver. At each time step, the state of charge of the battery is computed:

$$\frac{dE_{battery}}{dt} = \begin{cases} P_{Generated}(t) - P_{Load}(t) & \text{if } E_{battery}(t) < E_{battery,max} \\ 0 & \text{if } E_{battery}(t) = E_{battery,max} \end{cases} \quad (5.23)$$

An example of a transient analysis of the power loads is shown in Figure 5.6. In Figure 5.6(a), the incoming power from the solar panels, power load, and power supplied by the battery is shown. The battery supplies all power at nighttime and continues to provide some power during dawn. From Figure 5.6(b) it can be seen that the battery depth of discharge does not exceed 80%.



(a) Transient power analysis for 100 kg class lunar lander

(b) Battery charge state vs. time

Figure 5.6: Transient power analysis results

5.7 Orbits Subsystem

5.7.1 Overview

The orbits model takes as an input the orbit type: a Hohmann transfer orbit or a Weak-Stability Boundary (WSB) Orbit. The model determines the launch characteristic energy, the arrival ΔV , and the landing ΔV for each orbit type, as well as the transit duration. For the Hohmann transfer case, the arrival ΔV is 822 m/s; for the WSB case, the arrival ΔV is 629 m/s. For both cases, the landing ΔV is assumed to

be 2,100 m/s. The details of these calculations are presented in the following sections.

5.7.2 Low Energy Transfer Orbits

In 1991, the Japanese Hiten spacecraft first demonstrated the use of a new class of low-energy lunar transfer orbits.[49] These Weak-Stability Boundary orbits, developed by Edward Belbruno and James Miller,[50] take advantage of chaotic solutions to the n-body problem. An example of a WSB trajectory is shown in Figure 5.7.

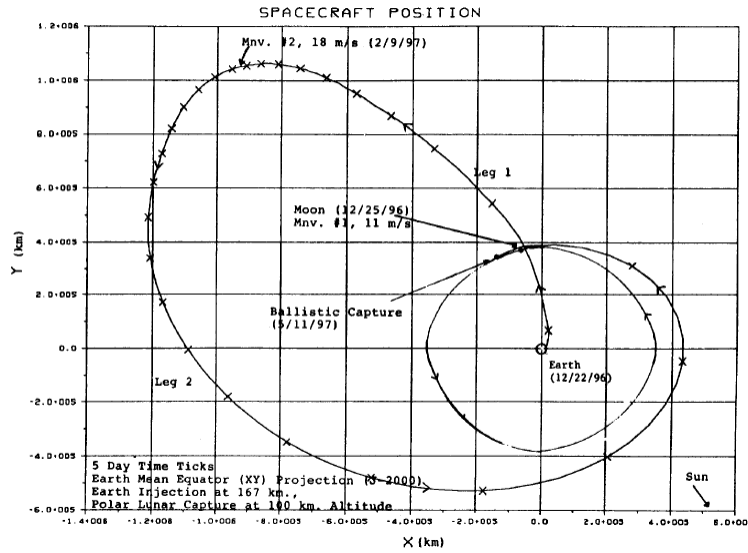


Figure 5.7: Schematic of a Weak-Stability Boundary transfer trajectory [50]

Due to the chaotic nature of these trajectories, analytic solutions for the ΔV required for these trajectories do not exist. The trajectories must be numerically integrated in order to find the needed ΔV . Implementing a solver for this problem is beyond the scope of this project, so estimates of the ΔV for a WSB trajectory were taken from a study by Pernicka, *et al.*[51]. This work examined a number of transfer orbits in the WSB class with starting and ending points in a 167 km altitude circular Earth orbit and a 100 km altitude circular lunar orbit, respectively. The results of this study are shown in Table 5.8.

For the orbits model, an Earth-departure ΔV of 3,194 m/s and a Moon-arrival ΔV of 629 m/s are assumed.

Table 5.8: Summary of Earth-to-Moon Transfers from Pernicka, et al. [51]

TYPE	MODEL	TOTAL ΔV (km/sec)	EARTH INJECTION ΔV (km/sec)	MOON INSERTION ΔV (km/sec)
Minimum ¹	3-Body	3.721	3.099	0.627
This Study	3-Body	3.824	3.194*	0.629*
Belbruno/Miller	Real World	3.838	3.187*	0.651
Biparabolic	2-Body	3.946	3.232	0.714
Hohmann	2-Body	3.959	3.140	0.819

*Includes mid-course maneuvers

5.7.3 Hohmann Transfer Trajectory Analysis

The simplest case for the ΔV required to get to the Moon is the Hohmann Transfer. The assumptions for this orbit are that it begins in LEO at 500 km, transits to Lunar altitude of 384,400 km, and then transfers to Lunar orbit via a hyperbolic insertion maneuver. A diagram of the propulsive maneuvers required for this trajectory are shown in Figure 5.8. It is assumed that the launch vehicle will provide the Earth-departure ΔV , as discussed in the section on Characteristic energy.

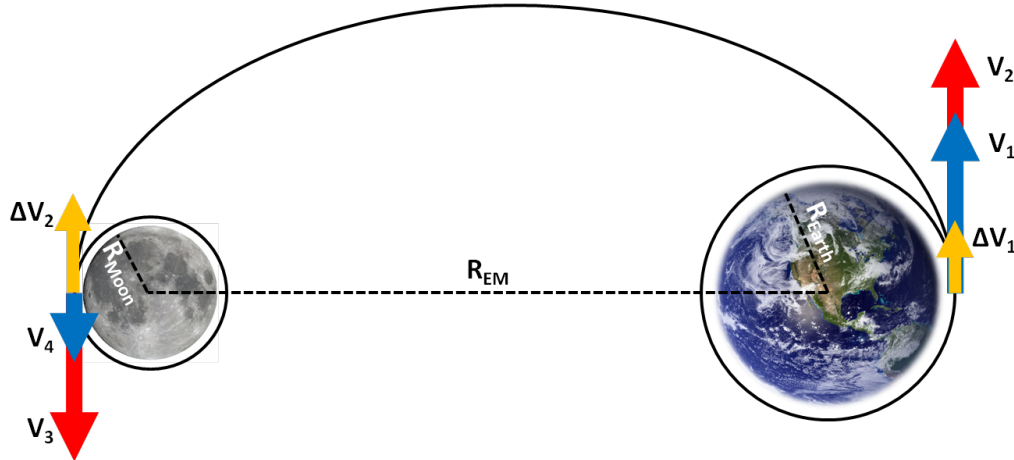


Figure 5.8: Schematic of a Hohmann transfer trajectory

Constants

The relevant parameters of the Earth and Moon for solving this problem are given below in Table 5.9.

Table 5.9: Properties of the Earth and Moon

Property	Units	Earth	Moon	
μ	Gravitational parameter	m^3/s^2	3.98601×10^{14}	4.903×10^{12}
R	Radius	km	6,378	1,738
a	Semi-major axis	km	149,598,261	384,399
V_{orbit}	Orbital velocity	m/s	29,780	1,022
g	Surface gravity	m/s^2	9.81	1.622

Low Earth Orbit

The initial orbit is assumed to be at an altitude of 500 [km].

$$R_{LEO} = 500 [km] + R_{earth} = 6878 [km] \quad (5.24)$$

The velocity of the initial circular orbit is:

$$V_{LEO} = \sqrt{\frac{\mu_{earth}}{R_{LEO}}} = 7612 \left[\frac{m}{s} \right] \quad (5.25)$$

Transfer Orbit

The semi-major axis of the orbit is:

$$R_a = R_{EM} + R_{moon} + 100[km] + R_{LEO} \quad (5.26)$$

The perigee velocity for the transfer orbit is:

$$V_p = \sqrt{\frac{2\mu_{earth}R_a}{R_{LEO}(R_a + R_{LEO})}} = 10672 \left[\frac{m}{s} \right] \quad (5.27)$$

The ΔV for Trans-Lunar Insertion is:

$$\Delta V_1 = V_p - V_{LEO} = 3060 \left[\frac{m}{s} \right] \quad (5.28)$$

The velocity of the spacecraft upon arrival at the moon is:

$$V_a = \sqrt{\frac{2\mu_{earth}R_{LEO}}{R_a(R_a + R_{LEO})}} = 186 \left[\frac{m}{s} \right] \quad (5.29)$$

Hyperbolic Insertion

In the moon's reference frame, the spacecraft is arriving on a hyperbolic trajectory. A burn must be completed at perilune to circularize around the moon.

The velocity of the spacecraft in the moon's reference frame along an asymptote in a hyperbolic trajectory is:

$$V_\infty = V_a - V_{moon} = -835 \left[\frac{m}{s} \right] \quad (5.30)$$

The velocity of the spacecraft at perilune in the moon's reference frame is:

$$V_{perilune} = \sqrt{V_\infty^2 + 2\frac{\mu_{moon}}{R_{LMO}}} = 2456 \left[\frac{m}{s} \right] \quad (5.31)$$

Low Moon Orbit

For a 100 km Low Moon Orbit the radius and velocity are as follows:

$$R_{LMO} = 100[km] + R_{moon} = 1838 [km] \quad (5.32)$$

$$V_{LMO} = \sqrt{\frac{\mu_{moon}}{R_{LMO}}} = 1633 \left[\frac{m}{s} \right] \quad (5.33)$$

The ΔV required for Lunar Orbit Insertion is:

$$\Delta V_2 = V_{LMO} - V_{perilune} = -822 \left[\frac{m}{s} \right] \quad (5.34)$$

From this analysis, the relevant value for the orbits model is the Lunar arrival ΔV of 882 m/s

Characteristic Energy, C_3

The energy required for an interplanetary trajectory is denoted by the *characteristic energy*, or C_3 , which is a measure of the additional velocity of a trajectory required beyond the escape velocity for a particular body. C_3 has units of km^2/s^2 . This value is used in launch vehicle selection: the amount of mass a given launch vehicle can put into an interplanetary trajectory decreases for trajectories with a higher value of C_3 . The expression for finding the characteristic energy is:

$$C_3 = v^2 - \frac{2\mu}{r} \quad (5.35)$$

5.7.4 Landing Trajectories

In order to get from Lunar orbit to the surface of the moon, additional ΔV must be expended to land. In the limiting case, two impulsive maneuvers could be conducted: 1) null out the horizontal orbital velocity (V_{LMO}), and 2) null out the vertical velocity after experience a free fall from the orbital altitude ($V_{Surface} = \sqrt{2h_{LMO}g_{Moon}}$). For a 100 km orbital altitude, this establishes the limiting case as 1400 m/s.

The limiting case is unachievable, however, as it would require an infinite thrust-to-weight (T/W) ratio. A more reasonable alternative is to use a gravity turn, in which the spacecraft provides a constant thrust for a period of time, with the spacecraft slowly turning from a horizontal orientation in orbit to a vertical orientation upon landing. Determining the Delta-V required for a given gravity turn trajectory requires numerically integrating the following system of equations for the spacecraft mass, m , thrust-axis velocity, v , and the off-vertical angle β for a given profile of thrust-to-weight ratio (TW) vs. time.[52]

$$TW(t) = \frac{\dot{m}(t)I_{sp} g_0}{mg} \quad (5.36)$$

$$\dot{v} = g(TW(t) - \cos \beta) \quad (5.37)$$

$$v\dot{\beta} = g \sin \beta \quad (5.38)$$

In order to increase the model runtime, estimates of the total landing ΔV required were taken from a study by Wilhite, *et al.*[53] From these estimates, based on the landing ΔV for the Apollo Lunar Excursion Module, a conservative ΔV of 2100 m/s is used in this study.

	Assumptions			ΔV , m/s		
	Conservative	Nominal	Optimistic	Conservative	Nominal	Optimistic
Nominal Trajectory	Pre-Mission Apollo	FPA=-45	Optimized	2081	2015	1877
T/W	1.8	2.4	3.0	0	-20	-30
Dispersions, ΔV m/s	53	27	0	53	27	0
Approach Time, sec	120	60	0	0	-10	-20
Vertical Descent Time, sec	46	23	12	0	-37	-55
Vertical Descent Margin, ΔV m/s	17	8	0	27	14	0
Redesignation footprint radius, m	305	50	25	0	15	8
Instantaneous Impact Cross Range, m	1000	500	200	19	10	5
Hardware Uncertainties, ΔV m/s	25	12	0	25	12	0
Additional Margin, ΔV m/s	57	28	14	57	28	14
	Total Mission ΔV, m/s			2262	2053	1799

Figure 5.9: Conceptual lunar landing trajectories [53]

5.8 Thermal Subsystem

5.8.1 Overview

The thermal module is responsible for estimating the expected heat loads on the spacecraft and sizing a thermal management system capable of keeping the temperature within a set of prescribed limits. The thermal module consists of: an environmental section, which determines the thermal conditions of the lunar surface; an energy balance section, which integrates the expected heat loads; and a thermal sizing section which synthesizes this information into a feasible thermal subsystem architecture. The inputs for the thermal module are:

- *Internal heat loads*
- *Spacecraft mass*
- *Landing latitude*

The outputs for the thermal module are:

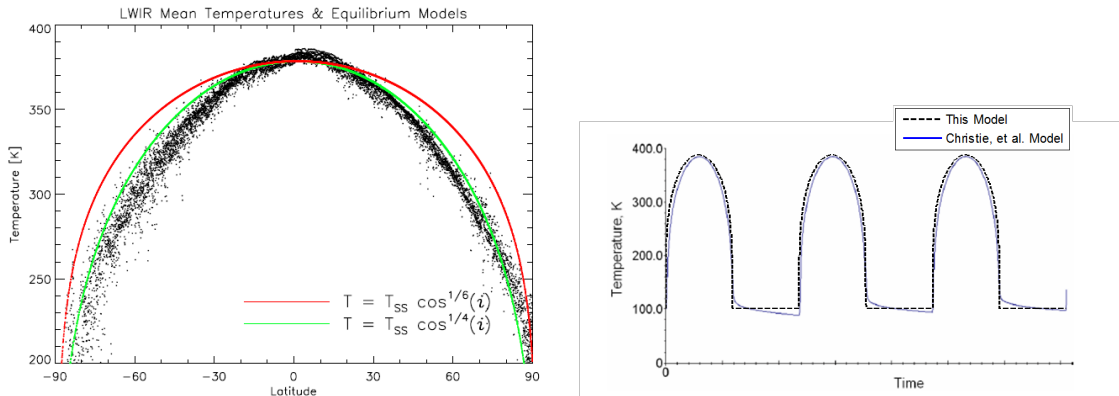
- *Number of radioisotope heaters*
- *Radiator mass*

- *MLI mass*
- *Thermal system mass and power*

This thermal model makes a number of simplifying assumptions about the spacecraft: namely, the spacecraft is assumed to be a single spherical thermal node with a uniform fixed density. The spacecraft temperature is found by calculating the equilibrium temperature for the various heat loads present in the system. The following sections walk through the thermal environment model, the energy balance equations, and the equipment sizing.

5.8.2 Thermal Environment Model

In order to accurately size a thermal subsystem, an accurate model of the lunar surface thermal environment as a function of time and latitude is needed. The Long-Wave Infrared (LWIR) camera on the Clementine Spacecraft mapped the local-noon surface temperature of the moon (see Figure 5.10(a) [54]). These data show that the Moon behaves as a Lambertian surface, and accordingly its surface temperature varies as $\cos^{1/4}(Lat)$.



(a) Local noon surface temperature at the lunar equator from Clementine LWIR data [54] (b) Lunar surface temperatures vs. time at the lunar equator [55]

Figure 5.10: Thermal Environment Data

Christie, *et al.* at NASA Glenn [55] have developed a high-fidelity lunar surface temperature model, which determines the transient lunar surface temperature. This model includes the effects of the lunar regolith “fluff” layer on the radiative equilib-

rium temperature. From a curve fit to the data presented by this model, it was found that the transient temperature is best modeled by:

$$T = \begin{cases} (T_{max} - T_{min}) \sin^{1/4} \left(\frac{t - t_{lunarDay}n}{2\pi t_{lunarDay}} \right) + T_{min} & \text{if } t - t_{lunarDay}n \leq \frac{t_{lunarDay}}{2}, n = 0, 1, \dots \\ T_{min} & \text{otherwise} \end{cases} \quad (5.39)$$

A comparison of this curve fit to the lunar surface thermal profile at the equator is shown in Figure 5.10(b). The maximum and minimum surface temperatures at varying latitudes are found by using the maximum and minimum equatorial temperatures found from the Christie, *et al.*[55] model and applying the Lambertian surface assumption demonstrated by Lawson *et al.*[54]. The result is:

$$T_{max} = 384 \cos^{1/4}(Lat)[K] \quad (5.40)$$

$$T_{min} = 102 \cos^{1/4}(Lat)[K] \quad (5.41)$$

The result is a complete estimate for the lunar surface temperature for any latitude or time during the lunar day. It should be noted that the accuracy of this model degrades very close to the lunar pole, where a temperature of 0 K would be predicted.

5.8.3 Energy Balance Model

With a thermal environment model in place, the next step is to develop a heat flow model to find the equilibrium temperature of the lander. The thermal model implemented to perform these calculations assumes a single thermal node (equivalent to a constant density spherical lander).[56] Equation 5.42 is solved to find the temperature vs. time profile:

$$mC_p \frac{dT}{dt} = \dot{Q}_{Sun} + \dot{Q}_{Reflected} + \dot{Q}_{Body} + \dot{Q}_{Internal} - \dot{Q}_{Emitted} \quad (5.42)$$

Figure 5.11 illustrates each of the terms of Equation 5.42. The following heat

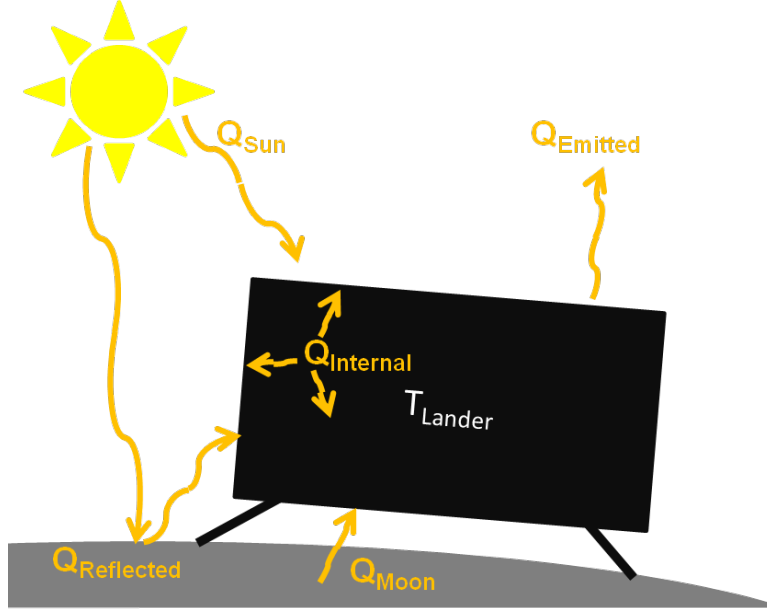


Figure 5.11: Lander Heat Flow Paths

loads are assumed in this model: radiation from the sun, radiation from the moon, reflected radiation off the moon from the sun, and internal heat sources. These must be balanced by the outgoing radiation of the spacecraft. A lander density of 100 kg/m^3 was assumed [57], as well as a C_p of 500 J/kg/K (slightly less than Aluminum).

The terms in Equation 5.42 are broken down as follows:

$$\dot{Q}_{Sun} = A_{SC} \pi r_{SC}^2 \sigma T_{Sun}^4 \frac{r_{Sun}^2}{R_{SunBody}^2} \quad (5.43)$$

$$\dot{Q}_{Reflected} = \alpha_{Body} A_{SC} \pi r_{SC}^2 \sigma T_{Sun}^4 \frac{r_{Sun}^2}{R_{SunBody}^2} \quad (5.44)$$

$$\dot{Q}_{Body} = A_{SC} \pi r_{SC}^2 \sigma \epsilon_{Body} T_{Body}^4 \quad (5.45)$$

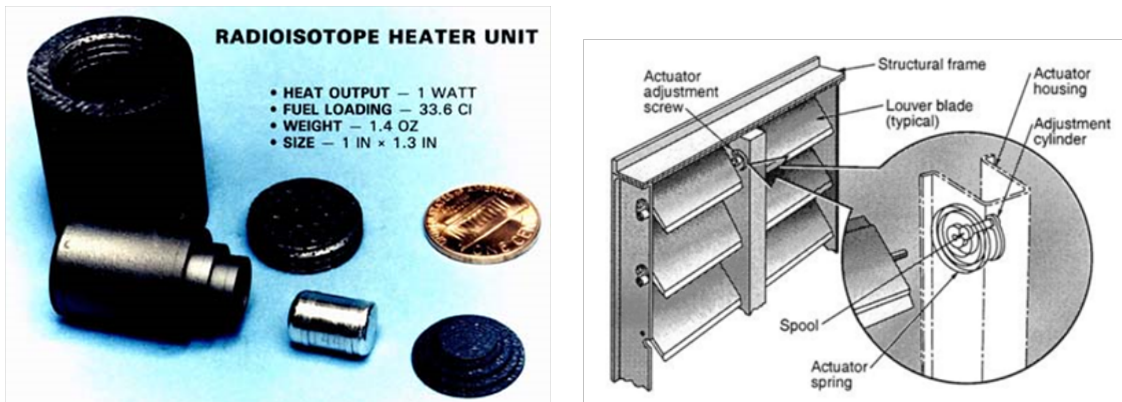
$$\dot{Q}_{Internal} = \sum P_{Internal} + \dot{Q}_{Heaters} \quad (5.46)$$

- where
- A_{SC} = Spacecraft absorbtivity
 - r_{SC} = Equivalent spherical spacecraft radius
 - σ = Stephan-Botlzmann constant
 - r_{Sun} = Radius of the Sun
 - $R_{SunBody}$ = Sun-target body distance
 - T_{Sun} = Solar temperature (5778 K)
 - α = Bond albedo
 - ϵ = Emissivity
 - T_{Body} = Target body temperature
 - $P_{Internal}$ = Spacecraft electrical power
 - $\dot{Q}_{Heaters}$ = Power output of heaters

Equation 5.42, the spacecraft heat flow equation, is solved along with Equations 5.43 through Equation 5.46 for several cases, outlined in the following section, to determine the necessary size of the thermal subsystem.

5.8.4 Thermal Subsystem Sizing

This model assumes that the spacecraft's temperature is maintained withing a set of specified limits through the use of Radioisotope Heater Units (RHUs), a passive radiator, and Multi-layer Insulation (MLI).



(a) Radioisotope Heater Units [58]

(b) Passive Louvers [45]

Figure 5.12: Thermal control mechanisms

Examples of RHUs and louvers are shown in Figure 5.12. An RHU is small device,

weighting 40 grams and containing an amount of radioactive material which decays at a known rate, producing 1 W of heat.

For heat rejection, it is assumed a fraction of the spacecraft surface area will be covered with a high-emissivity paint, and have passive louvers situated on top of it. The high emissivity paint acts as a passive radiator. The louvers open above a set temperature, due to an expansion of a metal coil, exposing the radiator to space, thereby radiating heat away from the spacecraft. Below the set temperature they close, keeping the heat within the spacecraft.

Additionally, the entire body of the spacecraft (with the exception of the radiator) is assumed to be covered in MLI. The sizing of these elements is given using the two cases below:

Radiator Sizing

The driving case for radiator sizing is the maximum daytime temperature. In the steady state, the spacecraft temperature is constant, so the heat input equals the heat output. The radiator covers some fraction of the spacecraft's surface area, F ; under this condition the emitted heat is:

$$\dot{Q}_{Emitted} = [(1 - F) \epsilon_{MLI} + F \epsilon_{Radiator}] 4\pi r_{SC}^2 \sigma T_{SCmax}^4 \quad (5.47)$$

Using this formulation for $\dot{Q}_{Emitted}$, Equation 5.42 is solved to find F , and thereby the radiator area. A louver/radiator mass of $4.5 [kg/m^2]$ is assumed.[45]

RHU Sizing

The driving case for heater sizing is the minimum nighttime temperature. In this case it is assumed the louvers are closed, so:

$$\dot{Q}_{Emitted} = \epsilon_{MLI} 4\pi r_{SC}^2 \sigma T_{SCmin}^4 \quad (5.48)$$

The required heater power to maintain the spacecraft at T_{SCmin} is:

$$\dot{Q}_{Heaters} = \dot{Q}_{Emitted} - \frac{\int_{LunarDay/2}^{LunarDay} P_{Internal} dt}{LunarDay/2} - \dot{Q}_{Body} \quad (5.49)$$

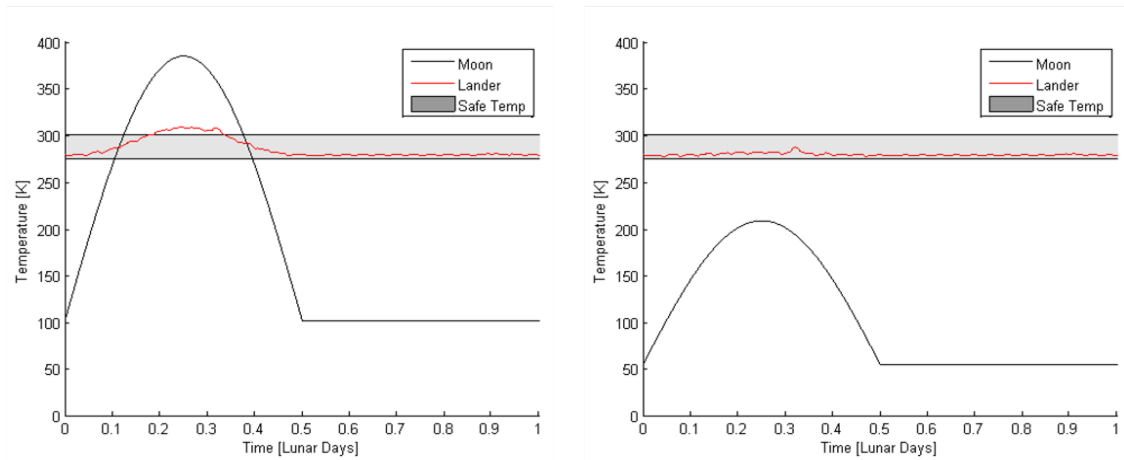
The number of RHUs required to supply this much heat is found, given that each RHU produces 1 W. As stated previously, each RHU weights 0.04 kg.[58]

Other Thermal Equipment Sizing

The spacecraft is assumed to be covered with MLI (with the exception of the radiator. An MLI density of $0.73 [kg/m^2]$ is assumed. Additionally $0.25 [kg]$ is allocated for thermal control mass and and 1 W for thermal control power.

5.8.5 Validation

To illustrate the effectiveness of this thermal sizing scheme, it was applied to a representative 100 [kg] class lunar lander architecture. Each of the heat loads was found as a function of time and transient temperature equation was solved. The results of this analysis, shown in Figure 5.13, show that this scheme can keep the temperature mostly within the given temperature limits (conservatively assumed to be a maximum of 300 [K] and a minimum of 275 [K]).



(a) Lander temperature vs. time at the Lunar equator (b) Lander temperature vs. time at 85°N on the Moon

Figure 5.13: Transient thermal model results

5.9 Structures Subsystem

The structures module is responsible for estimating the structural mass of the spacecraft. A simple mass fraction is used for this estimate, where the structural mass is expressed as a fraction of the landed dry mass:

$$m_{\text{structures}} = F_{\text{structures}} m_{\text{dry}} \quad (5.50)$$

Here $F_{\text{structures}}$ represents the structural mass fraction. Typical orbiting spacecraft have a structural mass in the range of 15% to 25% of their dry mass.[45] A planetary lander is likely to see higher loads than an orbiter due to the particulars of its mission profile: the spacecraft needs to withstand the deceleration of a landing burn and absorb some shock from a final freefall upon engine shutdown. Accordingly, the structural mass fractions of landers are typically higher: in the 25% to 30% range.

A quick survey was conducted of the structural mass fractions of several historical landers for which data was available: JPL's Lunette mission concept, ESA's Huygens lander, NASA's NEARER mission concept, and the Apollo Ascent Module. These mass fractions are plotted against the lander dry mass in Figure 5.14.

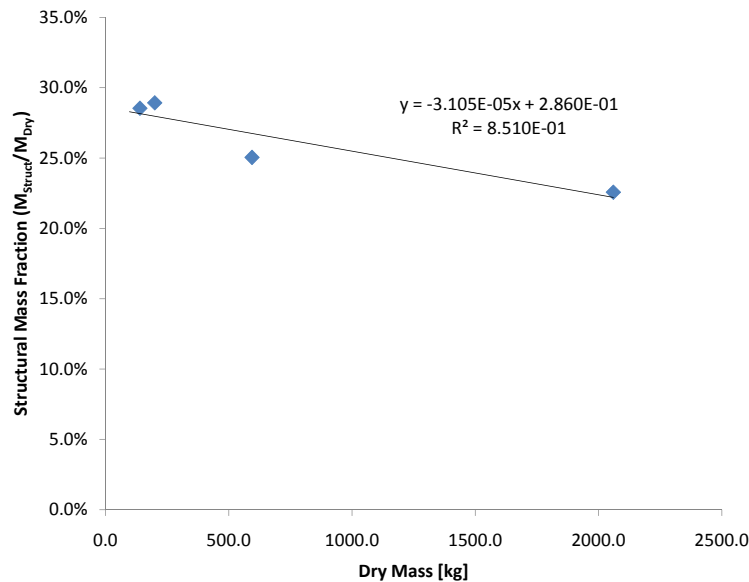


Figure 5.14: Lander structural mass fractions

In the dry mass range below 500 kg, the structural mass fraction is estimated to be 27.5%. This value of $F_{\text{structures}}$ is used in the engineering model.

5.10 ACS/GNC Subsystem

The GNC module is responsible for sizing the Guidance, Navigation and Control equipment. In this model, the GNC subsystem is assumed to only consist of the sensors for determining position, navigation state, and orientation for both cruise and landing. The orientation of the spacecraft is controlled by twelve attitude control thrusters held by the propulsion subsystem. The details of these thrusters are given at the end of Section 5.11.2.

The mass of the terminal landing GNC sensors, m_{GNC} , is assumed to be 2 kg. The mass of the in-transit GNC sensors is assumed to be carried as part of the carrier subsystem mass. The GNC module is an area which is open for improvement in future iterations of this work.

5.11 Propulsion Subsystem

5.11.1 Overview

The propulsion module is responsible for determining the size of the propulsion subsystem, in both the wet launch configuration and the final dry landed configuration. The primary role of the propulsion system is to provide the ΔV needed for arrival and landing at the target body. It is also responsible for any mid-course correction and propulsive attitude adjustment that may be needed. The inputs for the propulsion system are:

- *Propulsion system staging*: Design input (Solid & Liquid; or Liquid Only)
- *Liquid propulsion type*: Design input (Monopropellant; or Bipropellant)
- *Mid-course ΔV* : From orbits module
- *Arrival ΔV* : From orbits module
- *Landing ΔV* : From orbits module

- *Number of tanks*: Parameter
- *Lander dry mass*: From mass module

Due to the need for precise control during the landing of a mission, there is no solid-only propulsion option. It is also assumed that the launch vehicle will provide an Earth-escape trajectory for the spacecraft, so no Earth-departure ΔV needs to be provided by this propulsion system.

5.11.2 Propulsion Subsystem Design

The propulsion system design consists of two high level architectural decisions: Solid & Liquid vs. Liquid Only, and Monopropellant vs. Bipropellant. This section walks through the background and design process for the four architectures possible from these two choices.

Staging vs. Single Engine

The inspiration for the two staged propulsion approach comes from the 1960's era design of NASA's Surveyor spacecraft which conducted soft landings on the Moon.[59] A schematic of the Surveyor landing time line is shown in Figure 5.15.

In this staged architecture, a majority of the arrival and landing ΔV is provided by a solid rocket motor. After the solid rocket motor has burned out, it is dropped, reducing the mass of the lander. The remaining small amount of ΔV required to null out the spacecraft's vertical velocity coincident with the spacecraft's arrival at the surface is provided by a second liquid engine.

The alternate to this staged approach is to use a liquid engine to provide all of the ΔV necessary for both arrival and landing, similar to the approach used by the Apollo lunar module during its landing phase (illustrated in Figure 5.16). [60]

It should be noted that these two architectures (staged and non-staged landing) are only applicable to the Moon or other airless target bodies. For arrival at Mars (or any other target body with an atmosphere), a more sophisticated entry, descent, and landing (EDL) scheme involving an aerothermal protection stage would be required.

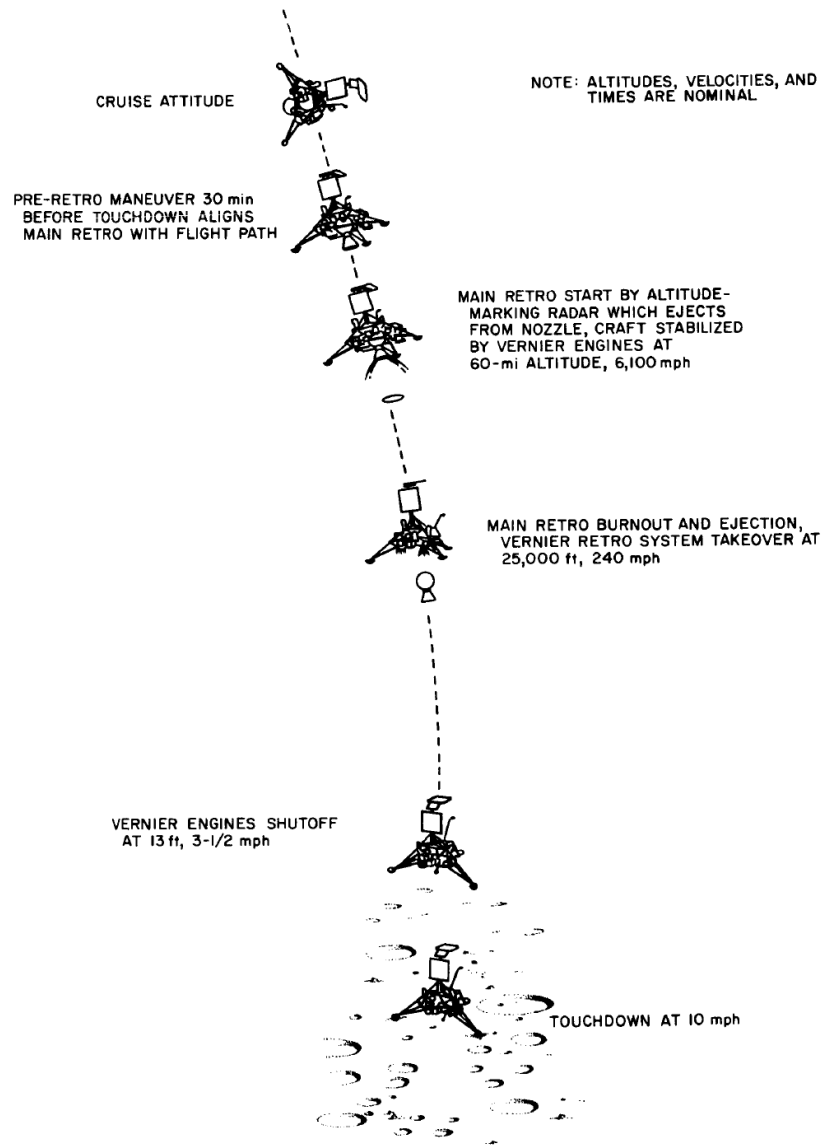


Figure 5.15: Schematic of Surveyor's Two-Stage Landing Method [59]

Solid Rocket Motor For two-stage propulsion architectures, the solid rocket motor is chosen by computing the propellant mass needed in the solid rocket motor, then looking up the smallest solid motor that will meet the requirements from a catalog of solids. From the rocket equation, the minimum propellant needed in the solid is:

$$m_{prop_{solid}} = \left[\exp \left(\frac{\Delta V}{I_{sp} \text{ solid} g_0} \right) - 1 \right] (m_{wet_{lander}} + m_{empty_{solid}}) \quad (5.51)$$

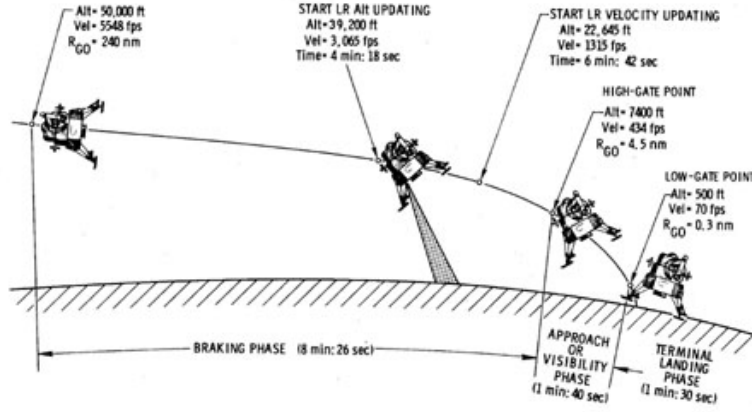


Figure 5.16: Schematic of the Apollo Lunar Module's Landing Phase [60]

- where $m_{prop_{solid}}$ = Propulsion mass of the solid motor
 $m_{empty_{solid}}$ = Inert mass of the solid motor
 $m_{wet_{lander}}$ = Wet mass of the lander (without solid stage)
 ΔV = Velocity change of the lander
 $I_{sp_{solid}}$ = Specific impulse of the solid

It should be noted that the ΔV used here is the sum of the $\Delta V_{Landing}$ and $\Delta V_{Arrival}$. The liquid propulsion system is allocated $0.25\Delta V_{Landing}$ for the terminal descent, allowing for 25% margin on the descent ΔV . As mentioned above, using the computed value of $m_{prop_{solid}}$, the appropriate solid rocket motor is determined from a lookup table (Table 5.10, taken from a subset of the ATK Space Propulsion Catalog).

Table 5.10: Solid Motor Selection [61]

Name	I_{sp} [s]	Total Mass [kg]	Empty Mass [kg]	Prop. Mass [kg]
Star 17A	286.7	125.6	13.3	112.3
Star 24	282.9	218.2	18.3	199.9
Star 27	289.0	365.0	27.4	337.6
Star 30	293.0	542.8	26.6	516.2

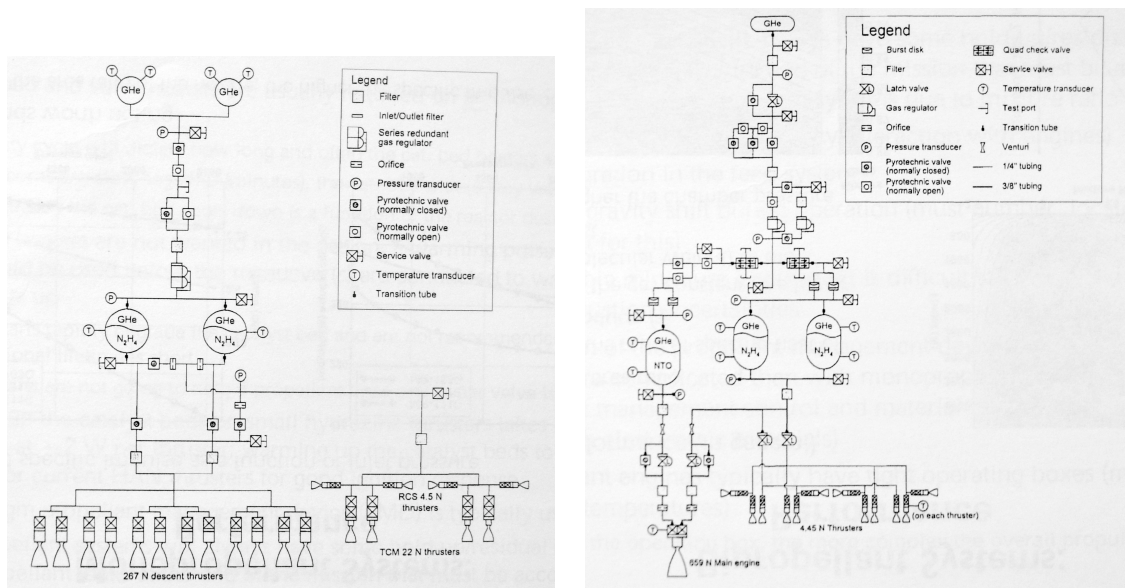
If the required propellant is less than the max propellant load of the motor, the motor is only partially loaded to 110% of the required propellant mass or the maximum propellant load (whichever is less).

If there is no staging, then the liquid propulsion system is responsible for providing the full ΔV ($\Delta V_{Liquid} = \Delta V_{Landing} + \Delta V_{Arrival}$).

Monopropellant vs. Bipropellant

The second decision is whether to use a monopropellant system or bipropellant system. Both have flight heritage in a landing application: the Lunar Surveyor missions used a bipropellant terminal descent system, and the Mars Viking missions used a monopropellant terminal descent system. A bipropellant system will typically have a larger inert mass, due to having twice the number of propellant tanks; a larger number of valves, filters, and other fillings; and heavier engines. A bipropellant system has a higher I_{sp} , which can offset the larger higher inert masses for bigger propulsion systems.

To illustrate the additional complexity of a bipropellant system, flow diagrams of the Mars Polar Lander (monopropellant) and Mars Global Surveyor (bipropellant) liquid propulsion systems are shown in Figure 5.17.



(a) Flow Diagram of the Mars Polar Lander Propulsion System (Monopropellant) (b) Flow Diagram of the Mars Global Surveyor Propulsion System (Bipropellant)

Figure 5.17: Comparison of Monopropellant and Bipropellant Propulsion Systems [62]

For the purposes of this project, the following propellant characteristics are assumed about the two liquid propulsion options:

The trade off between monopropellant and bipropellant systems typically occurs

Table 5.11: Propellant Characteristics

	Fuel	ρ_{Fuel} [kg/m ³]	Oxidizer	ρ_{Ox} [kg/m ³]	I_{sp} [s]
Monopropellant	N_2H_4	1004	-	-	230
Bipropellant	N_2H_4	1004	N_2O_4	1450	330

around 20,000 N-s of total impulse according to reference [63], as shown in Figure 5.18. For a given terminal ΔV , one can calculate the lander dry mass below which it would be more mass efficient to use a monopropellant system:

$$\frac{20000[Ns]}{\exp\left(\frac{\Delta V}{230[s]g_0}\right) - 1230[s]g_0} = m_{dry} \quad (5.52)$$

For a 300 m/s terminal ΔV , this corresponds to 63 kg.

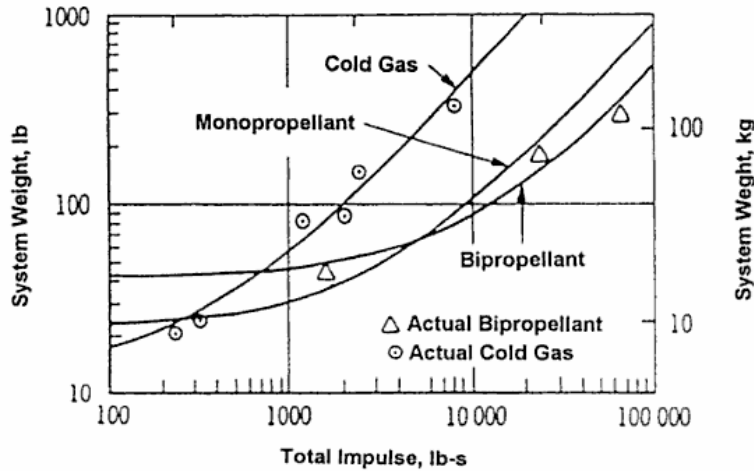


Figure 5.18: Liquid Propulsion System Weight Comparison [63]

Liquid Engine Sizing To select the components of the propulsion system, again lookup tables are utilized. In order to select the terminal descent engine(s), it is assumed that the engine(s) must provide a thrust equal to twice the wet weight of the lander on the target body:

$$T_{\text{req}} = 2g_{\text{body}}m_{\text{wet}} \quad (5.53)$$

For a monopropellant propulsion system, find the engine with the lowest mass, with a thrust greater than T_{req} , in Table 5.12:

Table 5.12: Monopropellant Engine Selection

Name	Thrust [N]	Number	Unit Mass [kg]	Total Mass [kg]
MR-107B	178	1	0.88	0.88
MR-107B	356	2	0.88	1.76
MR-107B	534	3	0.88	2.64
MR-107B	712	4	0.88	3.52
MR-107N	1184	4	0.74	2.96
MR-104	2288	4	1.86	7.44
MR-104	3432	6	1.86	11.16

For a bipropellant propulsion system, find the engine with the lowest mass, with a thrust greater than T_{req} , in Table 5.13:

Table 5.13: Bipropellant Engine Selection

Name	Thrust [N]	O/F Ratio	Number	Unit Mass [kg]	Total Mass [kg]
R1-E	111	1.65	1	2.0	2.0
R1-E	222	1.65	2	2.0	4.0
R1-E	333	1.65	3	2.0	6.0
R4-D	490	1.65	1	3.76	3.76
R-42	890	1.65	1	4.53	4.53
R-42	1780	1.65	2	4.53	9.06
R-42	2670	1.65	3	4.53	13.59
R-40A	3870	1.60	1	10	10

Propellant and Tank Sizing To calculate the propellant and tank masses, an iterative method is used. The tank, propellant and pressurant masses are initially set to zero. In each step of the iteration, the values are recalculated, using values from the previous iteration to converge on a viable solution.

The first step is to find the propellant mass, which is calculated with the rocket equation:

$$m_{\text{prop}} = m_{\text{dry}} \left(\exp \left(\frac{\Delta V}{I_{\text{sp}} g_0} \right) - 1 \right) \quad (5.54)$$

For the bipropellant option, the fraction of propellant mass that is fuel or oxidizer is found as a function of the oxidizer-to-fuel (O/F) ratio:

$$m_{\text{fuel}} = m_{\text{prop}} \left(\frac{1}{1 + OF} \right) \quad (5.55)$$

$$m_{\text{fuel}} = m_{\text{prop}} \left(\frac{OF}{1 + OF} \right) \quad (5.56)$$

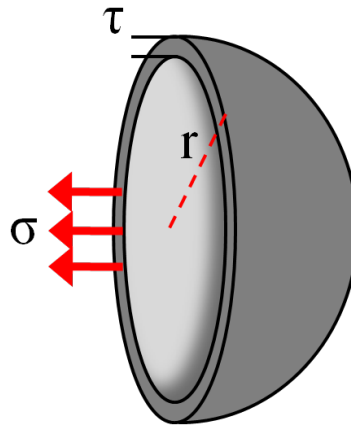


Figure 5.19: Cutaway Diagram of a Spherical Tank

It is assumed that spherical Titanium tanks (Figure 5.19) are used. The formulas for finding the radius and mass of a generic spherical tank are as follows:

$$r_{\text{tank}} = \left(\frac{3}{4} \frac{m_{\text{liq}}}{\rho_{\text{liq}} N_{\text{tanks}} \pi} \right)^{1/3} \quad (5.57)$$

$$m_{\text{tank}} = 4\pi r_{\text{tank}}^2 \left(P_{\text{tank}} \frac{r_{\text{tank}} SF}{2\sigma_{\text{tank}}} \right) \rho_{\text{tank}} N_{\text{tanks}} \quad (5.58)$$

where m_{liq} = Mass of tank fluid
 ρ_{liq} = Density of tank fluid
 N_{tanks} = Number of tanks
 P_{tank} = Tank pressure
 σ_{tank} = Tank material maximum allowable stress (after safety factor)
 ρ_{tank} = Tank material density
 SF = Tank safety factor

For the purposes of this analysis, it is assumed that the propellant tanks are operated at a pressure of 2 MPa, using Titanium ($\sigma = 900$ MPa) and a safety factor of 3.

The liquid propulsion system is assumed to be pressure fed. A tank containing high pressure helium is regulated down to pressurize the fuel and oxidizer tanks. The volume of pressurant is:

$$V_{pres} = \frac{V_{fuel} + V_{ox}}{PR^{1/\gamma} - 1} \quad (5.59)$$

From the ideal gas law, the mass of pressurant is:

$$m_{pres} = \frac{P_{tank}PRV_{pres}}{R_{He}T} \quad (5.60)$$

where V_{pres} = Pressurant volume
 V_{fuel} = Fuel volume
 V_{ox} = Oxidizer volume
 PR = Pressurant tank pressure ratio (assumed to be 10)
 γ = Ratio of specific heats
 m_{pres} = Pressurant mass
 R_{He} = Pressurant gas constant (2057 J/kg/K for He)
 T = Pressurant temperature (assumed to be 200 K)

The pressurant tank mass is found by the same method described for the fuel and

oxidizer tank masses.

Other Inert Mass Other inter masses for the propulsion system include lines, valves, regulators and other fillings. All lines are assumed to have a mass of 5 kg. Due to the added complexity of the bipropellant system, it will have more valves and fittings than the monopropellant system. An estimate of the number of fill valves, filters, pyro valves, regulators, orifices, and latch valves that would be needed for each system was made, and masses were estimated for each valve type. These valves are assumed to have a total mass of 5.65 kg for the monopropellant system and 10.40 kg for the bipropellant system.

Finally, for attitude control the propulsion subsystem is assumed to have twelve 1 N monopropellant thrusters. Representative properties for an Aerojet MR-103C thruster are shown in Table 5.14. A total of 4 kg is allocated for these ACS thrusters.

Table 5.14: Attitude Control Thruster Characteristics

Property	Unit	Aerojet MR-103C
Mass	[kg]	0.33
Thrust	[N]	0.22 - 1.02
Propellant	[-]	N_2H_4
Isp	[s]	209 - 224

5.11.3 Propulsion Validation

The propulsion system model was validated by comparing its results to the known masses of four missions: JPL's Lunette mission concept, NASA's Surveyor lunar lander, and the Russian Luna 15 and Luna 21 missions to the moon.[8, 59, 56] Surveyor used a two-staged solid/bi-propellant propulsion system to achieve a soft lunar landing. The Lunette mission proposes to use a solid/mono-propellant propulsion system for landing. The Luna missions used a bi-propellant only propulsion system to land on the moon. The landed dry masses and launch masses for these four systems are shown in Figure 5.20, along with the dry and launch masses for 1000 randomly generated lander architectures.

In Figure 5.20(a), both the Surveyor and Lunette masses lie very close to the predicted masses for a two-staged bipropellant and two-staged monopropellant system respectively. In Figure 5.20(b), the two Luna missions follow the mass trend exhibited by the bipropellant only architectures as calculated by the propulsion model.

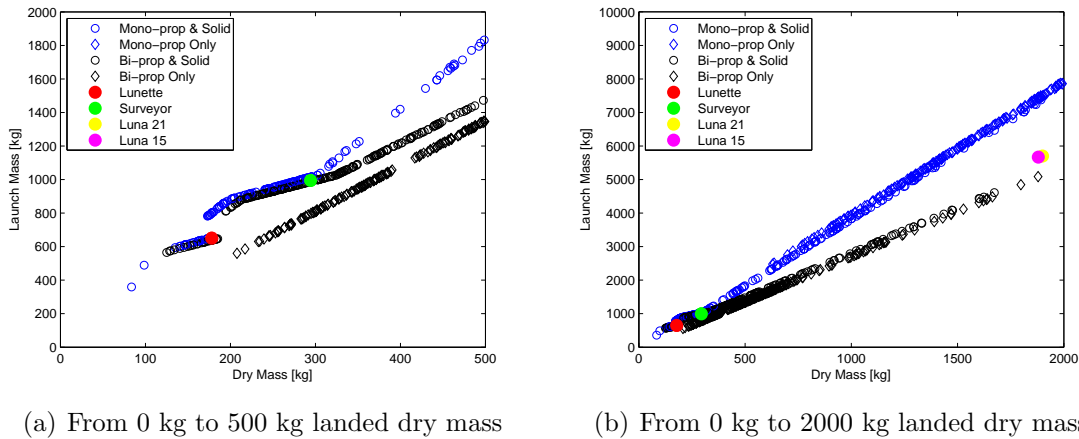


Figure 5.20: Launch mass vs. landed dry mass for sample lunar lander architectures

5.12 Mass Module

The mass properties module is responsible for determining the overall mass of the spacecraft at different points throughout the mission. Masses from all the other subsystems are given as inputs to the mass module, which in turn reports the spacecraft total mass as its output. The three masses reported by this module are:

- *Dry mass*: Mass of the spacecraft without propellant, solid motor, or carrier stage.
- *Wet mass*: Dry mass and propellant mass
- *Launch mass*: Wet mass, solid rocket motor mass, and carrier stage mass

The expressions for these masses are:

$$m_{\text{dry}} = m_{\text{instruments}} + m_{\text{comm}} + m_{\text{avionics}} + m_{\text{GNC}} + \dots$$

$$m_{\text{power}} + m_{\text{thermal}} + m_{\text{structures}} + m_{\text{propulsion,dry}} \quad (5.61)$$

$$m_{\text{wet}} = m_{\text{dry}} + m_{\text{propellant}} \quad (5.62)$$

$$m_{\text{launch}} = m_{\text{wet}} + m_{\text{solid rocket}} + m_{\text{carrier}} \quad (5.63)$$

The mass module is included in an iterative loop along with the Power, Thermal, Propulsion, Structures and Carrier modules. This loop iterates until the spacecraft mass converges.

5.13 Carrier Module

The carrier module is responsible for sizing an additional element of the flight system, the carrier or cruise stage, which remains attached to the spacecraft from launch, through cruise, and until the beginning of the descent phase. This flight system is responsible for providing any additional power the spacecraft may need during cruise, sensing the orientation and position of the spacecraft during cruise, and providing structural interface in the launch vehicle. If a two stage solid-liquid descent architecture is chosen, the solid rocket motor would be integrated with the carrier stage.

The mass of the carrier stage is estimated to be 10% of the launch mass:

$$m_{\text{carrier}} = 0.1m_{\text{launch}} \quad (5.64)$$

5.14 Launch Module

The launch module determines which launch vehicle the spacecraft will fit on. The inputs to this model are the required C^3 (characteristic energy) from the orbits module; and m_{launch} (mass at launch) from the mass module. A launch vehicle mass margin of 30% is assumed; ie. the launch vehicle must be capable of carrying:

$$m_{\text{payload}} = m_{\text{launch}}(1 + LV_{\text{margin}}) \quad (5.65)$$

Using this information, the smallest launch vehicle capable of carrying this mass is determined. This is done by interpolating the launch mass capability of a launch vehicle based on the data in Table 5.15 and the required C^3 . The values in Table 5.15 come from the NASA Launch Services Program.[64]

Table 5.15: Launch Vehicle Payload Mass [kg] vs. C^3 [km^2/s^2]

Characteristic Energy C^3	-5	-2	0	2.5	5
Delta II (2920-10L)	715	640	570	460	325
Delta II (2920-10)	745	670	600	490	355
Delta II (2920-9.5)	820	740	665	595	530
Delta II (2425-10)	835	790	750	700	675
Delta II (2425-9.5)	865	815	775	710	690
Delta II (2920H-10L)	940	855	775	730	630
Delta II (2920H-10)	970	885	805	730	660
Delta II (2920H-9.5)	1015	925	845	770	695
Delta II (2925-10L)	1290	1220	1155	1095	1040
Delta II (2925-10)	1315	1245	1180	1120	1060
Delta II (2925-9.5)	1375	1300	1235	1170	1110
Delta II (2925H-10L)	1520	1440	1370	1295	1230
Delta II (2925H-10)	1550	1465	1390	1320	1250
Delta II (2925H-9.5)	1585	1500	1425	1350	1280
Falcon 9 (9)	2385	2195	2010	1835	1670
Atlas V (501)	2975	2825	2680	2540	2405
Delta IV (4040-12)	3075	2900	2735	2570	2415
Atlas V (401)	3785	3615	3445	3285	3130
Atlas V (511)	4155	3955	3765	3595	3435
Delta IV (4240-12)	4520	4290	4075	3860	3660
Atlas V (521)	4965	4750	4545	4345	4120
Delta IV (4450-14)	5075	4825	4580	4345	4145
Atlas V (531)	5700	5450	5210	4980	4760
Atlas V (541)	6360	6085	5820	5570	5325
Atlas V (551)	6920	6620	6330	6055	5790
Delta IV (4050H-19)	10115	9695	9305	8920	8545

A quadratic interpolation scheme is used to find the mass performance of the launch vehicles as a function of C^3 , as the mass performance of a launch vehicle is typically a second-order polynomial function of C^3 . In Figure 5.21, example curves

of launch vehicle mass performance vs. C^3 are shown.

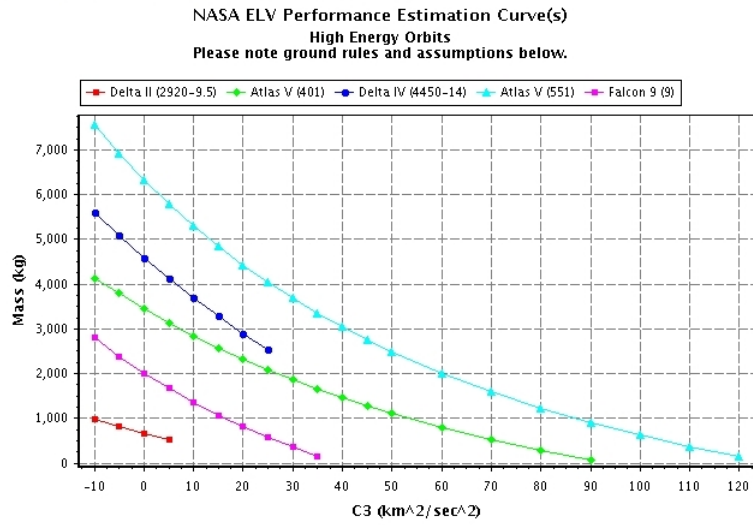


Figure 5.21: Launch vehicle performance vs. C^3 [64]

5.15 Conclusion

In closing, this Chapter has demonstrated a methodology for estimating the overall size of a planetary lander spacecraft, including the specific subsystem masses and power properties, the required launch vehicle, as well as a number of other performance parameters.

The following Chapter outlines how this Engineering Model along with the Science Value Model developed in Chapter 4 may be used together to conduct a tradespace exploration. The systems level validation of the Engineering Model is also presented in the following chapter.

Chapter 6

In Situ Lunar Mission Case Study

6.1 Overview

In Chapter 3 we explained the mathematical framework for tradespace exploration and optimization. In Chapter 4 we developed a model for estimating the science value of a scientific payload. In Chapter 5 we developed an engineering model for conducting the preliminary sizing a robotic lunar lander. The goal of this chapter is to bring these three elements together and to present an integrated view of the tradespace exploration of potential *in situ* lunar spacecraft designs.

This chapter is organized as follows: Section 6.2 details the validation of the engineering model presented in Chapter 5. The design of Lunette, the JPL mission concept against which the model is validated, serves as the basis for further investigations with this model. In Section 6.3, probabilistic Monte Carlo trade space exploration method is demonstrated, as well as several alternate science utility metrics. Finally, in Section 6.4, a Multi-Objective Simulated Annealing method is demonstrated.

6.2 Engineering Model Validation

In order to gain confidence in the engineering model presented in Chapter 5, it is validated against historical spacecraft data and detailed mission concept studies. The validation process is conducted by constructing a design vector representative of a

reference mission, running the design through the engineering model, and comparing the results of the model to the reference design.

In this section the four missions used for validation are described, then results from a subsystem-level validation and a system-level validation are presented.

6.2.1 Validation Reference Missions

Four reference missions are used to validate the engineering model. They are: JPL's Lunette mission concept [8, 9, 10], NASA's International Lunar Network mission concept (a nuclear and solar variant) [65], and NASA's Lunar Surveyor spacecraft from the 1960's [59, 66, 56]. All four of these designs are *in situ* spacecraft—they are designed for a soft landing on the lunar surface and a sustained operational duration of weeks to years. Figure 6.2 shows the designs of the four missions that were used for validation of the engineering model.

This set of validation missions is not an exhaustive list of *in situ* robotic lunar spacecraft. The Soviet Union had a robust program of lunar exploration from 1959 to 1976 under the *Luna* program. This included seven successful soft landings on the moon, with two *Lunokhod* rovers, and three sample return missions.[56] Unfortunately little data is available on the specific designs of these missions, so they are not used in this validation effort.

The Apollo Lunar Module (LM) also conducted soft landing on the moon six times from 1969 to 1972. Due to the fact that these were manned missions and in the 10,000 kg class, their designs are significantly outside the range of validity for this model, and as such are not used for validation.

There are also a number of proposed future missions to the moon, including several soft landers not already mentioned. The European Space Agency has plans to send a lander (see Figure 6.1(a)) under the MoonNEXT program to the Moon's South Pole-Aitken Basin in the 2013–2015 time frame. This proposed lander would be in the 650 to 800 kg range; it is currently undergoing Pre-Phase A studies. [67]

The Japanese Space Agency (JAXA) is also undertaking studies for a lander under the auspices of the SELENE-2 program (see Figure 6.1(b)). Preliminary studies for

this 2015–2020 mission have identified three options: a 1000 kg lander with a 100 kg rover and a dedicated 100 kg lunar communications satellite; a 800 kg lander with a 100 kg rover and 500 kg lunar orbiter; and a network mission of two or more 500 kg landers. [68]



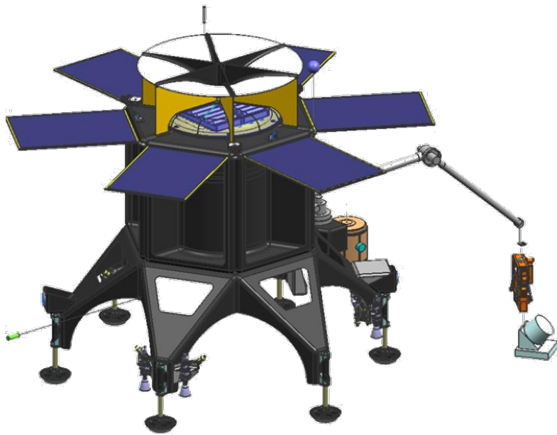
(a) ESA's proposed MoonNEXT lander concept



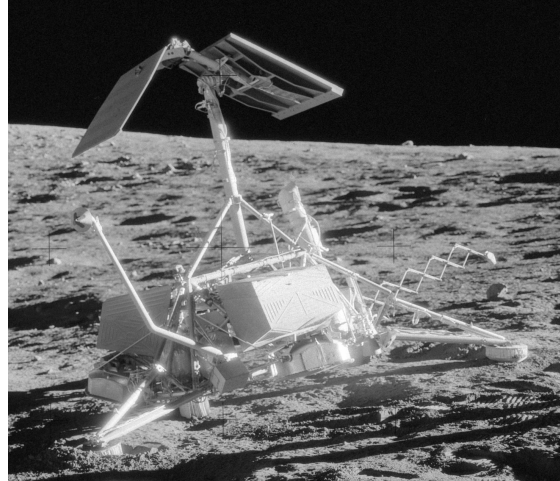
(b) Equatorial variant of JAXA's proposed SELENE-2 lander

Figure 6.1: Proposed lunar lander missions

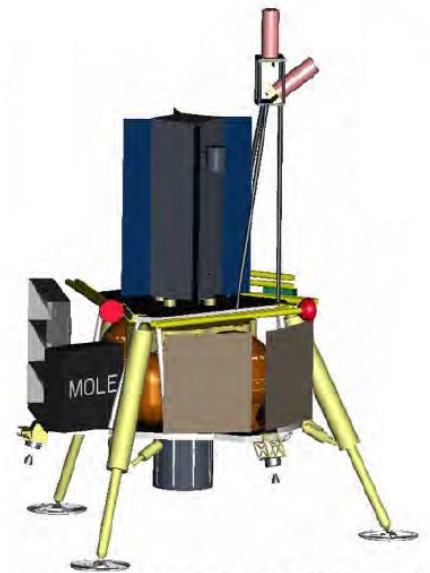
Unfortunately insufficient data about the MoonNEXT or SELENE-2 missions was available to validate the model using their designs.



(a) Lunette geophysical lander [10]



(b) Surveyor 3 (Photo by Apollo 12 Crew)



(c) ILN nuclear variant [65]



(d) ILN solar variant [65]

Figure 6.2: Missions for engineering model validation

Lunette

Lunette is a Discovery-class mission concept currently being developed by NASA's Jet Propulsion Laboratory. The scientific goals of this mission are to establish a two-node geophysical network on the moon and study its internal properties. These goals are strongly aligned with SCEM Concept 2 (see Section 4.2.2). The science payload will include: a seismometer, an electric field sensor, a magnetometer, a Langmuir probe, a heat flow probe, and a retro-reflector. This mission has been designed with the goal

of minimizing the cost where ever feasible, drawing from off-the-shelf equipment and limiting the use of technologies still in development. An image of the Lunette lander is shown in Figure 6.2(a).

Using detailed subsystem mass numbers from the most recent Lunette mission study provided by JPL [10], Lunette is used as the basis for validation of the engineering model's subsystem mass estimates. The results of this validation are shown in Section 6.2.2.

International Lunar Network

The International Lunar Network (ILN) is a mission concept being developed by NASA under the Lunar Precursor Robotic Program.[4] The scientific goals of the ILN are to study the internal structure and properties of the moon, in line with SCEM Concept 2 (see Section 4.2.2). The ILN would consist of 2 to 4 landers distributed globally over the lunar surface. The data from these landers could be coupled with landers from other concurrent geophysical landers developed by international partners to improve the science value. The baseline science payload for the ILN consists of a seismometer, an electrometer, a magnetometer, a Langmuir probe, a heat flow probe, and a retro-reflector.[69]

In its early studies for the ILN, NASA has identified two design variants: a nuclear powered lander (Figure 6.2(c)) and a solar powered lander (Figure 6.2(d)). The nuclear powered lander uses an Advanced Sterling Radioisotope Generator to provide power; this allows it to operate at full power over the lunar night, and does not require large batteries. The ILN nuclear variant has a payload mass of 23 kg, a wet mass of 200 kg (260 kg after 30% contingency), and a launch mass of 613 kg (798 kg after 30% contingency).

The solar variant of the ILN lander must operate in a low power mode during the lunar night, resulting in lower total science data return. It is significantly larger than the nuclear variant due to the large batteries required for operations during the 14 day lunar night. The ILN solar variant has a payload mass of 19 kg, a wet mass of 325 kg (422 kg after 30% contingency), and a launch mass of 895 kg (1164 kg after

30% contingency).

Surveyor

The Surveyor program consisted of seven missions from 1966 to 1968, developed by JPL, with the goal of a soft landing on the lunar surface. Five of these missions were successful in landing. The science goals of Surveyor were to characterize the lunar environment prior to the manned Apollo landings, demonstrate the technology required for a soft landing, and to broadly “add to the scientific knowledge of the moon”. [66] The scientific payload included on the Surveyor missions was: a TV camera, strain gauges, the soil mechanics surface sampler (only on 3,4 & 7), an α -proton spectrometer (only on 5, 6, & 7), temperature sensors, and magnets. [56] These missions did not operate at night, but were capable of surviving the lunar nighttime. For the purposes of validation, the instruments and masses from Surveyor 7 are used). An image of Surveyor 3 is shown in Figure 6.2(b).

Validation Design Vector

The next step in the model validation process is to generate design vectors that are representative of the reference missions. Using the four missions outlined above: Lunette, ILN (Solar & Nuclear), and Surveyor 7, design vectors have been constructed for each. These are shown in Table 6.1.

Table 6.1: Validation Design Vector

Parameter	Units	Lunette	ILN Nuclear	ILN Solar	Sur- veyor
Payload Mass	[kg]	12.7	23.0	19.2	32.2
Payload Power	[W]	26.4	74	14.9	30.5
Lifetime	[yr]	2	6	6	0.25
Landing Latitude	[°]	85	30	30	0
Power Source	-	Solar	RPS	Solar	Solar
Battery Type	-	LiIon	LiIon	LiIon	NiH
Solar Panel Type	-	Multi junction GaAs	-	Multi junction GaAs	Si
Radio Frequency	[GHz]	2.1	2.1	2.1	2.1
Data Rate	[bits/s]	45×10^3	20×10^3	20×10^3	4400
Antenna Gain	[dB]	7	0	0	27
Transfer Orbit	-	WSB	Hohmann	Hohmann	Hohmann
Descent Method	-	Staged	Staged	Staged	Staged
Propellant	-	Monoprop	Biprop	Biprop	Biprop

6.2.2 Validation Results

The next step in the model validation process is to run a mission representative design vector through the engineering model and compare the results to values from the reference mission study or spacecraft. Due to the lack of detailed subsystem mass data available for all four missions, this step is divided into two parts: a subsystem level validation and a flight system level validation.

Subsystem Validation

The subsystem level validation is conducted with the Lunette design vector. (See Table 6.1) These variables were fed into the engineering model; the masses of each spacecraft subsystem generated by the engineering model were then compared to the Lunette MEL (Master Equipment List). This comparison is shown in Figure 6.3 and Table 6.2.

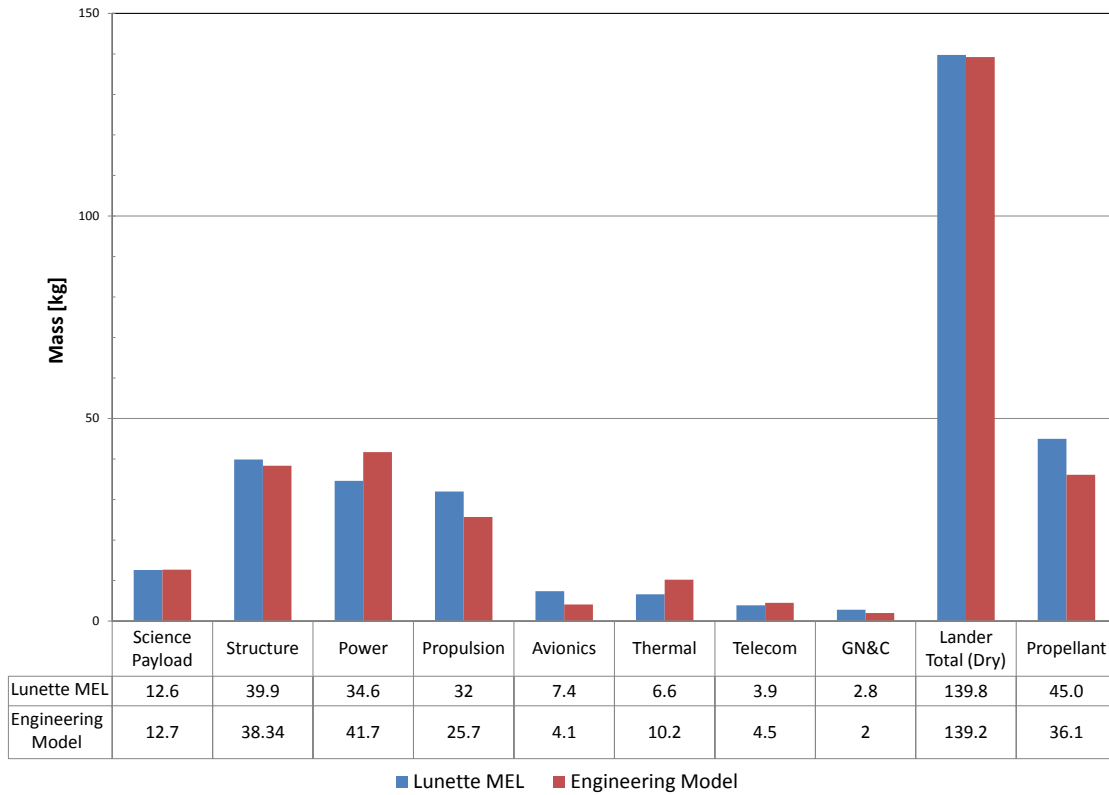


Figure 6.3: Engineering model subsystem validation against JPL’s Lunette mission concept

Table 6.2: Engineering model subsystem validation against JPL’s Lunette mission concept with differences highlighted

	Lunette MEL	Engineering Model	Difference [%]	Difference [kg]
Science Payload	12.6	12.7	0.79%	0.1
Structure	39.9	38.34	-3.91%	-1.6
Power	34.6	41.7	20.52%	7.1
Propulsion	32	25.7	-19.69%	-6.3
Avionics	7.4	4.1	-44.59%	-3.3
Thermal	6.6	10.2	54.55%	3.6
Telecom	3.9	4.5	15.38%	0.6
GNC	2.8	2	-28.57%	-0.8
Lander Total (Dry)	139.8	139.2	-0.37%	-0.5
Propellant	45.0	36.1	-19.78%	-8.9

The overall dry mass discrepancy between the detailed Lunette study and the engineering model is less than 1%, however this does not tell the whole story. Four subsystems out of nine have mass discrepancies greater than 20% (Power, Propulsion, Avionics, and Thermal). No mass discrepancy is greater than 10 kg, and these four largest are the only discrepancies to exceed 4 kg. Each of these discrepancies can be explained in some way.

Upon closer inspection, the main deficit in the as-modeled propulsion subsystem mass is due to an undersizing of the tanks. This is due to two factors: a slight underestimation of the empty tank density, and a lower estimate of the tank volume (and thus mass). The low tank volume is tied to the underestimation of the propellant mass. This in turn is due to the extra propellant and Delta-V margins held by JPL at this stage in the design process. This engineering model does not include margins, which accounts for some of the discrepancy. The thermal subsystem was validated more completely in Section 5.11.3, in which it was shown to provide robust values across a wider range of inputs.

The avionics mass estimate is based on a very simple model, given solely as a function of the system's data rate. This obviously does not capture the level of complexity of the spacecraft's avionics system and should be an area of future work.

Finally, the power and thermal models both over estimate their subsystem masses. The power mass error can primarily be linked to uncertainty about the nighttime power loads. The thermal subsystem error is likely due to the simplified single node thermal model. The Lunette thermal design is also rather novel, involving a warm enclosure box and a variable position radiator. A more detailed model accounting for the heat conductivity of the avionics enclosure would likely resolve this issue, and lower the required mass for dissipating thermal energy.

In conclusion, while this engineering model has a number shortfalls and there are many areas that have been identified for improvement, this model does demonstrate rough order accuracy sufficient for broad trade studies. Overall, the average subsystem mass accuracy is 17%. Mass estimates from this model should be considered to be valid only to within 15-20% as a result of this validation. Further work may be

able to increase the confidence in this model.

Flight-System Mass Validation

The flight system level validation is conducted with a broader set of four missions outlined previously. Again, the same design vector inputs displayed in Table 6.1 are used for the flight system level validation. In this validation, only payload mass, spacecraft dry mass, spacecraft wet mass (dry mass + liquid propellant mass), and spacecraft launch mass (wet mass + carrier stage mass) are considered. Only wet mass and launch mass numbers were available for the ILN missions; for Surveyor only dry mass and launch mass numbers were available. Unfortunately detailed subsystem mass level data was not available for any of these missions other than Lunette. It should be noted that only pre-contingency mass numbers are used, to make sure that a level field is used as the basis for these comparisons.

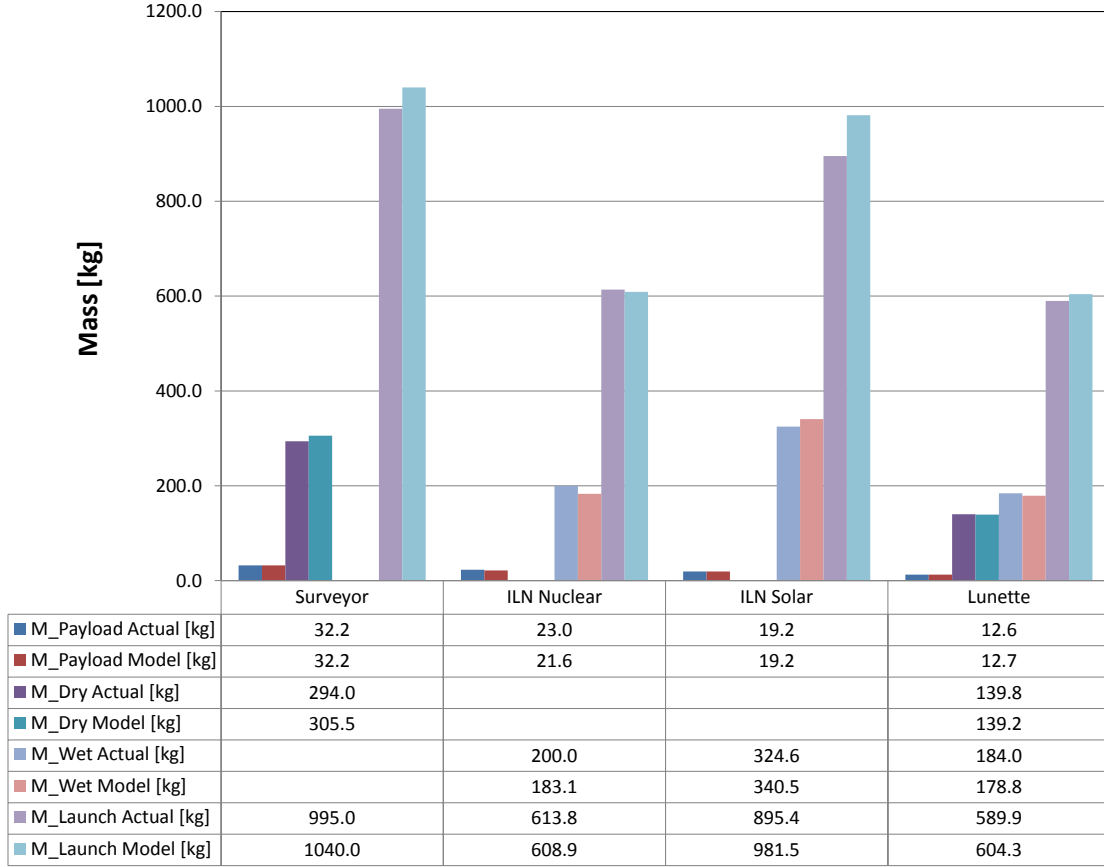


Figure 6.4: Engineering model validation against NASA’s Surveyor missions, NASA’s ILN mission concept, and JPL’s Lunette mission concept

Table 6.3: Engineering model validation against NASA’s Surveyor missions, NASA’s ILN mission concept, and JPL’s Lunette mission concept with differences highlighted

	M_{Dry}				M_{Wet}				M_{Launch}			
	Actual	Model	Error	Error	Actual	Model	Error	Error	Actual	Model	Error	Error
	[kg]	[kg]	[kg]	%	[kg]	[kg]	[kg]	%	[kg]	[kg]	[kg]	%
Surveyor	294.0	305.5	11.5	4%					995.0	1040.0	45.0	5%
ILN Nuclear					200.0	183.1	-17.0	-8%	613.8	608.9	-4.9	-1%
ILN Solar					324.6	340.5	15.9	5%	895.4	981.5	86.1	10%
Lunette	139.8	139.2	-0.6	0%	184.0	178.8	-5.2	-3%	589.9	604.3	14.4	2%

After generating masses from the engineering model for these four missions at the flight system level, the results are shown in Figure 6.4. In the accompanying table, the masses for each flight system configuration from the detailed studies and from the engineering model are shown. Of the missions compared here, the engineering model predicted the mass of every flight system to within 10%.

Without more specific subsystem mass numbers, it is difficult to pin down the reasons for the mass discrepancies seen here. These results are in keeping with the same conclusion reached in the previous section—that the engineering model produces results which are accurate to within 15% to 20%.

6.3 Monte Carlo Analysis

Now that the engineering model has been validated, the next step is begin to explore the shape of the trade space for the *in situ* lunar spacecraft design problem. A first step in understanding the shape of the trade space is to conduct a probabilistic exploration. This is done using a Monte Carlo method (as previously outlined in Section 3.3.3). The design variable space is randomly sampled to generate a set of architectures, the objective values for these are calculated, and the results are plotted. In general, there are two main reasons for mapping the trade space in this way: a current design can be compared to the optimal set of designs, and design updates can be made accordingly; designers can also use this information to select a new design from scratch. After interrogating the trade space, a point design can be selected based on the results of such a study.

In this section we use the Monte Carlo trade space exploration technique to compare JPL’s Lunette mission to the set of optimal architectures. The Pareto optimal solutions, their design specifics, and their interrelationships are also explored.

6.3.1 Sampling the Design Space

The first step in conducting a Monte Carlo trade space exploration is to sample the design space. The variables that make up the design space, and the levels which

they can take, were originally discussed in Section 5.2. They are repeated here for reference, with the exception that the landing latitude and mission lifetime are fixed as parameters, with values taken from the Lunette design of 85° and 2 years respectively.

Table 6.4: Design Variables

Variable	Units	Levels				
Instrument 1	[-]	0	1			
⋮						
Instrument 14	[-]	0	1			
Power Source	[-]	Solar	Nuclear			
Battery Type	[-]	Ni-Cd	Ni-H I	Ni-H II	Ni-H III	LiIon
Solar Panel Type	[-]	Si	Amorp. Si	Ga-As	In-P	Multi junction Ga-As
Data Rate	[bits/s]	5e4	5e5	5e6	5e7	5e8
Antenna Size	[m]	0.05	0.3	1		
Transfer Orbit	[-]	WSB	Hohmann			
Descent Method	[-]	Solid-Staged	Liquid-Direct			
Propellant	[-]	Monopropellant	Bipropellant			

In each step of the Monte Carlo simulation, the variables in Table 6.4 are uniformly sampled to build up a design vector, \mathbf{x} .

The number of possible architectures in the trade space is given by equation 3.8. For the design space we consider here, the number of possible architectures is:

$$\Omega = 2^{14} \cdot 2 \cdot 5 \cdot 5 \cdot 5 \cdot 3 \cdot 2 \cdot 2 \cdot 2 = 98,304,000 \quad (6.1)$$

The Monte Carlo analysis run here, with 2000 iterations, represents approximately 0.002% of the design space.

6.3.2 Running the Model

In each iteration of this analysis, the new design vector was run through the science and engineering models and the objective functions were calculated. The reader will recall that the objective function, \mathbf{J} , consists of the science utility, U , (Equation 4.11) and the lander dry mass, m_{dry} , (Equation 5.63).

The simulation was run over 2000 iterations, and the objective functions for this analysis were plotted, shown in Figure 6.5. Note that only feasible architectures have

been plotted. The Pareto set of optimal designs is highlighted in red. The objective functions for a design vector corresponding to the Lunette mission were also calculated and are plotted in Figure 6.5 as well. These “simulated” Lunette values were used in order to ensure that a similar data set is being compared.

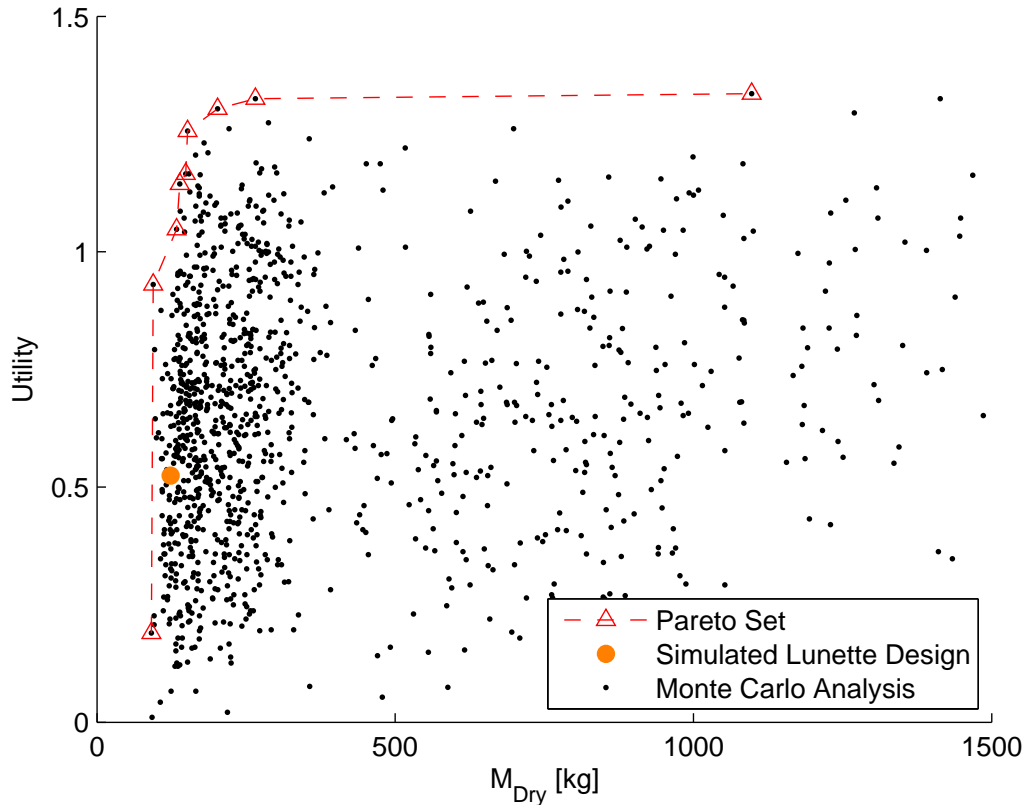


Figure 6.5: Monte Carlo Simulation results of science utility vs. dry mass for 2000 runs

There are a number of features evident in Figure 6.5. The most immediately obvious point is that for the set of instruments investigated here, nearly all of the value can be delivered by a 250 kg class lander. Furthermore, the lightest lander in the Pareto set is approximately 90 kg. The Lunette mission architecture is situated close to the Pareto front, however it only achieves half the utility of the architectures with the highest science utility.

6.3.3 Concept Utility Analysis

One of the downsides of this analysis is that using a single utility metric does not give very much information about the breadth of science of which a mission may be capable. It is unlikely that a mission would ever be flown with the goal of assessing all the lunar science objectives simultaneously; we therefore need a more appropriate science utility metric that provides more granularity. The solution to this is to use the science concept utility vector defined in Equation 4.12. We now have a vector of eight utilities, corresponding to how well a mission assesses each of the eight science concepts for the moon outlined in SCEM.

These eight science utility values were calculated for the same designs as presented in the single utility value Monte Carlo analysis shown in Figure 6.5. Eight plots of each science concept utility versus dry mass for each of the 2000 designs are displayed in Figure 6.6. Here the Pareto front for each science utility value is shown, as well as the Lunette utility values and simulated dry mass.

Figure 6.6 gives a much more complete understanding of the trade space. A number of features can be noted:

- 1) The Pareto optimal designs for science concepts 1, 2, and 3 provide the most value to the planetary science community as recognized by the higher utility values for these concepts (relative to concept 8, for instance).

- 2) The relatively steep slopes of the Pareto fronts for concepts 1, 2, and 5 indicate that the instruments assessing these objectives offer much value for little mass impact.

- 3) The Lunette mission concept has much different utility values for each of the science concepts. Recalling Figure 6.5, Lunette is not Pareto optimal with regards to the overall science utility value, but it is on the Pareto front for SCEM concept 2, and nearly on the Pareto front for SCEM concept 3. SCEM concept 2 is: *The structure and composition of the lunar interior provide fundamental information on the evolution of a differentiated planetary body.* As Lunette is designed as geophysical mission to probe the interior of the moon, this result indicates that the instruments were well selected for this science objective and that the mass has been minimized to

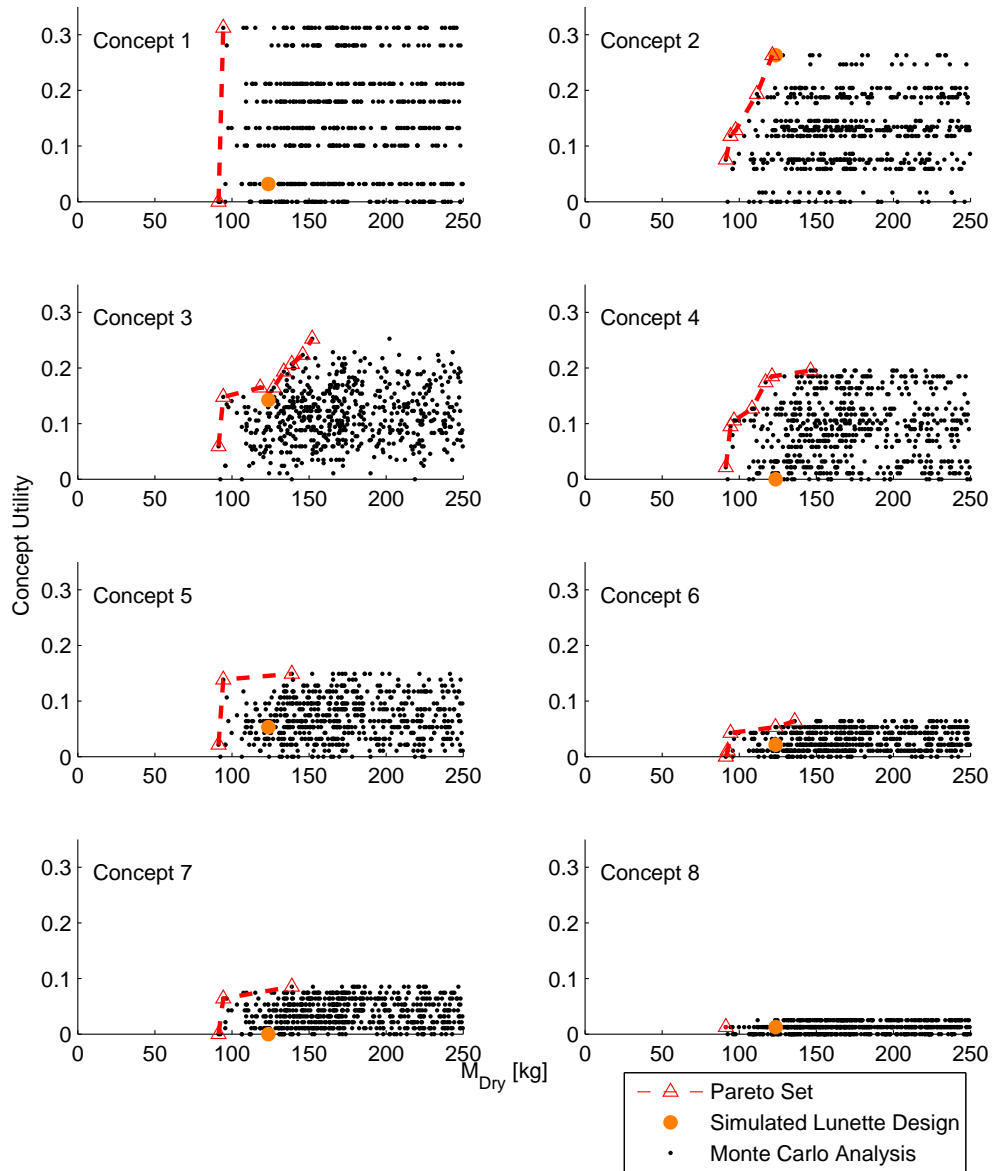


Figure 6.6: Monte Carlo Simulation results of eight elements concept science utility vs. dry mass for 2000 runs

limits according to this model.

6.3.4 Pareto Front Interactions

The results from the science concept utility analysis are promising. We can understand how a mission assesses a set of science goals and identify its strengths and

weaknesses. The next step is to determine if we can use this information to improve a design. Again using the Lunette design as an example, we have shown that it is within the Pareto front for SCEM concept 2, and close to the Pareto front for SCEM concept 3, but is not Pareto optimal when the single utility value is considered.

In order to understand how different the different utility of a design compare to one another, the eight Pareto sets (one for each of the science value concepts) can be plotted together. One of the science concepts can be selected and the eight Pareto sets can be plotted in the space of U_i versus M_{Dry} . Using such a plot, we can identify if there are any architectures which are Pareto optimal with respect to one utility metric and also in the Pareto set for another utility metric, or at least near the Pareto front.

In Figure 6.7, SCEM concept 2 is used as a baseline and the eight Pareto sets are plotted in the U_2 versus M_{Dry} space:

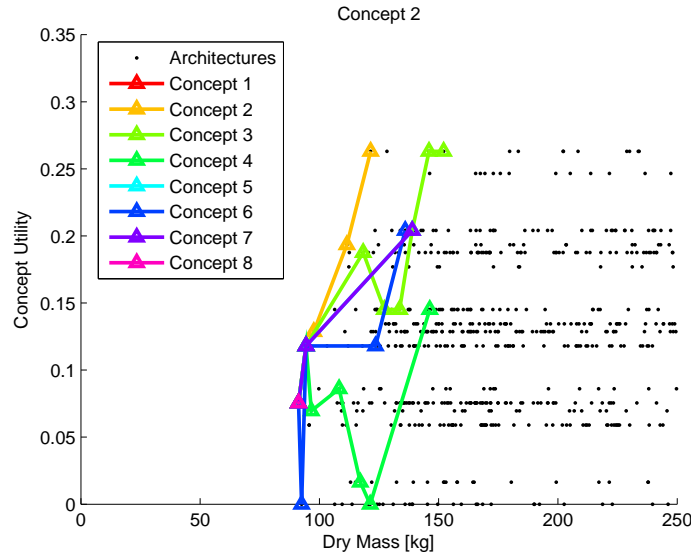


Figure 6.7: Concept 2 Utility vs. Dry Mass for eight concept Pareto sets

From this, we can see that in the 95 kg range, the architectures which are Pareto optimal with regard to concept 2 are Pareto optimal with regard to concepts 3, 4, 6, and 7 as well. We can also see that there are two architectures which are Pareto optimal for concept 3, and which have the maximum utility of concept 2. The instruments selected for these architectures, and for Lunette are shown together with their objective values in Table 6.5. These two designs maintain the same concept

2 utility as Lunette, while providing an 80% and 140% increase in the total utility respectively. The increase in mass required to accommodate these changes is relatively modest: only 4% and 9% respectively.

Table 6.5: Instruments and objective functions for two designs in the SCEM concept 3 Pareto set

Variable	Units	Lunette	Design 1550	Design 1391
Instrument 1 (AGE)	[-]	0	0	1
Instrument 2 (Camera)	[-]	1	1	1
Instrument 3 (MECA)	[-]	0	1	1
Instrument 4 (VAPoR)	[-]	0	0	0
Instrument 5 (LIDAR)	[-]	0	0	0
Instrument 6 (Mini-TES)	[-]	0	0	1
Instrument 7 (APXS)	[-]	0	1	1
Instrument 8 (CP)	[-]	0	0	0
Instrument 9 (EM)	[-]	1	1	1
Instrument 10 (SEIS)	[-]	1	1	1
Instrument 11 (RAD)	[-]	0	1	1
Instrument 12 (MAG)	[-]	1	1	1
Instrument 13 (HF)	[-]	1	1	1
Instrument 14 (Retro)	[-]	1	1	1
Total Utility	[-]	0.524	0.952	1.256
Concept 1 Utility	[-]	0.032	0.133	0.312
Concept 2 Utility	[-]	0.263	0.263	0.263
Concept 3 Utility	[-]	0.142	0.223	0.252
Concept 4 Utility	[-]	0.000	0.127	0.137
Concept 5 Utility	[-]	0.053	0.085	0.149
Concept 6 Utility	[-]	0.021	0.053	0.053
Concept 7 Utility	[-]	0.000	0.043	0.064
Concept 8 Utility	[-]	0.013	0.025	0.025
M_{Dry}	[-]	139	145	152
M_{Launch}	[-]	604	609	603

Overall, this is a very useful method for determining where value can be added to a design in a particular area, while minimizing impacts to other areas.

6.4 Optimization Analysis

As was mentioned before, the Monte Carlo method is not guaranteed to find a globally optimal Pareto set, additionally it explores only a very small fraction of the trade space and can waste time looking in regions which are of no interest to a designer. In order to move closer to a globally optimal set of architectures, more quickly explore the trade space, and reduce the computational effort spent evaluating designs of little interest, a heuristic algorithm is needed.

Here, a Multi-Objective Simulated Annealing (MOSA) algorithm is used. The details of this method are described in Section 3.3.4. A 500 iteration run of the

simulated annealing algorithm was conducted, with the objectives of minimizing the landed dry mass and maximizing the total science utility of the mission.

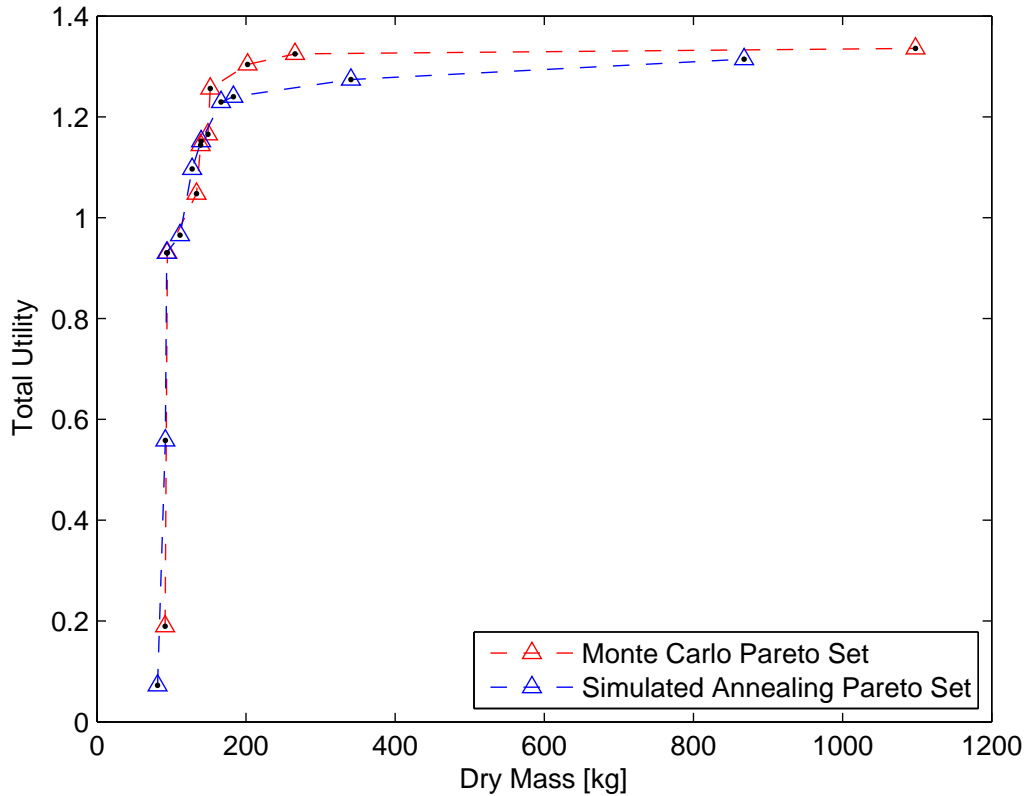


Figure 6.8: Pareto sets for Monte Carlo Analysis and Multi-Objective Simulated Annealing Analysis

The Pareto set identified by the MOSA algorithm is shown, along with the Pareto set identified by the Monte Carlo method in Figure 6.8. From this plot we can see that the Monte Carlo method and the MOSA method identify the same architectures below 175 kg. Above this point, the Monte Carlo simulation performs better.

Future work is needed to understand why the heuristic algorithm does not identify solutions in this region.

The greatest advantage conferred by the use of MOSA is the decrease in run time. With a quarter of the iterations, we can reliably find Pareto set that performs as well as the Monte Carlo method over the region of interest.

6.5 Conclusion

In this chapter we have validated the engineering model, and demonstrated its effectiveness when combined with the science value model to map out a trade space of lunar lander designs. Several science value metrics have been demonstrated which allow a designer to understand the science performance of a mission according to multiple attributes.

Chapter 7

Uncertainty Analysis

Uncertainty is an inherent part of any model. Sometimes the range of uncertainty within a model can be quantified by a designer, and other times the values of the uncertainty remain unknown. This chapter reviews the impact of uncertainty on optimality conditions within a trade space and presents a method for trade space exploration under uncertainty.

7.1 Model Errors

In this study, both the mass estimates generated by the engineering model and the science utility values generated by the science model contain some amount of error. Through the model validation presented in Section 6.2, we can estimate that the masses reported are known within 15% to 20%. The uncertainties in the science model may come from the instrument-objective weights being incorrect or not properly reflecting the sentiments of the planetary science community. The model itself may be flawed if the conditions for using Multi-Attribute Utility Theory (see Section 4.6) are not met.

Whatever the sources of uncertainty, we can be certain that they exist. The uncertainties present in the model will affect the optimal set of architectures this methodology might report to a designer. An example of how this problem presents itself is shown in Figure 7.1.

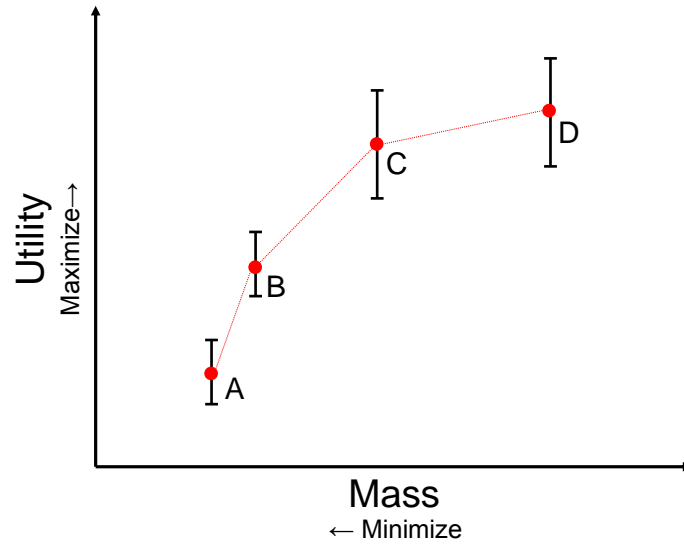


Figure 7.1: Example of uncertainty in architectures

Here we have four architectures: A, B, C, and D, each which have uncertain utility values as indicated by the error bars. It is clear that architectures A and B are non-dominated with respect to one another, even under uncertainty, as their error bars do not overlap. Even if the utility of A takes its maximum value and the utility of B takes its minimum value, the utility of architecture B will be greater than that of architecture A.

Looking at architectures C and D, it is no longer clear that they are always non-dominated. As their utility error bars overlap, it is possible that architecture C dominates architecture D. Based on this example, in order to be able to make intelligent decisions with these uncertain models, it is important for designers to have an understanding of how this uncertainty maps to the trade space.

7.2 Trade Space Exploration Under Uncertainty

There are several ways to estimate the effects of model uncertainty. The traditional method is to estimate all the errors present in the models, and combine them into a single error measurement for each dimension of the objective function. This is a cumbersome process and requires a detailed level of knowledge about the deficiencies

of the model — information that may be difficult or impossible to get for a problem with little historical or analogous reference data.

A second method to estimate the effects of model uncertainty is to ask the question: *How uncertain does the model have to be in order to affect the outcome?* If our goal is to find Pareto optimal designs, we can use this method to determine how far into the trade space we may have to look to find the possible set of Pareto architectures in an uncertain environment. This is done by varying the estimates of uncertainty and mapping the Pareto-field. Designers can estimate what they think the uncertainty within an objective might be, then use more detailed methods depending on the level of overlap within the design space.

7.2.1 ϵ -Pareto Set

Our goal is to find all the architectures that are within some distance, dictated by the level of uncertainty, from the Pareto set. In order to find this “ ϵ -Pareto set” we introduce the concept of ϵ -dominance.[70] This is related to the concept of dominance presented in Section 3.2. The mathematic statement of ϵ -dominance is:

For two objective vectors: $\mathbf{J}^1 = \mathbf{J}(\mathbf{x}^1)$ and $\mathbf{J}^2 = \mathbf{J}(\mathbf{x}^2)$ with i elements, \mathbf{J}^1 ϵ -dominates \mathbf{J}^2 with some uncertainty $\epsilon_i > 0$ iff:

$$\begin{aligned} (1 + \epsilon_i)\mathbf{J}_i^1 &\leq \mathbf{J}_i^2 \quad \forall i, i \in \{1, 2, \dots, n\} \\ \text{and } (1 + \epsilon_j)\mathbf{J}_j^1 &< \mathbf{J}_j^2 \quad \text{for at least one } j, j \in \{1, 2, \dots, n\} \end{aligned} \tag{7.1}$$

This concept is illustrated graphically in Figure 7.2:

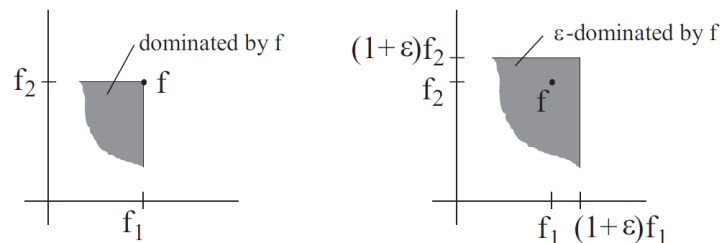


Figure 7.2: Plot illustrating the concept of ϵ -dominance [70]

As in Section 3.2, we can find the ϵ -Pareto set by conducting a pairwise comparison

of all designs to check for ϵ -dominance. Any designs left at the end of this comparison which were not found to be ϵ -dominated by at least one other design comprise the ϵ -Pareto set.

7.3 Example ϵ -Pareto Set Exploration

We use the trade space mapped in Section 6.3 to illustrate several ϵ -Pareto sets corresponding to different levels of uncertainty (0%, 20%, and 50%) within the objective functions. The ϵ -Pareto sets are mapped out for these nine cases in Figure 7.3.

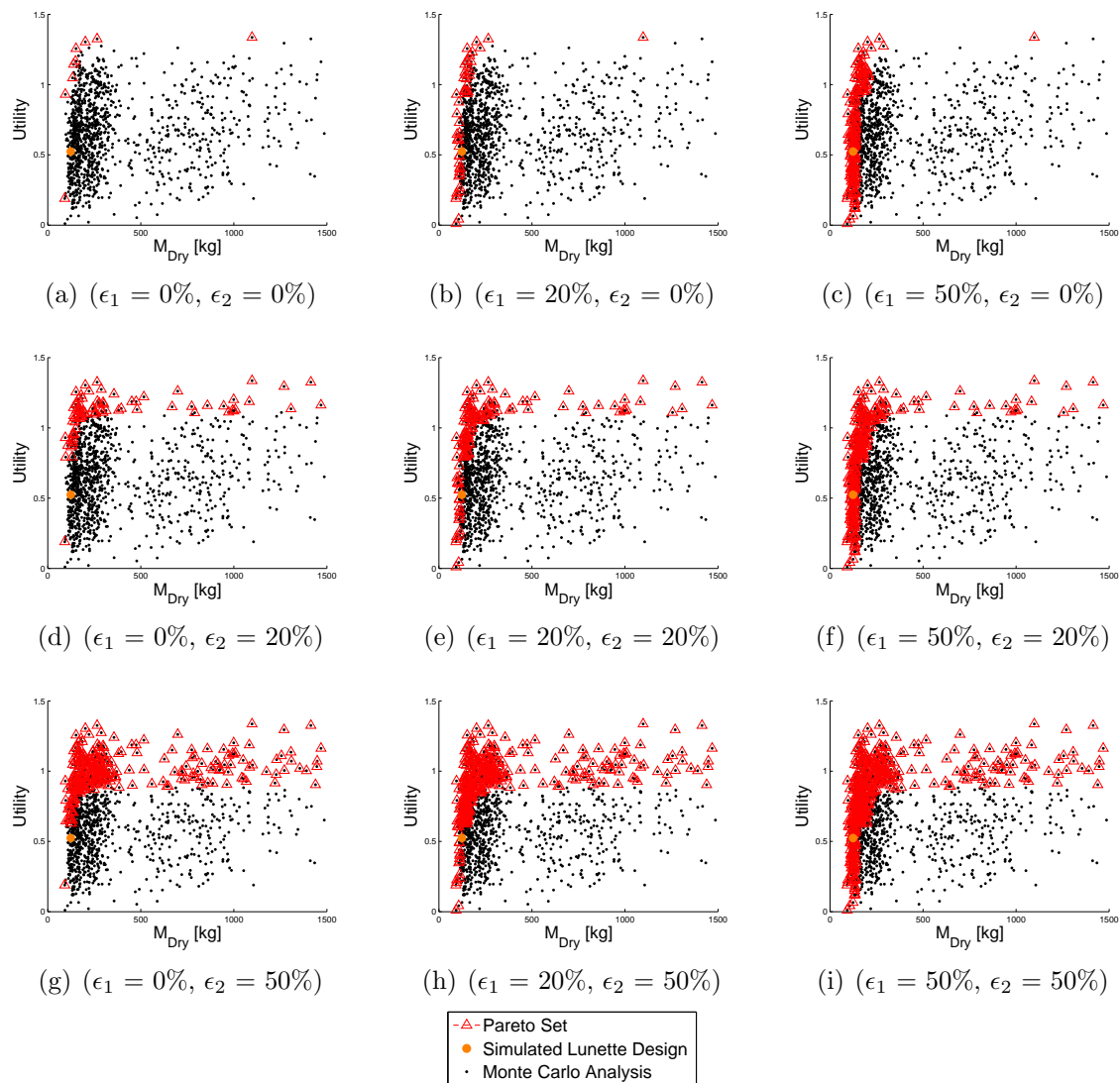


Figure 7.3: ϵ -Pareto sets for $\epsilon_{i,j} \in 0, 0.2, 0.5$

A designer could look at this plot in a particular region of interest. For illustrative purposes, we will use the Lunette mission, here plotted in orange, as an example. One would use these plots to check for the degree of overlap among designs. If the ϵ -Pareto set extends far away from the true Pareto set, then the guarantee that a design picked from that region will actually be truly optimal is low. If requirements dictate picking a design from such a region, then a more traditional error quantification method may be needed.

Looking at the case corresponding to $(\epsilon_1 = 20\%, \epsilon_2 = 50\%)$, shown in Figure 7.4, we see that despite the very high uncertainty in utility metric, because of Lunette's location in the trade space close to a steep feature in the Pareto front, there is little overlapping of designs. This shows that in spite of the uncertainty that may exist, we may still be confident of the near-optimality of this design.

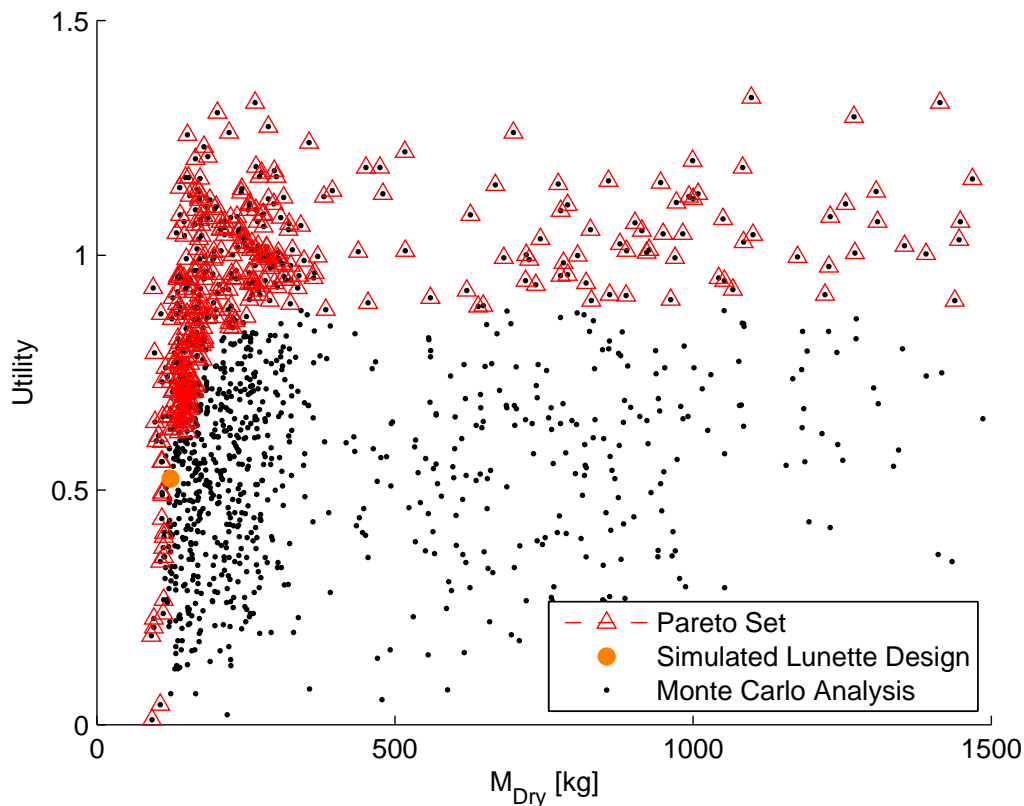


Figure 7.4: ϵ -Pareto set with 20% mass uncertainty and 50% science utility uncertainty

Chapter 8

Conclusion

8.1 Summary

The goal of this thesis was to develop a trade space exploration tool to aid in the design of lunar landers, and to demonstrate the usefulness of this tool.

In Chapter 4, a science utility model was developed, drawing on utility theory from the field of economics, and work on the Science Value Matrix from space systems engineering. For a given set of science instruments and science objectives, a designer can map the contributions of each instrument to each science objective, and use this model to aggregate this information into a single utility value or vector of utility values.

Chapter 5 presented the development of an engineering model that can estimate the mass of an *in situ* lunar lander, given some design vector. The engineering model presented is multidisciplinary in nature, with twelve subsystem modules contained within it, spanning disciplines from power and propulsion to astrodynamics and communications. A validation of the engineering module was presented in Chapter 6, using JPL's Lunette mission concept, as well as data from NASA's Surveyor missions and the proposed International Lunar Network.

The remainder of Chapter 6 used probabilistic and heuristic trade space exploration methods to map out the objective functions developed by analysing mission designs with the science and engineering models. Specific examples of how these trade

space exploration techniques could be used to evaluate the optimality of a mission design were presented using the Lunette mission concept as a case study.

Finally, in Chapter 7, the ideas presented in the previous chapters were expanded upon for cases when uncertainty is present. A method for evaluating confidence in the optimality of a design within the trade space was presented, using the concept of an ϵ -Pareto set.

8.2 Future Work

Throughout this thesis, a number of areas have been identified for future work.

Optimization

The trade space exploration methods used in this project leave a great deal of room open for improvement. One heuristic optimization method, Multi-Objective Simulated Annealing, was used, however many other optimization methods exist, such as Genetic or Evolutionary Algorithms, which are well suited for a highly discrete problem such as this one.

Science Value Model

There are two primary areas for improvement in the Science Value Model:

- 1) A model could be developed to include cases when preferential independence, utility independence or additive independence do not apply. A number of such cases may exist; for instance having simultaneous spectral measurements of the same lunar feature across several wavelengths may be more than twice as advantageous as having just one or the other.

- 2) The model could be improved to include the effects of non-instrument payloads such as drills, arms, and mobility systems, on utility.

Engineering Model

A number of the modules within the engineering model are parametric relations or fixed allocations and could be improved by adding more details. Specifically these include: the structures module and the ACS & GNC module. The thermal module also included a number of simplifying assumptions which and could be improved to have a higher fidelity.

Program Trade Space Exploration

One of the most exciting areas of future work is in the implementation of this model as part of a program systems engineering model. In such a model, a catalog of possible lunar missions could be developed using this tool, and then evaluated to see how well all the missions satisfy the lunar science objectives over time. The use of such a model may help to eliminate areas of unnecessary overlap between missions or to identify areas of interest that are not identified by any current missions.

Appendix A

Lunar Science Value Matrix

Table A.1: Lunar Science Value Matrix based on SCEM Goals

Concept	#	Objective	Rank	Weight	Utility	Instrument																															
						Measurement			Argon Geochronology Experiment (AGE)			Camera		Microscopy, Electrochemistry, and Conductivity Analyzer (MECA)		Pyrolysis Mass Spectrometer (VAPoR)		LIDAR		IR Imager (Mini-TES)		Alpha Particle X-Ray Spectrometer (APXS)		Cone penetrometer		E-field boom		Seismometer (SEIS)		Radiation Assessment Detector (RAD)		Magnetometer		Heat Flow Probe		Retroreflector	
						Regolith Properties	Regolith Volatile Content	Topography	Thermal Environment	Mineralogy/Water Maps	Regolith Cohesion/Mechanical Properties	Electric Field, Regolith/Dust Electrostatic Charge	Seismic Activity/Moonquakes	Radiation Environment	Magnetic Field	Heat Flux	Orbital Elements	Geochronology	Lighting	Regolith Properties	Regolith Volatile Content	Topography	Thermal Environment	Mineralogy/Water Maps	Regolith Cohesion/Mechanical Properties	Electric Field, Regolith/Dust Electrostatic Charge	Seismic Activity/Moonquakes	Radiation Environment	Magnetic Field	Heat Flux	Orbital Elements						
						Max Power [W]	Power [W]	Mass [kg]	180	6	30	25	30	5.4	1.5	10	3	3	4.1	0.9	3	0	5.4	1.5	10	3	3	4.1	0.9	3	0	5.4	1.5	10	3	3	4.1
						0.281	0.041	0.032	0.066	0.010	0.010	0.356	0.010	0.112	0.100	0.020	0.100	0.132	0.039																		
The bombardment history of the inner solar system is uniquely revealed on the Moon.	1a	1a. Test the cataclysm hypothesis by determining the spacing in time of the creation of lunar basins.	1	3.00	2.00	1	0.5	0	0	0	0	0	0.5	0	0	0	0	0	0	0	0	0	0	0	0	0	0	0	0	0	0	0	0	0			
	1b	1b. Anchor the early Earth-Moon impact flux curve by determining the age of the oldest lunar basin (South Pole-Aitken Basin).	2	2.82	1.50	1	0	0	0	0	0	0	0.5	0	0	0	0	0	0	0	0	0	0	0	0	0	0	0	0	0	0	0	0	0	0		
	1c	1c. Establish a precise absolute chronology.	3	2.64	1.50	1	0	0	0	0	0	0	0.5	0	0	0	0	0	0	0	0	0	0	0	0	0	0	0	0	0	0	0	0	0	0	0	
	1d	1d. Assess the recent impact flux.	12	1.00	0.00	0	0	0	0	0	0	0	0	0	0	0	0	0	0	0	0	0	0	0	0	0	0	0	0	0	0	0	0	0	0	0	
	1e	1e. Study the role of secondary impact craters on crater counts.	12	1.00	0.50	0	0	0	0	0	0	0	0.5	0	0	0	0	0	0	0	0	0	0	0	0	0	0	0	0	0	0	0	0	0	0	0	0
The structure and composition of the lunar interior provide fundamental information on the evolution of a differentiated planetary body.	2a	2a. Determine the thickness of the lunar crust (upper and lower) and characterize its lateral variability on regional and global scales.	6	2.09	2.00	0	0	0	0	0	0	0	0	0.5	0.5	0	0.5	0.5	0	0.5	0.5	0	0.5	0.5	0	0.5	0.5	0	0.5	0.5	0	0.5	0.5	0	0.5	0.5	
	2b	2b. Characterize the chemical/physical stratification in the mantle, particularly the nature of the putative 500-km discontinuity and the composition of the lower mantle.	7	1.91	2.00	0	0	0	0	0	0	0	0	0.5	0.5	0	0.5	0.5	0	0.5	0.5	0	0.5	0.5	0	0.5	0.5	0	0.5	0.5	0	0.5	0.5	0	0.5	0.5	
	2c	2c. Determine the size, composition, and state (solid/liquid) of the core of the Moon.	9	1.55	2.50	0	0	0	0	0	0	0	0	0.5	0.5	0	0.5	0.5	0	0.5	0.5	0	0.5	0.5	0	0.5	0.5	0	0.5	0.5	0	0.5	0.5	0	0.5	0.5	
	2d	2d. Characterize the thermal state of the interior and elucidate the workings of the planetary heat engine.		3.18	0.50	0	0	0	0	0	0	0	0	0	0	0	0	0	0	0	0	0	0	0	0	0	0	0	0	0	0	0	0	0	0	0	0
Key planetary processes are manifested in the diversity of lunar crustal rocks.	3a	3a. Determine the extent and composition of the primary feldspathic crust, KREEP layer, and other products of planetary differentiation.	5	2.27	3.00	0	0	0	0	0	0	0.5	0	0.5	0.5	0	0.5	0.5	0	0.5	0.5	0	0.5	0.5	0	0.5	0.5	0	0.5	0.5	0	0.5	0.5	0	0.5	0.5	
	3b	3b. Inventory the variety, age, distribution, and origin of lunar rock types.	10	1.36	1.50	1	0	0	0	0	0	0.5	0	0	0	0	0	0	0	0	0	0	0	0	0	0	0	0	0	0	0	0	0	0	0	0	0
	3c	3c. Determine the composition of the lower crust and bulk Moon.	12	1.00	0.50	0	0	0	0	0	0	0.5	0	0	0	0	0	0	0	0	0	0	0	0	0	0	0	0	0	0	0	0	0	0	0	0	0
	3d	3d. Quantify the local and regional complexity of the current lunar crust.	12	1.00	1.50	0	0	0	0	0	0	0.5	0	0	0.5	0	0	0	0	0.5	0	0	0	0	0	0	0.5	0	0	0.5	0	0	0.5	0	0	0.5	0
	3e	3e. Determine the vertical extent and structure of the megaregolith.	12	1.00	1.00	0	0	0.5	0	0	0	0.5	0	0	0	0	0	0	0	0.5	0	0	0	0	0	0	0	0	0	0	0	0	0	0	0	0	0

Table A.2: Lunar Science Value Matrix based on SCEM Goals (Continued)

The lunar poles are special environments that may bear witness to the volatile flux over the latter part of solar system history.	4a	4a. Determine the compositional state (elemental, isotopic, mineralogic) and compositional distribution (lateral and depth) of the volatile component in lunar polar regions.	4	2.45	1.50	0	0	0	0.5	0	0	1	0	0	0	0	0	0	0
	4b	4b. Determine the source(s) for lunar polar volatiles.	12	1.00	1.00	0	0	0	0.5	0	0	0	0	0	0	0.5	0	0	0
	4c	4c. Understand the transport, retention, alteration, and loss processes that operate on volatile materials at permanently shaded lunar regions.	12	1.00	1.50	0	0	0	0	0	0.5	0.5	0	0	0	0.5	0	0	0
	4d	4d. Understand the physical properties of the extremely cold (and possibly volatile rich) polar regolith.	12	1.00	1.00	0	0	0.5	0	0	0	0.5	0	0	0	0	0	0	0
	4e	4e. Determine what the cold polar regolith reveals about the ancient solar environment.	12	1.00	2.00	0	0	0	1	0	0	1	0	0	0	0	0	0	0
Lunar volcanism provides a window into the thermal and compositional evolution of the Moon.	5a	5a. Determine the origin and variability of lunar basalts.	12	1.00	3.00	1	0	0	0	0	0.5	0	0.5	0	0.5	0.5	0	0	
	5b	5b. Determine the age of the youngest and oldest mare basalts.	12	1.00	1.50	1	0	0	0	0	0.5	0	0	0	0	0	0	0	
	5c	5c. Determine the compositional range and extent of lunar pyroclastic deposits.	12	1.00	0.50	0	0	0	0	0	0.5	0	0	0	0	0	0	0	
	5d	5d. Determine the flux of lunar volcanism and its evolution through space and time.	12	1.00	2.00	1	0	0	0	0	0	0	0	0.5	0	0	0.5	0	
The Moon is an accessible laboratory for studying the impact process on planetary scales.	6a	6a. Characterize the existence and extent of melt sheet differentiation.	12	1.00	0.50	0	0	0	0	0	0.5	0	0	0	0	0	0	0	
	6b	6b. Determine the structure of multi-ring impact basins.	12	1.00	0.50	0	0	0	0	0	0	0	0	0	0.5	0	0	0	
	6c	6c. Quantify the effects of planetary characteristics (composition, density, impact velocities) on crater formation and morphology.	12	1.00	1.50	0	0.5	0	0	0.5	0	0.5	0	0	0	0	0	0	
	6d	6d. Measure the extent of lateral and vertical mixing of local and ejecta material.	12	1.00	0.50	0	0	0	0	0	0.5	0	0	0	0	0	0	0	
The Moon is a natural laboratory for regolith processes and weathering on anhydrous airless bodies.	7a	7a. Search for and characterize ancient regolith.	12	1.00	2.00	1	0	0	0	0	0	1	0	0	0	0	0	0	
	7b	7b. Determine physical properties of the regolith at diverse locations of expected human activity.	12	1.00	1.50	0	0	0	0.5	0	0	0.5	0.5	0	0	0	0	0	
	7c	7c. Understand regolith modification processes (including space weathering), particularly deposition of volatile materials.	12	1.00	0.00	0	0	0	0	0	0	0	0	0	0	0	0	0	
	7d	7d. Separate and study rare materials in the lunar regolith.	12	1.00	0.50	0	0	0	0	0	0	0.5	0	0	0	0	0	0	
Processes involved with the atmosphere and dust environment of the Moon are accessible for scientific study while the environment remains in a pristine state.	8a	8a. Determine the global density, composition, and time variability of the fragile lunar atmosphere before it is perturbed by further human activity.	8	1.73	0.00	0	0	0	0	0	0	0	0	0	0	0	0	0	
	8b	8b. Determine the size, charge, and spatial distribution of electrostatically transported dust grains and assess their likely effects on lunar exploration and lunar-based astronomy.	11	1.18	1.00	0	0	0.5	0	0	0	0	0	0.5	0	0	0	0	
	8c	8c. Use the time-variable release rate of atmospheric species such as ⁴⁰ Ar and Radon to learn more about the inner workings of the lunar interior.	12	1.00	0.00	0	0	0	0	0	0	0	0	0	0	0	0	0	
	8d	8d. Learn how water vapor and other volatiles are released from the lunar surface and migrate to the poles where they are adsorbed in polar cold traps.	12	1.00	0.00	0	0	0	0	0	0	0	0	0	0	0	0	0	

Appendix B

Engineering Model Variables

Table B.1: Working Variables

#	Name	Units	Range
Design Vector			
1	Instrument Vector	-	-
2	Lifetime	yr	-
3	Landing Latitude	°	-
4	Power Source	-	Solar, Nuclear
5	Battery Type	-	Ni-Cd, Nh-H, LiIon
6	Solar Panel Type	-	Si, Amorphous Si, Ga-As, In-P, Multijunction Ga-As
7	Data Rate	bits/s	-
8	Antenna Size	m	-
9	Transfer Orbit	-	Hohmann, WSB
10	Descent Method	-	Solid-Staged, Liquid-Direct
11	Propellant	-	Monoprop, Biprop
Parameters Vector			
1	Solar Flux	W/m^2	
2	Communications Frequency	Hz	
3	Structural Mass Fraction	-	
4	Lander Heat Capacity	J/kg/K	-
5	Downlinks per Day	-	-
6	Ground Station Antenna Size	m	-

#	Name	Units	Range
7	Target Body Distance	m	-
8	Target Body Mass	kg	-
9	Target Body Radius	m	-
10	RPS Mass	kg	-
11	RPS Power	W	-
12	Landing ΔV	m/s	-
Instruments			
1	Data Rates	bits/s	
2	Duty Cycles	%	
3	Instruments Power	W	
4	Instrument Mass	kg	
Avionics			
1	Storage Capacity	bits	
2	Avionics Power	W	
3	Avionics Mass	kg	
4	Data Transmission Rate	bits/s	
5	Uplink Period	day^{-1}	
Communications			
1	Antenna Diameter	m	
2	Communications Power	W	
3	Communications Mass	kg	
Power			
1	Battery Capacity	J	
2	Solar Panel Area	m^2	
3	Radioisotope Mass	kg	
4	Heat Flux	W	
5	Power System Mass	kg	
Orbit			
1	Mid-course ΔV		
2	Arrival ΔV	m/s	
3	Launch C3	km^2/s^2	
Thermal			
1	Thermal Mass	kg	
2	Thermal Power	kg	
Structures			
1	Structural Mass	kg	

#	Name	Units	Range
ACS/GNC			
1	ACS/GNC Mass	kg	
Propulsion			
1	Thrust	N	
2	Propellant Mass	kg	
3	Propulsion Dry Mass	kg	
Mass			
1	Total Spacecraft Dry Mass	kg	
2	Total Spacecraft Wet Arrival Mass	kg	
3	Total Spacecraft Launch Mass	kg	
Launch Vehicle			
1	Launch Vehicle	-	Atlas 4xx, Atlas 5xx, Delta II, Delta IV, Falcon 9

Bibliography

- [1] NASA, *The Vision for Space Exploration*, Washington, D.C., February 2004, NP-2004-01-334-HQ.
- [2] “Google Lunar X Prize,” <http://www.googlelunarxprize.org>.
- [3] NASA, *Fiscal Year 2011 Budget Estimates*, Washington, D.C., 1 February 2010, <http://www.nasa.gov/news/budget/index.html>.
- [4] NASA Marshall Space Flight Center, “Lunar Precursor Robotic Program,” <http://moon.msfc.nasa.gov/>.
- [5] Wieczorek, M. A., Jolliff, B. L., Khan, A., Pritchard, M. E., Weiss, B. P., Williams, J. G., Hood, L. L., Richter, K., Neal, C. R., Shearer, C. K., McCallum, I. S., Tompkins, S., Hawke, B. R., Peterson, C., Gillis, J. J., and Bussey, B., “The Constitution and Structure of the Lunar Interior,” *Reviews in Mineralogy and Geochemistry*, Vol. 60, No. 1, January 2006, pp. 221–364.
- [6] NASA, *Announcement of Opportunity: New Frontiers 2009*, April 20 2009, NNH09ZDA007O.
- [7] Committee on New Opportunities in Solar System Exploration, National Research Council, *Opening New Frontiers in Space: Choices for the Next New Frontiers Announcement of Opportunity*, The National Academies Press, Washington, D.C., 2008, <http://www.nap.edu/catalog/12175.html>.
- [8] Bob Kinsey, et al., “Lunette 2008-03 Study Final Report,” *Team X, Jet Propulsion Laboratory*, March 12 2008.
- [9] Elliott, J. and Alkalai, L., “Lunette: A Low-Cost Concept Enabling Multi-Lander Lunar Science and Exploration Missions,” *International Astronautical Congress*, Glasgow, Scotland, 2008, IAC-08-B4.8.4.
- [10] Elliott, J. O., Alkalai, L., and Banerdt, B., “Lunette Geophysical Lunar Network,” Internal JPL Presentation.
- [11] Vane, G., “Concept Maturity Level: Establishing A Shared Language To Articulate Maturity Of a Space-Science Mission Concept and Cost Uncertainty in the Early Formulation Phase,” *Presentation to the Planetary Science Decadal Survey Steering Group*, Washington, D.C., 6 July 2009.

- [12] Weiss, J. R., Smythe, W. D., and Lu, W., "Science Traceability," *2005 IEEE Aerospace Conference*, Big Sky, Montana, 5-12 March 2005.
- [13] Seher, T. K., *Campaign-Level Science Traceability for Earth Observation System Architecting*, Master's thesis, Massachusetts Institute of Technology, Cambridge, Massachusetts, May 2009.
- [14] Lamassoure, E. S., Wall, S. D., and Easter, R. W., "Model-Based Engineering Design for Trade Space Exploration throughout the Design Cycle," *AIAA Space 2004 Conference and Exhibition*, San Diego, California, 28-30 September 2004.
- [15] Hubbard, G. S., Naderi, F. M., and Garvin, J. B., "Following the Water: The New Program for Mars Exploration," *Acta Astronautica*, Vol. 51, No. 1-9, 2002, pp. 337-350.
- [16] MEPAG (2001), Scientific Goals, Objectives, Investigations, and Priorities, in *Science Planning for Exploring Mars*, JPL Publication 01-7, p. 9-38. Available on the web at <http://mepag.jpl.nasa.gov/reports/index.html>.
- [17] Committee on Assessing the Solar System Exploration Program, National Research Council, *Grading NASA's Solar System Exploration Program: A Midterm Review*, The National Academies Press, Washington, D.C., 2008.
- [18] de Weck, O. S. and Willcox, K., "16.888 / ESD.77 Multidisciplinary System Design Optimization Lecture Notes," <http://ocw.mit.edu/OcwWeb/Aeronautics-and-Astronautics/16-888Spring-2004/CourseHome/>, Spring 2010.
- [19] de Weck, O. S., "Multiobjective Optimization: History and Promise," *The Third China-Japan-Korea Joint Symposium on Optimization of Structural and Mechanical Systems*, No. GL2-2, Kanazawa, Japan, 30 October - 2 November 2004.
- [20] Jilla, C. D., *A Multiobjective, Multidisciplinary Design Optimization Methodology for the Conceptual Design of Distributed Satellite Systems*, Ph.D. thesis, Massachusetts Institute of Technology, Cambridge, Massachusetts, May 2002.
- [21] Mattso, C. A., Mullur, A. A., and Messac, A., "Smart Pareto Filter: Obtaining a Minimal Representation of Multiobjective Design Space," *Engineering Optimization*, Vol. 36, No. 6, 2004, pp. 721-740.
- [22] Ehrgott, M. and Gandibleux, X., "Approximative Solution Methods for Multiobjective Combinatorial Optimization," *TOP*, Vol. 12, No. 1, 2004, pp. 1-89.
- [23] Kirkpatrick, S., Gelatt, C. D., and Vecchi, M. P., "Optimization by Simulated Annealing," *Science*, Vol. 220, No. 4598, 13 May 1983, pp. 671-680.
- [24] Nam, D. and Park, C. H., "Multiobjective Simulated Annealing: A Comparative Study to Evolutionary Algorithms," *International Journal of Fuzzy Systems*, Vol. 2, No. 2, June 2000, pp. 87-97.

- [25] von Neumann, J. and Morgenstern, O., *Theory of Games and Economic Behavior*, Princeton University Press, Princeton, New Jersey, 3rd ed., 1953.
- [26] Ross, A. M., Hastings, D. E., Warmkessel, J. M., and Diller, N. P., “Multi-Attribute Tradespace Exploration as Front End for Effective Space System Design,” *Journal of Spacecraft and Rockets*, Vol. 41, No. 1, January 2004, pp. 20–28.
- [27] Richards, M. G., *Multi-Attribute Tradespace Exploration for Survivability*, Ph.D. thesis, Massachusetts Institute of Technology, Cambridge, Massachusetts, June 2009.
- [28] Lamamy, J., *Methods and Tools for the Formulation, Evaluation and Optimization of Rover Mission Concepts*, Ph.D. thesis, Massachusetts Institute of Technology, Cambridge, Massachusetts, June 2007.
- [29] Peterson, C. E., Balint, T., Curtis, J., Kwok, J., Hall, J. L., Senske, D., Kolowa, E., and Bullock, M., “Evaluating Low Concept Maturity Mission Elements and Architectures for a Venus Flagship Mission,” *AIAA Space 2009 Conference & Exhibition*, Pasadena, California, 1417 September 2009, AIAA-2009-6760.
- [30] Posavac, E. J. and Carey, R. G., *Program Evaluation: Methods and Case Studies*, Pearson Prentice Hall, Upper Saddle River, NJ, 7th ed., 2007.
- [31] Spilker, T., “JPL Rapid Mission Architecture (RMA) Neptune Study Report: Executive Summary,” *Solar System 2012 Giant Planets Panels*, Irvine, CA, 26 October 2009.
- [32] NASA, *Titan Saturn System Mission Study: Final Report*, No. JPL D-48148., Jan. 30 2008, <http://opfm.jpl.nasa.gov/library/>.
- [33] NASA, *Jupiter Europa Orbiter Mission Study: Final Report*, No. JPL D-48279, Jan. 30 2009, <http://opfm.jpl.nasa.gov/library/>.
- [34] Space Studies Board, National Research Council, *New Frontiers in the Solar System: An Integrated Exploration Strategy*, The National Academies Press, Washington, D. C., 2003.
- [35] *NASA’s Lunar Robotic Architecture Study*, National Aeronautics and Sapce Administration, Washington, D.C., July 2006.
- [36] Lunar Exploration Analysis Group, *Report of Analysis Results of the Geology-Geophysics Specific Action Team*, Lunar and Planetary Institute, November 2006.
- [37] Committee on the Scientific Context for the Exploration of the Moon, National Research Council, *The Scientific Context for the Exploration of the Moon*, The National Academies Press, Washington, D.C., 2007.

- [38] NASA Advisory Council, *NASA Advisory Council Workshop on Science Associated with the Lunar Exploration Architecture*, Tempe, Arizona, Feb. 27 – Mar 2 2007.
- [39] “SAO/NASA Astrophysics Data System,” <http://adswww.harvard.edu/>.
- [40] “Lunar and Planetary Institute Meeting Abstracts,” <http://www.lpi.usra.edu/publications/>.
- [41] Williams, D. R., “National Space Science Data Center,” <http://nssdc.gsfc.nasa.gov/>.
- [42] Thurston, D. L., “Real and Misconceived Limitations to Decision Based Design With Utility Analysis,” *Journal of Mechanical Design*, Vol. 123, No. 2, June 2001, pp. 176–182.
- [43] Design Decisions Laboratory, Carnegie Mellon University, “Design Decisions Wiki: Multiattribute Utility Theory,” http://ddl.me.cmu.edu/ddwiki/index.php/Multiattribute_utility_theory, March 17 2009.
- [44] Keeney, R. L. and Raiffa, H., *Decisions with Multiple Objectives: Preferences and Value Tradeoffs*, John Wiley & Sons, New York, NY, 1976.
- [45] Larson, W. J. and Wertz, J. R., *Space Mission Analysis and Design*, Microcosm Press, California, 3rd ed., 2007.
- [46] Lamamy, J., *Enhancing the Science Return of Mars Missions via Sample Preparation, Robotic Surface Exploration, and In-Orbit Fuel Production*, Master’s thesis, Massachusetts Institute of Technology, Cambridge, Massachusetts, June 2004.
- [47] Radioisotope Power Systems Committee, National Research Council, *Radioisotope Power Systems: An Imperative for Maintaining U.S. Leadership in Space Exploration*, The National Academies Press, Washington, D.C., 2009.
- [48] Shaltens, R. K. and Wong, W. A., “Advanced Stirling Technology Development at NASA Glenn Research Center,” Tech. Rep. TM2007-214930, NASA Glenn Research Center, Cleveland, Ohio, June 2007.
- [49] Uesugi, K., Matsuo, H., Kawaguchi, J., and Hayashi, T., “Japanese First Double Lunar Swingby Mission “Hiten”,” *Acta Astronautica*, Vol. 25, No. 7, July 1991, pp. 347–355.
- [50] Belbruno, E. A. and Miller, J. K., “Sun-Perturbed Earth-to-Moon Transfers with Ballistic Capture,” *Journal of Guidance, Control and Dynamics*, Vol. 16, No. 4, July–August 1993, pp. 770–775.

- [51] Pernicka, H. J., Scarberry, D. P., Marsh, S. M., and Sweetser, T. H., “A Search for Low Delta-V Earth-to-Moon Trajectories,” *AIAA/AAS Astrodynamics Conference*, AIAA-1994-3772, Scottsdale, Arizona, 1-3 August 1994, pp. 530–537.
- [52] Culler, G. J. and Fried, B. F., “Universal Gravity Turn Trajectories,” *Journal of Applied Physics*, Vol. 18, No. 6, June 1957, pp. 672–676.
- [53] Wilhite, A. W., Wagner, J., Tolson, R., and Moen, M. M., “Lunar Module Descent Mission Design,” *AIAA/AAS Astrodynamics Specialist Conference and Exhibit*, No. AIAA 2008-6939, AIAA/AAS, Honolulu, Hawaii, 18-21 August 2008.
- [54] Lawson, S. L. and Jakowsky, B. M., “Brightness Temperatures of the Lunar Surface: The Clementine Long-Wave Infrared Global Data Set,” *30th Annual Lunar and Planetary Science Conference*, No. 1892, Houston, Texas, 15-29 March 1999.
- [55] Christie, R. J., Plachta, D. W., and Hasan, M. M., “Transient Thermal Model and Analysis of the Lunar Surface and Regolith for Cryogenic Fluid Storage,” Tech. Rep. TM-2008-215300, NASA Glenn Research Center, Cleveland, Ohio, August 2008.
- [56] Ball, A. J., Garry, J. R. C., Lorenz, R. D., and Kerzhanovic, V. V., *Planetary Landers and Entry Probes*, Cambridge University Press, Cambridge, U.K., 2007.
- [57] Sarsfield, L. P., *The Cosmos on a Shoestring*, RAND Corporation, Santa Monica, California, 1998.
- [58] Department of Energy: Office of Nuclear Energy, “Radioisotope Heater Units,” <http://nuclear.gov/space/neSpace2f.html>.
- [59] NASA, “Surveyor I Mission Report: Part I. Mission Description and Performance,” Tech. Rep. 32-1023, Jet Propulsion Laboratory, Pasadena, California, August 31 1966.
- [60] Johnson, M. S. and Giller, D. R., “MIT’s Role in Project Apollo, Vol. V: The Software Effort,” Tech. rep., Charles Stark Draper Laboratories, Cambridge, Massachusetts, 1971.
- [61] Alliant Techsystems, Inc., Tactical Propulsion and Controls, “ATK Space Propulsion Products Catalog,” http://www.atk.com/capabilities_space/documents/ATK_Catalog_May_2008.pdf, May 2008.
- [62] Aerojet, Inc., Redmond, Washington., *Chemical Monopropellant Training Manual*, Unpublished.
- [63] Brown, C. D., *Spacecraft Propulsion*, AIAA, Washington, D. C., 1996.
- [64] NASA Launch Services Program, “ELV Mission Analysis Launch Vehicle Information,” <http://elvperf.ksc.nasa.gov>.

- [65] Tahu, G., Cohen, B., and Morse, B., “International Lunar Network (ILN) AnchorNodes,” *Presentation to Solar System 2012 Planetary Decadal Survey Inner Planets Panel*, Washington, D.C., 27 August 2009.
- [66] NASA, “Surveyor Program Results: Final Report,” Tech. Rep. NASA-SP-184, Washington, D.C., 1969.
- [67] Houdou, B. and Carpenter, J., “The MoonNEXT Mission,” *Joint Annual Meeting of LEAG-ICEUM-SRR*, Cape Canaveral, Florida, 28-31 October 2008.
- [68] Hashimoto, T., Tanaka, S., Hoshino, T., Otsuki, M., and Kawaguchi, J., “A Lunar Landing Mission SELENE-2,” *27th International Symposium on Space Technology and Science*, Tsukuba, Japan, 5-12 July 2009.
- [69] Cohen, B. A., the ILN Science Definition Team, and the MSFC/APL ILN Engineering Team, *International Lunar Network: Final Report of the Science Definition Team for the ILN Anchor Nodes*, NASA Marshall Space Flight Center, Huntsville, Alabama, January 2009.
- [70] Laumanns, M., Thiele, L., Deb, K., and Zitzler, E., “On the Convergence and Diversity-Preservation Properties of Multi-Objective Evolutionary Algorithms,” Tech. rep., Swiss Federal Institute of Technology (ETH), Zurich, Switzerland, 17 May 2001, TIK-Report No. 108.